NUMERICAL MODEL FOR THE LATERAL COMPRESSION RESPONSE OF A PLASTIC CUP

Ignacio Dapic Rodriguez

Thesis submitted to the Faculty of the

Virginia Polytechnic Institute and State University

in partial fulfillment of the requirements for the degree of

Master of Science

in

Aerospace Engineering

Dr. Eric Johnson, Chair

Dr. Scott Case, Committee Member

Dr. Donatus Ohanehi, Committee Member

Dr. Rakesh K. Kapania, Committee Member

July 2003

Blacksburg, Virginia

Keywords: High Impact Polystyrene, truncated conical shell, finite element analysis

NUMERICAL MODEL FOR THE LATERAL COMPRESSION RESPONSE OF A PLASTIC CUP

IGNACIO DAPIC RODRIGUEZ

(ABSTRACT)

A numerical analysis based on the finite element method is developed to simulate the mechanical response of a typical sixteen-ounce plastic drink cup subjected to a lateral compressive load. The aim of the analysis is to simulate a test in which the cup is supported horizontally in a fixture on a testing machine platen, and a loading nose attached to the actuator is displaced downward into the cup. The numerical model is developed using the software packages MSC.Patran, ABAQUS/CAE, and ABAQUS/Standard. The high impact polystyrene material of the cup is modeled as linear elastic, considering isotropic and orthotropic material behavior. The structural model of the cup is a truncated conical shell including a ring at the open end of the cup and circumferential stiffening ribs. The analysis is based on small strain, large rotation shell kinematics, and the loading apparatus of the test is simulated with a rigid, circular cylinder contacting the cup. Coupons cut from the wall of a cup are subjected to tension to determine the ranges of the meridional and circumferential moduli of elasticity. Rings cut from the open end of the cup were tested in diametrical tension to aid in validating the finite element modeling. Reasonable correlation of the simulation to available cup compression test data is achieved. Parametric studies are conducted for several meridional thickness distributions of the cup wall, and for a range of orthotropic material properties.

Dedication

In Memoriam of my grandparents Ignacio Dapic Usi and Alma Athie. This thesis is dedicated to you as a sign of love and gratitude. Thank you so much for all those good times and important lessons. We all miss you. Q.E.P.D

"Research is what I'm doing when I don't know what I'm doing."

- Wernher Von Braun (1912-1977)

Acknowledgments

First and foremost I would like to thank my parents Ignacio Dapic Sr. and Violeta Rodriguez for their love, support and inspiration. Because of you I have become what I am now, all my dreams and goals are based on your wisdom and hope. Thanks for believing always on me and being for me in every stage of my life. You are the greatest role models I could ever asked for.

I would also like to thank my grandfather Col. Florentino “Abu” Rodriguez Cota for his great inspiration and support. Your hard work and extraordinary flight abilities made my dream come true. It is a privilege and an honor to have a grandfather like you.

To my brother Eduardo “Huevillo” Dapic -a future mechatronics engineer-, to my sisters Violeta “Pimpi” Dapic and Yazmin “Seta” Dapic thank you for being a part of such a loving family. Having you as brother and sisters is the best thing, keep working hard to reach all those goals you have.

I want to thank my grandmother Delfina “Pina” Gomez for her support and for the important lessons she has taught me. Also, my aunt Rocio Rodriguez who has been always very close to me providing motivation and support.

To my girlfriend Sandra Quirino who has also been a great source of love, motivation and support. Thank you for being such a great inspiration.

I would like to acknowledge my advisor and mentor Dr. Eric Johnson for his hard work, help and coaching. His motivation and confidence on me played a very important role on the completition of my degree. The experiences and lessons learned from him will stand forever. I also like to thank my committee members Dr. Scott Case, Dr. Donatus Ohanehi and Dr. Rakesh Kapania.

This research is sponsored by The DOW Chemical Company. The financial support provided by this company is gratefully acknowledged. I also wish to thank Dr. Charles Berglund, the technical monitor for this project.

To my friends Aristides “Pyrogreek” Bonanos, Vinay “Winay” Goyal, Serhat “Mr. Serhat” Hosder, Leifer “Hip-hop Leif” Leifsson, Dhaval Makhecha and Rafael “Rafi” Perez thanks for your friendship, help, support and all the good moments while being part of the 101st Lborne Division.

Table of Contents

List of Figures

List of Tables

CHAPTER 1

Technology of a Plastic Drink Cup

The plastic drink cup is an ubiquitous consumer item with an interesting technology. The material science and manufacturing process are important parts of this technology, and are briefly reviewed in this chapter. However, the main subject of this work is the development of a computational model to predict the mechanical response of a plastic drink cup subjected to a lateral compressive load. In laboratory tests, an empty cup is held horizontally in a fixture, and a vertical compressive load is applied by a universal testing machine. This test is intended to mimic the pressure exerted by the hand of a person holding the cup. The computational model is developed for a typical drink cup manufactured by the thermoforming process from a sheet of high impact polystyrene (HIPS) material.

1.1 High Impact Polystyrene

High Impact Polystyrene (HIPS) is a blend of polystyrene monomers toughened by butadiene rubber produced by the process called co-polymerization. All blends of polystyrene are manufactured in stabilized form in both tinted and tint-free granules. Polystyrene is a clear amorphous polymer that exhibits high stiffness, good dimensional stability, electrical insulation properties and low specific gravity. HIPS is opaque, provides improved impact properties while maintaining good stiffness, offers good gloss, excellent extrusion performance, and high heat resistance. Its superior cost to performance ratio

makes HIPS a very advantageous material.The versatility of HIPS makes it ideal for a range of end-use applications, including: food packaging, food service-ware, office supplies, point-of-purchase signs and displays, TV cabinets/housings, housewares and consumer goods, refrigerator trim/liners, small appliance parts, toys, medical products and packaging, building insulation, cosmetics packaging, and CD jewel boxes. When used unmodified for the manufacture of food contact articles, HIPS complies with the US Food, Drug and Cosmetic Act and Food Additive Regulation 21. One of the larger markets for high impact polystyrene is for thermoformed drink cups. Drink cups made of HIPS are thermoformed by forcing a heated sheet into a mold.

The chemical composition of the butadiene rubber blended with styrene is shown in Fig. 1.1 [1], and a graphic depiction of the HIPS molecule is shown in Fig. 1.2. Polybutadiene has double bonds in it that can polymerize with other materials. When the polybutadiene copolymerizes with the styrene monomer, a type of copolymer called a graft copolymer is obtained. This graft copolymer consists of a polystyrene chain with chains of polybutadiene growing out of it. Since polybutadiene and polystyrene are homopolymers that do not mix, the polybutadiene branches try as best as they can to phase separately and form little globes. But these little globes are always tied to the polystyrene phase. These globules of the styrene-butadiene copolymer act as crack inhibitors to increase its fracture toughness. They act to absorb energy when the polymer is subjected to impact loads. They also give the polymer a resilience that normal polystyrene does not have. The HIPS blend is tougher than polystyrene, and so HIPS is capable of absorbing more severe impacts before fracturing than is regular polystyrene.

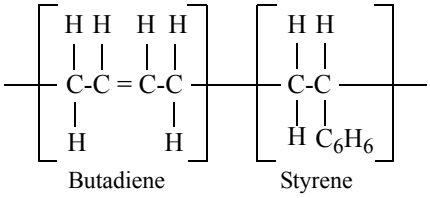

Fig. 1.1 Butadiene-styrene copolymer with carbon backbone

The polystyrene resin in HIPS offers several advantages over competitive resins, including higher stiffness, ease of processing and exceptional clarity. Due to its low density,

its yield strength is 20 to 30 percent greater than alternative resins such as polyester. HIPS mechanical properties are listed in Table 1.1.

Table 1.1 Typical Mechanical Properties of HIPS [2]

Property	Value
Tensile Yield Strength	4000 psi
Ultimate Tensile Strength	4080 psi
Ultimate Elongation	59%
Tensile Modulus	295000 psi
Flexural Strength	7500 psi
Flexural Modulus	350000 psi

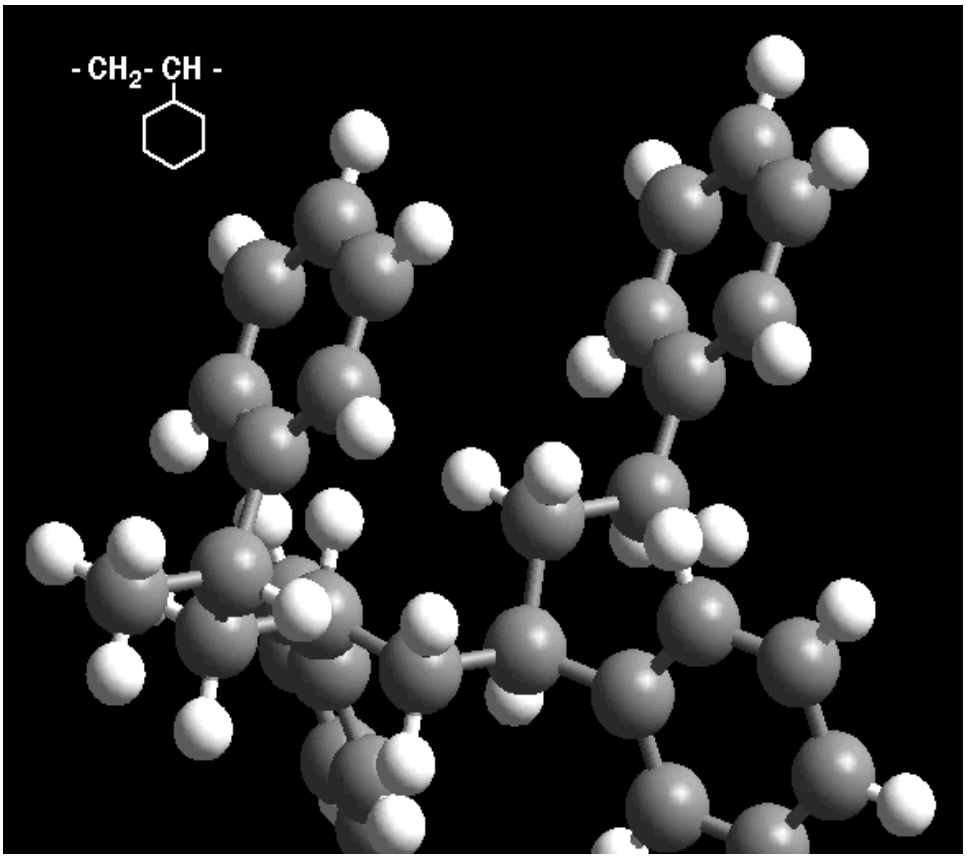

Fig. 1.2 HIPS molecule

1.2 The Thermoforming Process

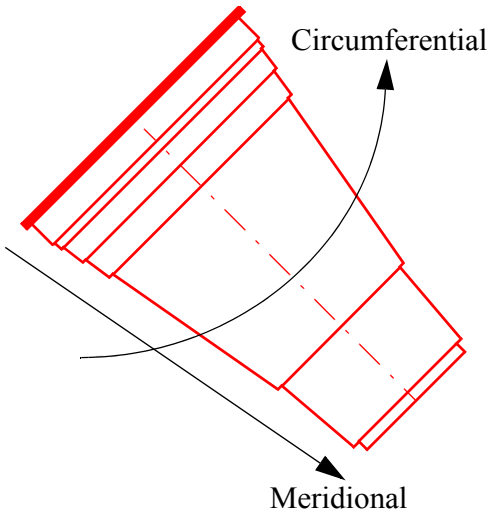

Fig. 1.3 Definition of cup directions

Thermoforming is the process where heat and pressure are used to change a sheet of plastic into any type of plastic part. This process takes a preheated sheet of plastic and inserts it into a mold that has the shape of the actual final product. The method allows for tight specifications, close tolerances and attention to detail. Thermoforming can be cost-effective and efficient, depending on the product. There is less mold shrinkage in thermoforming processes with polystyrene than other crystalline thermoplastics, such as polypropylene. HIPS is combined with a crystal polystyrene cap layer for high gloss and aesthetics to create a color-concentrated layer for a bright surface color. Polystyrene can be thermoformed or vacuum formed using standard aluminum tooling and equipment. The thermoforming and trim tooling needs to be designed with dimensions that will incorporate the typical polystyrene mold shrinkage rate. Polystyrene's low shrinkage provides good dimensional stability and part dimensional repeatability. It does not absorb moisture, so drying is not required prior to extrusion or thermoforming. During the forming process, material surface temperatures range between 250F to 300F, depending on the depth of draw and the forming rate. Because of its amorphous nature, polystyrene has good sheet integrity for forming operations.

Due to the thermoforming process, the HIPS wall material becomes orthotropic. In other words, the HIPS material acquires a different modulus of elasticity along the meridional direction of the cup than in the circumferential direction. These directions are shown on Fig. 1.3

1.3 The Cup Lateral Compression Test

Cup manufacturers seek to minimize the amount of material in a cup. However, there are limits on minimum amount of material based on cup rigidity, strength and fracture toughness. Apparently, cup manufacturers use subjective responses to evaluate cup designs; such as how the cup feels when squeezed by hand, and that the cup should not fracture when squeezed too hard. In order to translate customer acceptability on the feel of the cup to some quantitative measures, researchers at the Dow Chemical Company have developed a mechanical compression test. This compression test is depicted in the sketch of Fig. 1.4, and the measured cup response can be used to determine the acceptability of a design. As shown in the figure, the cup is supported horizontally in a fixture on the testing machine platen, and a loading nose attached to the actuator is displaced downward into the cup at one-third of the length of the cup from its opening. Data acquired in the test consists of the loads and corresponding lateral displacements of the cup wall, which are used to determine a representative stiffness of the cup.

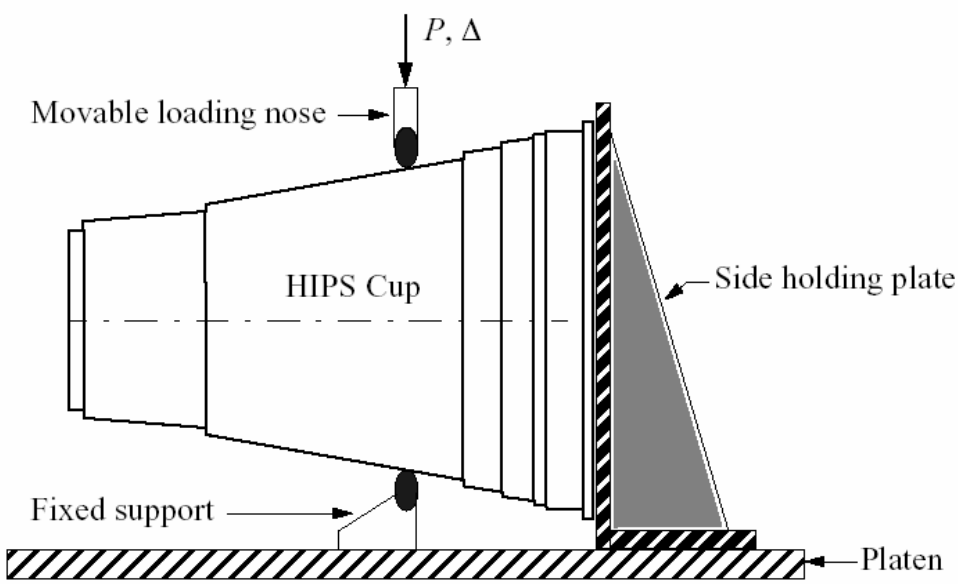

Fig. 1.4 Cup compression test

1.4 Objectives, Scope, and Contents

The objectives of this work are to develop a computational model of the cup compression test that can be used to better understand the mechanics of response, and to conduct parametric studies on the influence of geometric and material parameters on the compression response. The computational model is to be validated with respect to test data provided by Dow. The structural model of the cup is a truncated conical shell with one open end. Thermoforming results in a cup wall of variable thickness and variable orthotropic material properties along the meridian of the shell wall. In addition, the cup wall is not smooth, but consists of smooth shell segments between circumferential ribs.

Conical shell models of a typical sixteen-ounce drink cup are developed using the ABAQUS[1] finite element software. The model is intended to predict the three-dimensional compression response of the cup for an applied displacement of less than and equal to one inch. The scope of the project includes the following:

- A computational model validated with respect to existing compression test data from Dow. To achieve correlation with the test data, the model includes geometric nonlinearity, contact loading, non-uniform wall thickness, circumferential stiffening provided by the ring at the open end, circumferential ribs spaced along the meridional direction, and differing material moduli in the meridional and circumferential directions.
- A parametric study on the effects of wall thickness distribution on the compression response.
- A parametric study on the effects of the ratio of the meridional to circumferential modulus for a range of values that can be realized in the thermoforming manufacturing process.

The constitutive models for the HIPS material are an important part of the analysis effort. Dow has provided some material characterization data, but additional experiments were performed in the Engineering Science and Mechanics Department at Virginia Tech (ESM). These test data are presented in Chapter 2.

1. ABAQUS is a registered trademark of Hibbitt, Karlsson and Sorensen, Inc.

Before developing the finite element model of the actual cup, it is prudent to conduct a series of preliminary finite element analyses of simpler models. Chapter 3 presents the preliminary finite element analyses of structures that have known analytical solutions. Matching a finite element model to a known solution provides confidence in the use of the ABAQUS software.

Chapter 4 contains the development of the ABAQUS model of the cup. This development includes specification of the detailed geometry of the cup, mesh fidelity, contact modeling, element selection, and issues pertinent to use of the ABAQUS software to achieve solutions in reasonable agreement with compression tests conducted at Dow.

Chapter 5 contains the parametric studies on the effects of the meridional thickness distribution, orthotropic material properties, and the circumferential ribs, on the lateral compressive response of the cup. Concluding remarks are given in Chapter 6.

This page is intentionally left blank

CHAPTER 2

Material Characterization and Rim Tests

Results in the form of stress-strain curves from several coupon tests were provided by Dow and are presented in Section 2.1. Additional coupon tests, and bending tests of the ring portion of the rim of the cup, were performed using the facilities in the Department of Engineering Science and Mechanics (ESM) at Virginia Tech and are presented in Sections 2.2 and 2.3, respectively. The modulus of elasticity in circumferential and meridional directions are determined from the coupon tensile tests. Instrumentation to measure Poisson's ratio was not available in these coupon tests, but a typical value for HIPS is in the range of 0.35 to 0.40. Also, no shear test data was available. Rim bending tests are used to assess the finite element modeling of the ring portion at the open end of the cup. Analysis of the rim test is presented in Section 3.5 on page 44.

2.1 Dow Coupon Test Data

Small rectangular pieces, or coupons, were cut from the wall of a cup wall at several locations and subjected to tension in a universal testing machine. These coupons were loaded in either the meridional and circumferential directions, and the measured force-displacement data was reduced to obtain stress-strain curves. The meridional stress-strain data at three meridional locations are plotted in Fig. 2.1, and the circumferential stress-strain data at three circumferential locations are plotted in Fig. 2.2. The stress-strain curves are characteristic of a ductile material with relative large strains after yield.

Unfortunately, the exact locations of the coupons cut from the cup were not available. However, the data in these figures illustrates the range in variability of the material characteristics with location that can be expected from a thermoformed cup.

Spatial variability of the material properties is likely due to the molecular alteration of HIPS while being thermoformed. Molecular changes are expected to occur in polymers while subjected to processes where high temperatures are involved. The fact that HIPS after thermoforming has such an irregular mechanical characteristics complicates analysis.

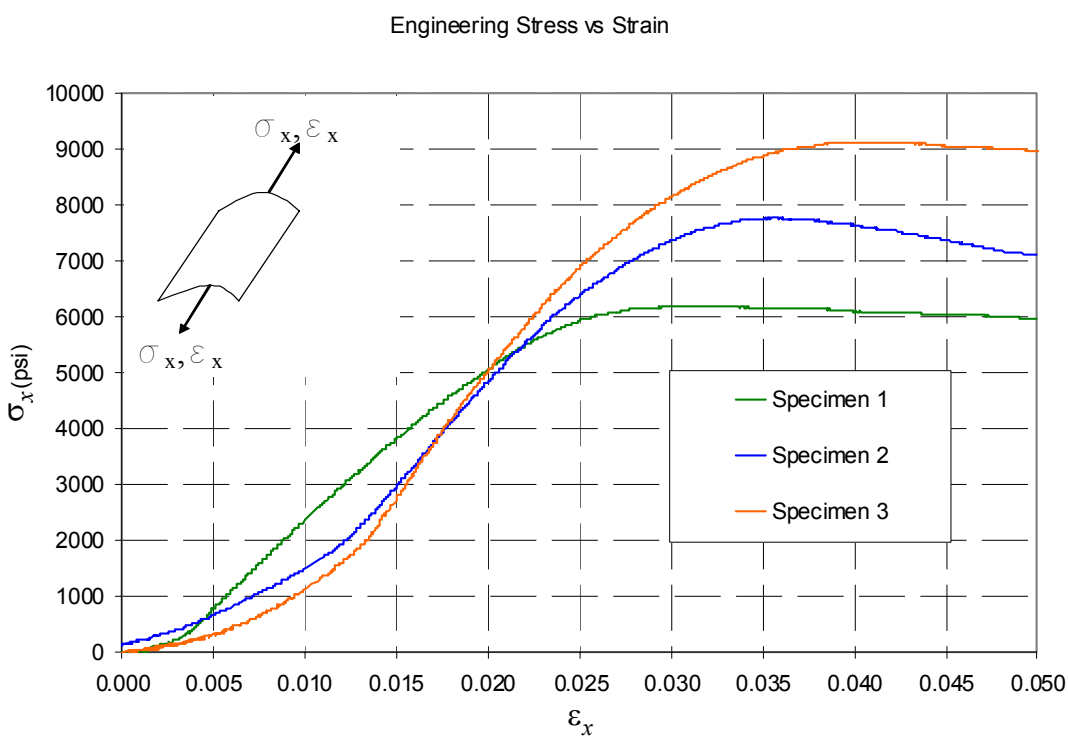

Fig. 2.1 Dow stress-strain curve in meridional direction

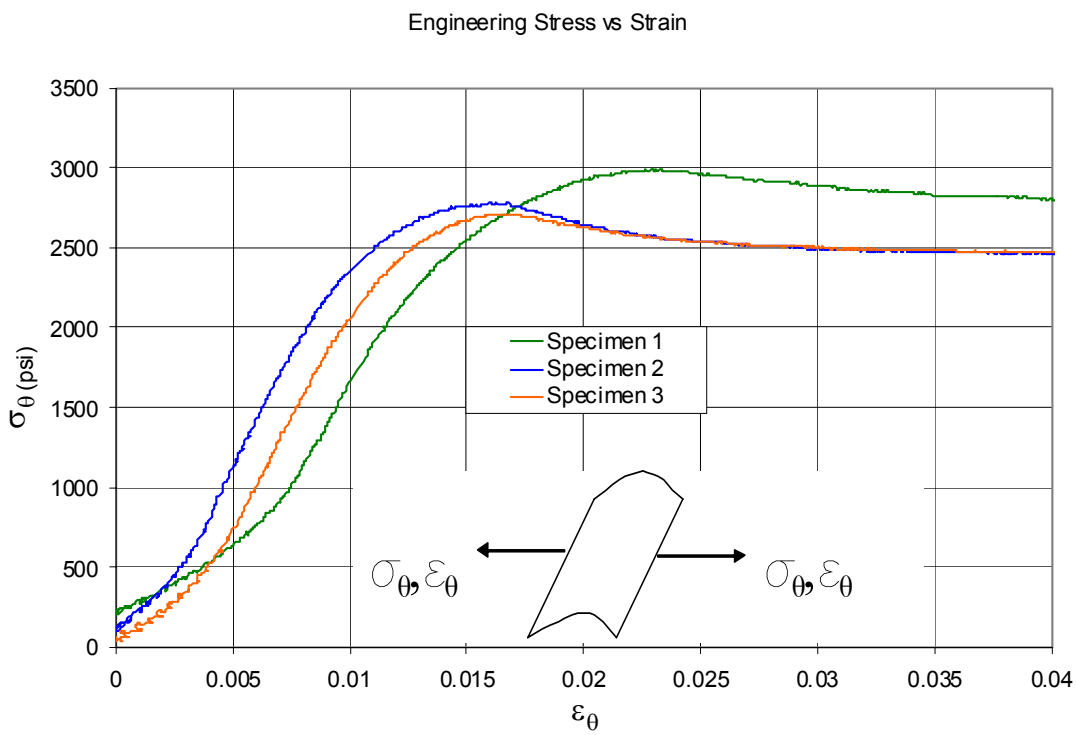

Fig. 2.2 Dow Stress-Strain curve in circumferential direction

2.2 ESM Coupon Tensile Tests

The goal of this portion of the effort was to determine the variation of the tensile stiffness and degree of orthotropy of the cup as a function of position along the meridian. In order to do so, specimens were fabricated by cutting cups in two different directions: along the meridian, and along the circumference.

2.2.1 Sample Preparation

Samples for making circumferential stiffness measurements were removed from two of the cup sections: the large middle section, and the smaller section above that. Within the middle section, samples were removed from the upper portion of that section (designated upper middle circumferential), the center of that section (designated middle circumferential), and the lower portion of that section (designated middle bottom circumferential). Each sample was cut from the cup section using a paper cutter in order to maintain straight sides. Nominal specimen dimensions were 3/8" wide, with a gage length of 4 inches. For the meridional samples, samples having a nominal width of 3/8" were removed from the cup with the use of a paper cutter. All samples were removed from cups marked 211 as part of the labeling. During this process, measurements were made of the thickness of the cup at different positions using micrometers and dial calipers. These results are summarized in Fig. 2.3.

The curves describe the ductility of the material. Polystyrene is a polymer characterized by its flexibility and by relatively high toughness. It is obvious that the results shown on Fig. 2.4 and Fig. 2.5 are not consistent and vary from coupon to coupon cut from the same cup. It is believed that the above results are not consistent due to factors such as temperature, location of strain gages, amount of butadiene added to the plastic, and most likely molecular alteration of HIPS while being thermoformed. Molecular changes are expected to occur in polymers while subjected to processes where high temperatures are involved. The fact that the HIPS has such an irregular mechanical characteristics made the later analysis more complex.

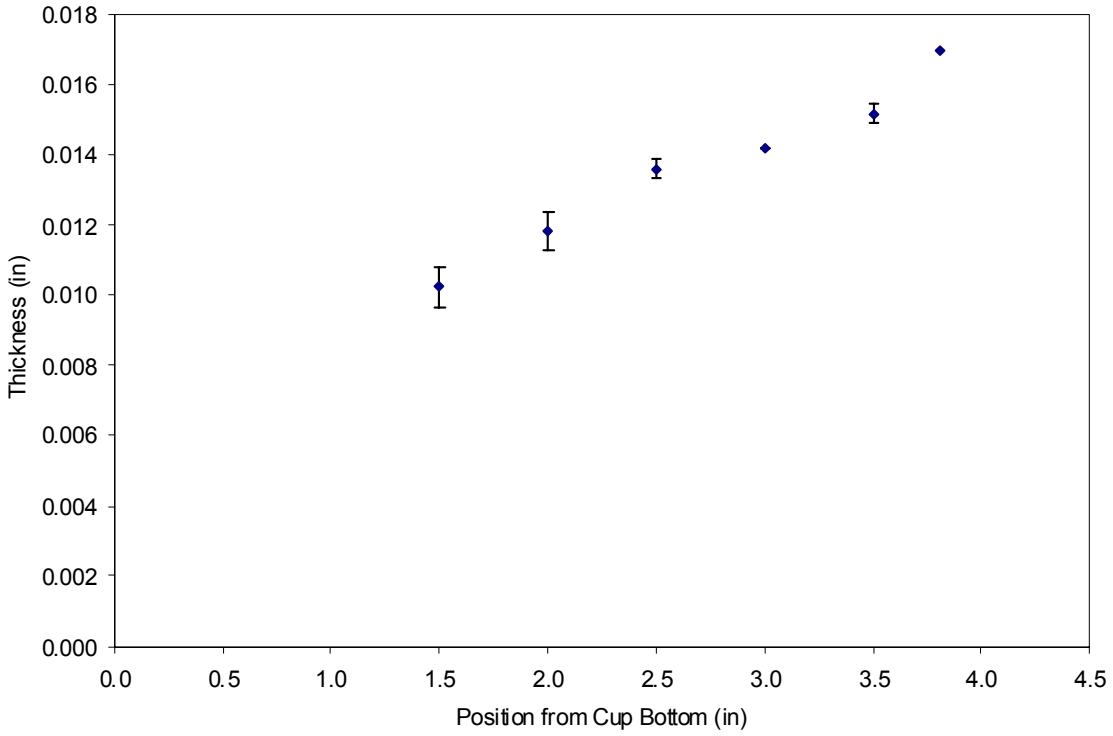

Fig. 2.3 Thickness measurements as a function of position from the cup bottom.

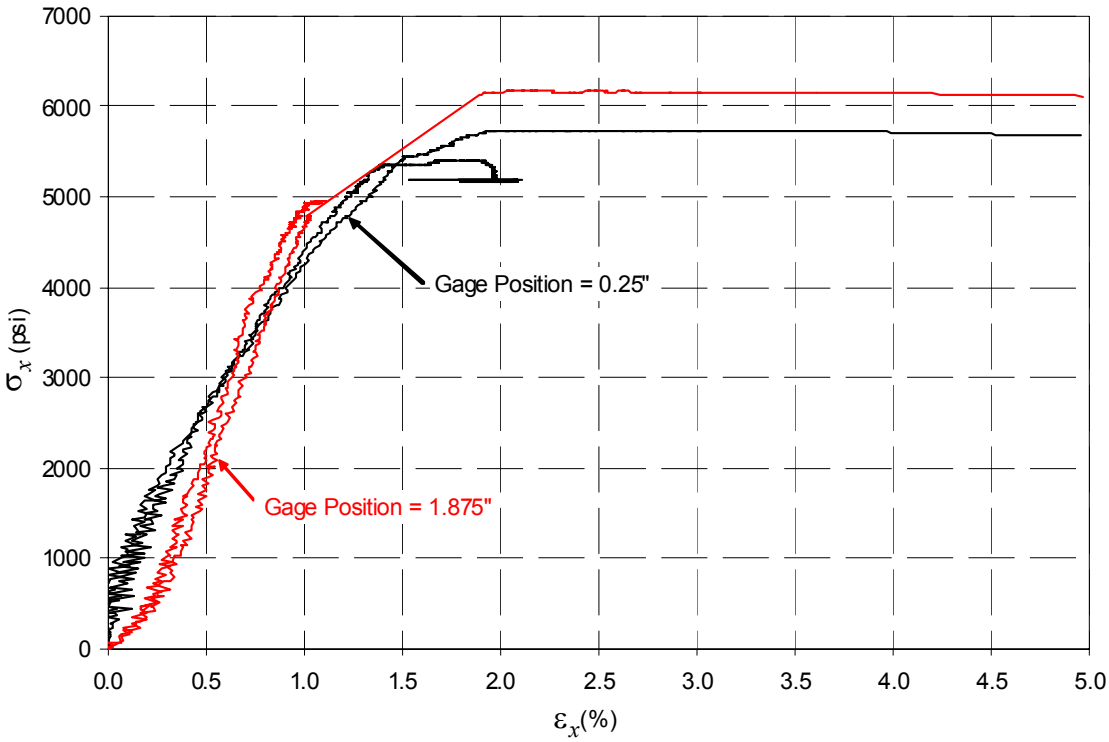

Fig. 2.4 Tensile test results for samples tested in the meridional direction

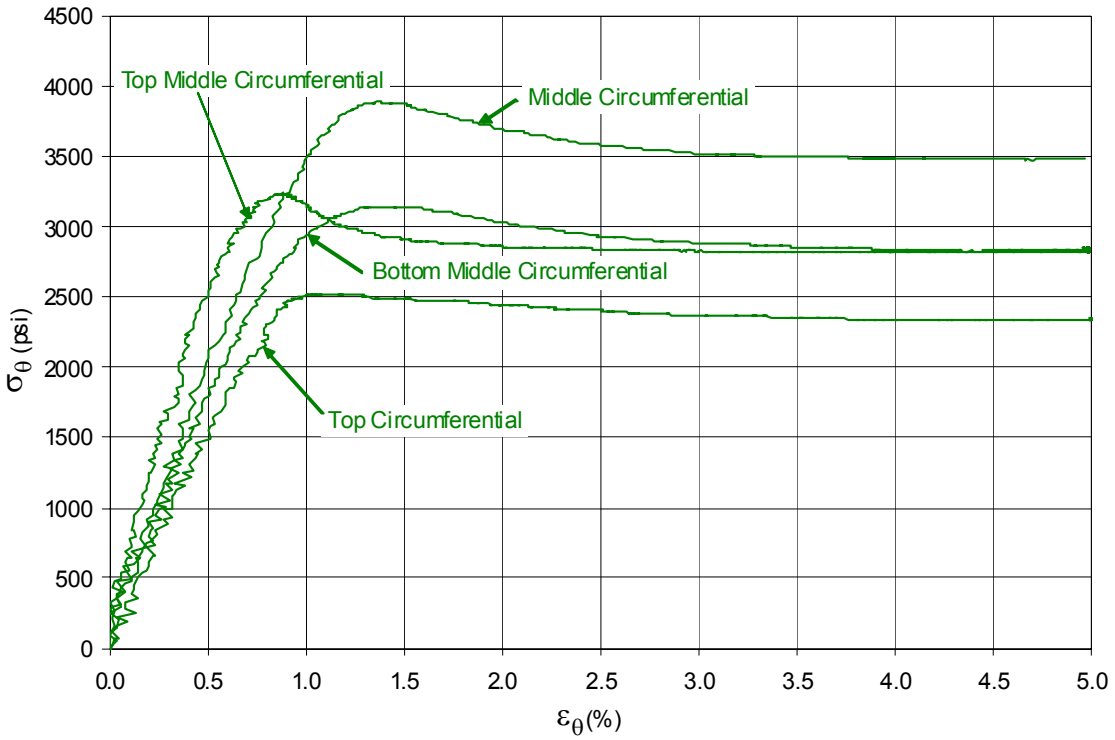

Fig. 2.5 Tensile test results for samples tested in the circumferential direction

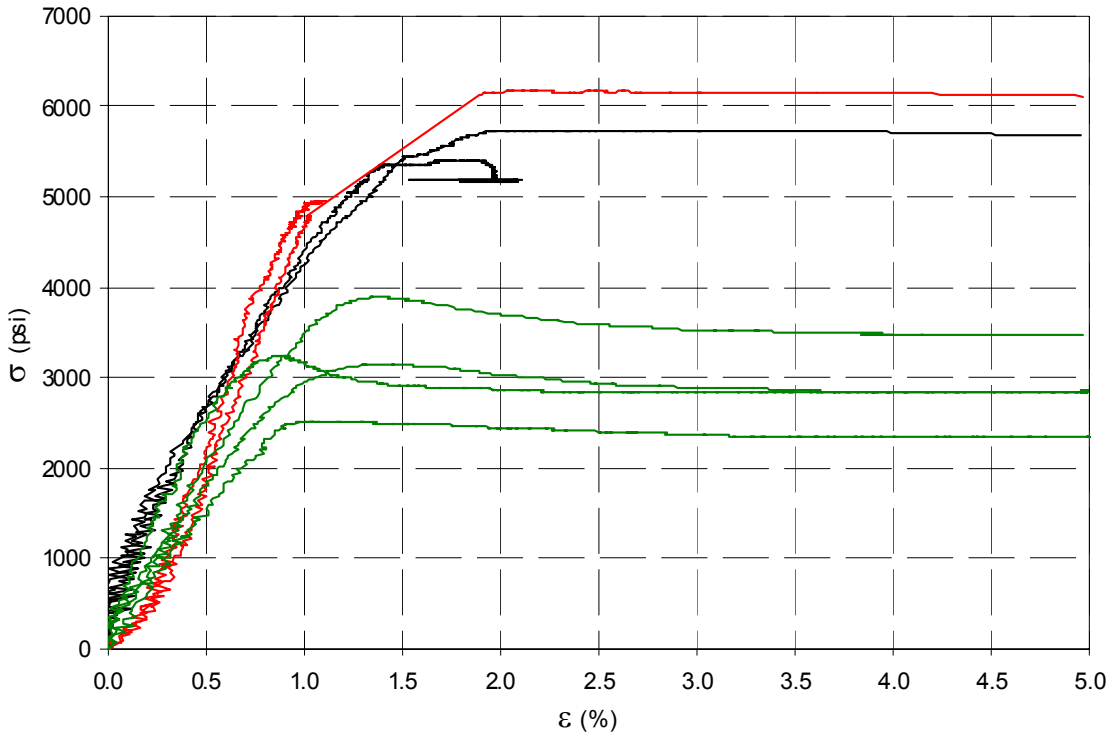

Fig. 2.6 Comparison of tensile test results for meridional and circumferential directions.

2.2.2 Test Techniques

All tensile tests were performed on a screw-driven Instron load frame equipped with pneumatic grips, and operated in displacement control at a displacement rate of 0.2 inches/ minute. Loads were measured using a 1 kN load cell. In order to measure strains, a Fiedler P-50 (class 0.2) laser extensometer was employed. This extensometer is used for non-contact measurement of strain in samples subjected to uniaxial loading conditions. Before starting the experiment, two marks are placed on the sample. The laser extensometer scans the measuring range with a visible laser beam. After automatically determining the reference length at the beginning, the positions of the marks are continuously observed throughout the experiment, enabling the calculation of strain, without relying on the crosshead displacement measurements, which may include substantial deformations in the vicinity of the grip region. Additionally, it facilitated making measurements of strain at two different locations along the meridian of the cup: 0.25" from the bottom and 1.875" from the bottom. The tests were continued until the point at which significant yielding was observed in the samples. During the course of the test, values of the load, crosshead displacement, and strain were recorded by a computer controlled data acquisition system at a rate of one sample per second.

2.2.3 Data Reduction and Results

Subsequent to the tests, the data recorded by the acquisition system was reduced to the form of stress and strain values. In order to determine the stress values, the thickness value at the location of the strain measurement was used to calculate the cross sectional area. Results for tests conducted in the meridional direction are shown in Figure 2.4 . These results suggest that (as expected) there is a difference in mechanical properties as a function of position in the cup due to the fabrication process.

Results for samples cut from the circumferential direction are shown in Figure 2.5 . These results suggest that the circumferential stiffness also varies as a function of position. Additionally, there is no clear progression in behavior as one takes samples from different positions along the meridian. There is a marked distinction in the behavior from that observed

in the samples cut in the direction of the meridian. To highlight such differences, we can compare the results directly, as shown in Figure 2.6 .

2.3 Modulus of Elasticity

After collecting the data from the experiments, we took a closer look at the stress-strain curves provided by DOW and by Dr. Case. We calculated the slope at the linear region of every curve in order to get the modulus of elasticity in the meridional and circumferential directions. After doing so, the average value in each direction for both sets of data was obtained. Table 2.1 lists the average value in each direction for both sets of data.

A valid comparison between the two sets of experiments cannot be made. The experiments performed at the two different locations did not use the same samples nor the same coupons. The cups that were tested came from different manufacturing molds. Furthermore, the coupons that were cut from the cup did not come from the same location along the meridian. However, both experiments are valid and provided important information about the ranges in the modulus of elasticity in the meridional and circumferential directions.

Table 2.1 Average Modulus of Elasticity

Source	Meridional (ksi)	Coefficient of Variation (%)	Circumferential (ksi)	Coefficient of Variation (%)
DOW	351	52.82	287	24.28
ESM	317	10.72	239	12.43

2.4 Rim Bending Tests

In addition to the tensile tests, bending tests were also conducted on the cup rims. In these tests, the upper rim was removed from cups purchased from a local grocery store using a utility knife. In all, fifteen rims were tested (five each from cups marked 211, 212, and 232). These rims were loaded in displacement control at a rate of 0.02 inches/minute using 0.25 in. diameter pins to apply the load on opposite sides of a diameter. During the course of these

tests, the load and corresponding displacement were recorded by a computer controlled data acquisition system at a rate of one sample per second. In addition, for six tests (two samples from each lot), the tests were interrupted to enable measurement of the opposite diameter as well using dial calipers.

2.4.1 Data Reduction and Results

Results from the rim tests were initially reduced to the form of load-displacement plots (load versus change in diameter) as shown in Figure 2.7 . The vertical lines in the load correspond to disturbances due to the measurement of the opposite diameter. These results demonstrate an initial linear response, followed by subsequent nonlinearity.

The results were further examined in the context of the flexural rigidity (*EI*) of rims. For a circular ring with tensile point loads applied to the diameter, the change in the vertical diameter (in the direction of the applied load) is given by $D_V = (0.1488WR^3)/(EI)$ where W is the applied load, R is the radius of the ring, and EI is the flexural rigidity [3]. The change in the horizontal diameter, D_H, is the given by $D_H = (-0.1366WR^3)/(EI)$.

Thus, we see that the expected ratio of the change in the vertical diameter to the change in the horizontal diameter is approximately $D_V/D_H = -1.0893$. We can compare this expected ratio to that measured in the rim tests, as shown in Figure 2.8 . We see that the comparison between the predicted ratio and that measured is very good for diameter changes of less than approximately 0.6 inches. For values greater than that, the measured changes in the horizontal diameter are greater than would be expected.

In addition, we may use the change in vertical diameter equation and the load versus change in vertical diameter information shown in Figure 2.7 to calculate an effective bending stiffness for the rims. Based upon the experimental results for all the rims tests, the value for *EI* is 2.58 ± 0.17 lb in^2 .

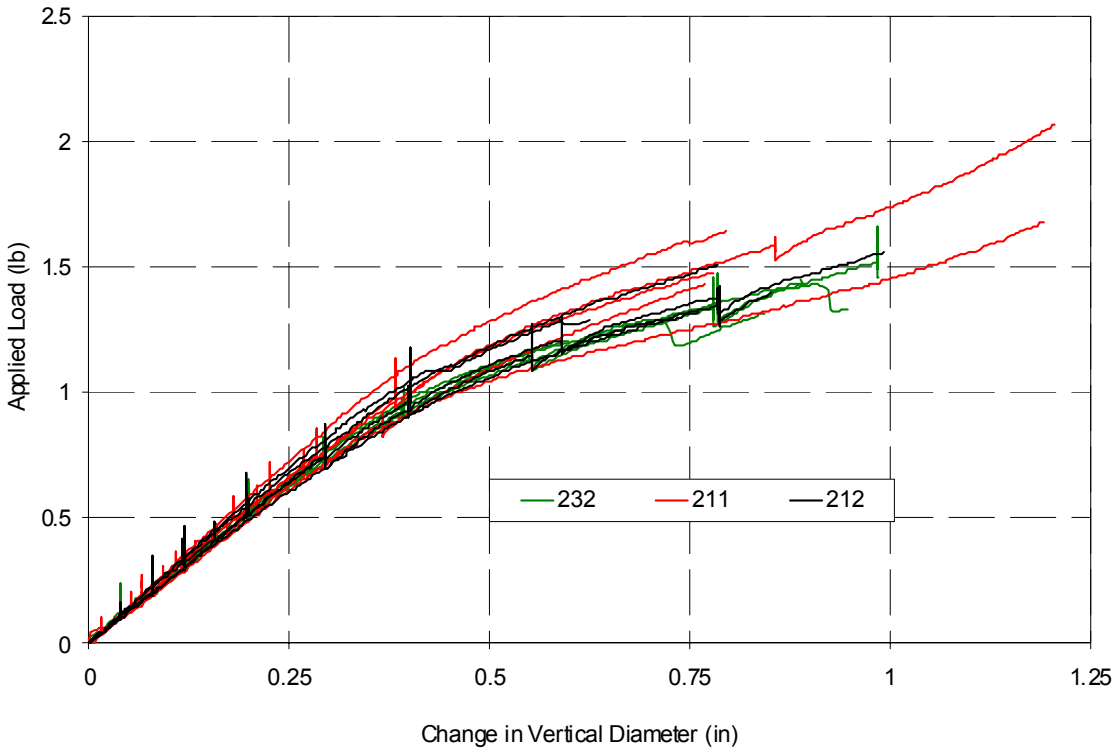

Fig. 2.7 Load-displacement results for rim tests.

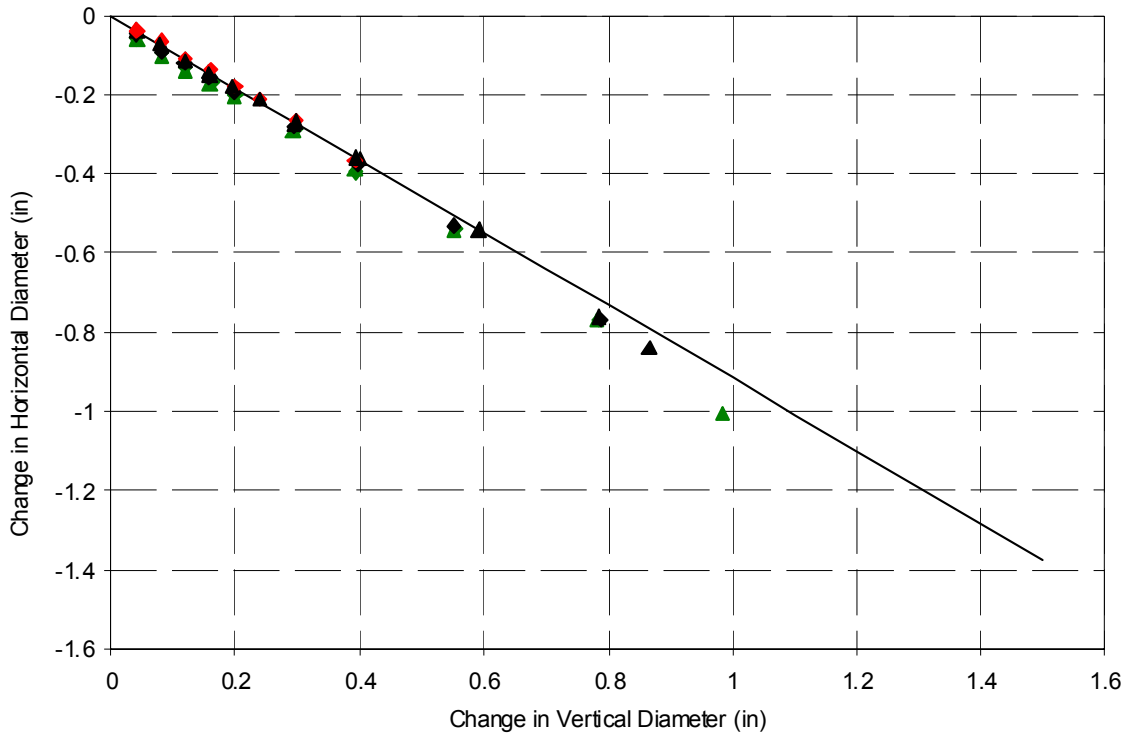

Fig. 2.8 Measured diameter changes for rim tests.

This page is intentionally left blank

CHAPTER 3

Preliminary Finite Element Analyses

Due to the complex geometry of the actual cup, it is prudent to conduct a series of preliminary finite element analyses of simpler models. We start with a beam in Section 3.1, followed by a ring in Section 3.2, and then a truncated conical shell in Section 3.3 and Section 3.4 For each of these structures, an analytical solution is available. Matching a finite element model to a known solution provides confidence in the use of the ABAQUS software. Finally, we present in Section 3.5 the analysis of the ring tests that were discussed in Section 2.4 on page 18.

3.1 The Beam Problem

Consider a simply supported, uniform, linear elastic beam. The length of the beam $L = 0.14$ in., and it has a solid square cross-section with dimensions $t \times t$ with $t = 0.007$ in.. The cross-sectional area $A = t^2$, and the second area moment of the cross section $I = t^4/12$. Take the positive x-axis to the left along neutral axis of the beam with origin at the right end, and take the positive y-axis downward from this origin. The material of the beam has a modulus of elasticity, $E = 344$ ksi. It is analyzed under two circumstances:

- A vertical point force of magnitude F located at one third the total length of the beam as shown in Fig. 3.1.

- A point force of magnitude F at $\theta = 20°$ with respect to the vertical, and located at one third the total length of the beam. as shown in Fig. 3.2.

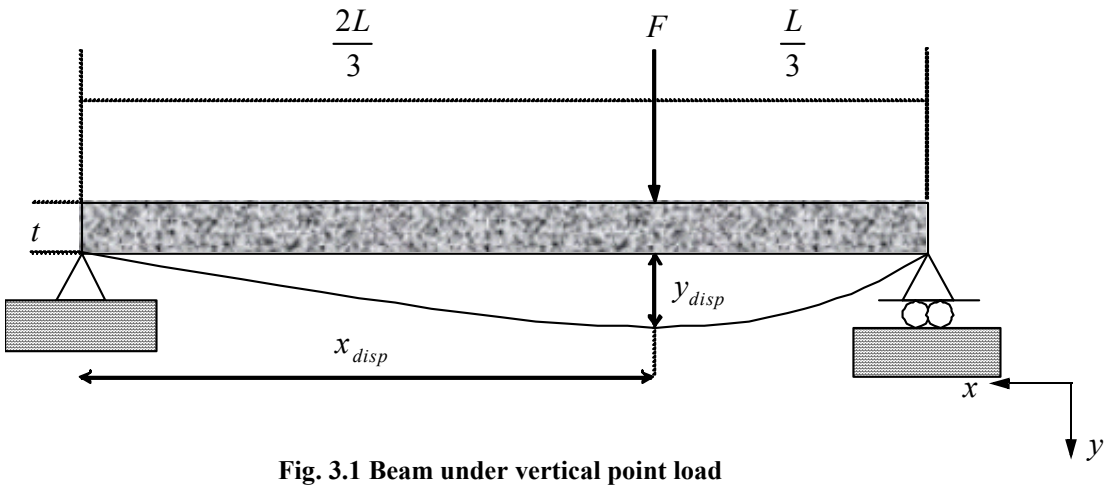

Fig. 3.1 Beam under vertical point load

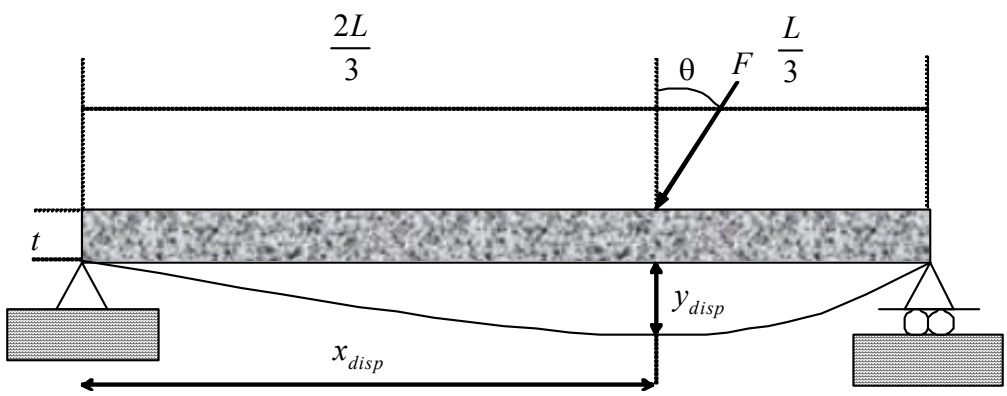

Fig. 3.2 Beam under point load at an angle

3.1.1 Analytical Solution

The applied force will cause deflection in the y direction if the force is vertical ($\theta = 0$), and deflections in both the x and y directions if the force is at an angle with respect to the vertical ($\theta \neq 0$). The displacement components at the point of application of the applied force are

determined from Castigliano's second theorem. The complementary strain energy, U, is given by

$$U = \int_0^L \frac{M^2}{2EI} dx + \int_0^L \frac{N^2}{2AE} dx \tag{1}$$

where M is the bending moment and N is the axial normal force in beam. In the formulas to follow, the distance $b = L/3$. The subscripts H and V in the letter F denote the horizontal and vertical components, respectively, of the applied force. The vertical reaction at the right end supported by a roller is denoted as S_y, and from equilibrium it equals $2F_V/3$. Equilibrium determines the distribution of the bending moment and the axial normal force, so that the complementary strain energy becomes

$$U = \int_0^{L/3} \frac{(S_y x)^2}{2EI} dx + \int_{L/3}^{L} \frac{(F_V(x-b) + S_y x)^2}{2EI} dx + \int_{L/3}^{L} \frac{F_H^2}{2AE} dx \tag{2}$$

Taking partial derivatives of the complementary strain energy with respect to F_V and F_H determines the vertical and horizontal displacements, respectively. For $F = 2$ lb. and $\theta = 20°$, the vertical displacement, y_{disp}, is 1.23 in., and the horizontal displacement, x_{disp}, is -0.00379 in. For $F = 2$ lb. and $\theta = 0$, the vertical displacement is 1.313 in., and the horizontal displacement is zero.

3.1.2 ABAQUS Solution for a Beam Under a Point Load

The ABAQUS model consist of nine beam elements denoted as B23 in the library of elements. The applied force of magnitude of 2 lb. located at $2L/3$ coincides with node 7 in the model. Table 3.1 lists the displacements in the horizontal and vertical directions. If the results for the displacements at node 7 are compared to the theoretical values obtained from the previous section, it can be seen that the displacement x and y are in agreement with the theoretical values for both loading cases.

Table 3.1 Comparison of displacements between analytical and ABAQUS results

Model with force at:	x_{disp} **(in)**	y_{disp} **(in)**
Analytic at 0 degrees	0	-1.3136
ABAQUS at 0 degrees	0	-1.313
Analytic at 20 degrees	-0.00379	-1.23
ABAQUS at 20 degrees	-0.00379	-1.234

3.2 The Ring Problem

One of the most important structural features of the plastic cup is the upper ring, which provides a substantial stiffness to the whole cup. This feature was modeled separately as a thin circular ring with mean radius r, with a solid circular cross-section of radius a, and subjected to equal and opposite tensile forces of magnitude F as shown on Fig. 3.3. The mean radius $r = 1.935\text{in.}$ and the cross sectional radius $a = 0.075\text{in.}$. The material is assumed to be isotropic with a modulus of elasticity $E = 344\text{ ksi}$ and Poisson's ratio $\nu = 0.35$.

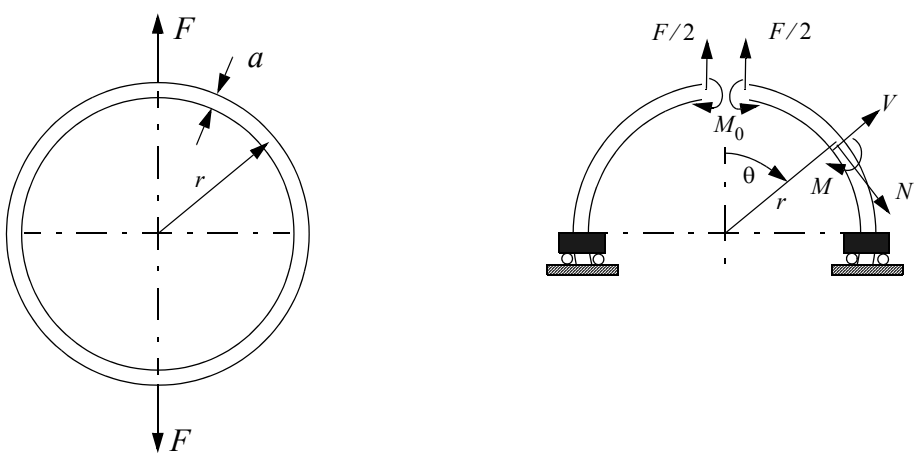

Fig. 3.3 Thin ring subjected to diametrical tension

3.2.1 Analytical Solution

The analytical solution for the displacement of the ring along the line of action of the applied loads is obtained by Castigliano's second theorem. The polar angle θ is measured clockwise from the load axis. Due to symmetry, the hoop force vanishes at the top of the ring where $\theta = 0$, and the only redundant action is the bending moment M_0 at $\theta = 0$. Only the upper half of the ring is modeled as is shown in the right-hand sketch of Fig. 3.3, and clamped roller supports represent symmetry conditions at $\theta = \pm\pi/2$. Using symmetry about the vertical axis of the half model, the total complementary strain energy is

$$U = 2\left\{ \int_0^{\pi/2} [M^2/(2EI) + N^2/(2EA) + V^2/(2GA_s)] r d\theta \right\} \tag{3}$$

where the hoop force is denoted by N, the bending moment by M, the transverse shear force by V, the bending stiffness by EI, the extensional stiffness by EA, and the transverse shear stiffness is denoted by GA_s. The area effective in shear, A_s, is equal to 9/10 of the actual cross-sectional area $A = \pi a^2$ for a solid circular section. The second area moment of the cross section $I = \pi a^4/4$. For $0 < \theta < \pi/2$, equilibrium gives

$$N = (F/2)\sin\theta \qquad V = -(F/2)\cos\theta \qquad M = M_0 - (F/2) r \sin\theta \tag{4}$$

We next substitute the equilibrium results for the bending moment from Eqs (4) into the complementary strain energy of Eq. (3). The redundant is determined by setting the partial derivative of complementary strain energy with respect M_0 to zero, which means that the rotation of the cross section on one side of the imaginary cut at $\theta = 0$ is equal to the rotation of the cross section on the other side of the cut. This leads to the value of the redundant in terms of the applied force; i.e., $M_0 = Fr/\pi$. Knowing the redundant, the bending moment is determined as

$$M = Fr[1/\pi - (\sin\theta)/2] \qquad 0 \le \theta \le \pi/2 \tag{5}$$

The bending moment distribution over one-quarter of the ring is sketched in Fig. 3.4.

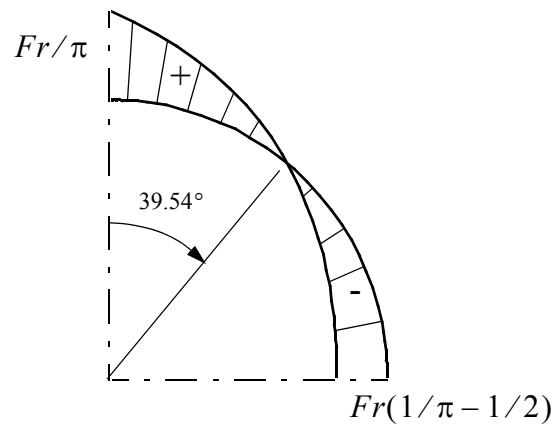

Fig. 3.4 Distribution of the bending moment over one-quarter of the ring

Now, substitute Eq. (5) for the bending moment, the first of Eqs. (4) for the hoop force, and the second of Eqs. (4) for the shear force, into the complementary strain energy given in (3). The partial derivative of this latter result with respect to F is equal to the displacement Δ corresponding to the applied load. The result is

$$\Delta = \underbrace{\pi Fr/(8EA)}_{\text{hoop extension}} + \underbrace{(-8+\pi^2)Fr^3/(8\pi EI)}_{\text{bending}} + \underbrace{\pi Fr/(8GA_s)}_{\text{transverse shear}} \tag{6}$$

For the applied force $F = 2$ lb, Eq. (6) gives $\Delta = 0.12719\text{in.}$. The contribution to the total displacement due to hoop extension is 0.00025 in., due to bending is 0.12619 in., and the contribution due to transverse shear is 0.00075 in.

3.2.2 ABAQUS Solution

Models in ABAQUS were programmed to compare to the theoretical calculations presented in the previous section. The finite element model has the same geometrical characteristics and constraints as those given in the previous section. In order to guarantee the displacement symmetry of the model, a clamped roller support was added to the point where the force was applied (Refer to Fig. 3.3). The clamped roller support restricts horizontal displacement as

well as the in-plane rotation. Different beam elements were used in order to pursue total agreement with the theoretical calculations.

The first ring model was programmed using library element B23, which has two nodes, cubic displacement interpolation, and its formulation is based on the classical Euler-Bernoulli assumption. Element B23 is limited to planar response in, say, the *x*-*y* plane, and connects the end nodes by a straight line. A total of forty elements were used. To approximate the circular geometry with straight line elements it is necessary to have as many elements as possible. Although forty straight line segments may be a good approximation to a circle, ABAQUS has library beam elements to model curvature. A second model was made of B22 elements that have three nodes and quadratic interpolation. Element B22 can model curvature and allows for transverse shear strain. This second ring model has twelve B22 elements and thirteen nodes, six of which are internal.

Table 3.2 lists the results from the analytical and ABAQUS solution results for displacement a the point of application and in the direction of the applied force. Fig. 3.5, Fig. 3.6, and Fig. 3.7 show the graphical comparison between the analytical solution and the ABAQUS solution for distributions of the hoop force, transverse shear force, and the bending moment, respectively. Since the ring is a curved beam, the three-node quadratic beam element B22 provide a better solution than the straight-line element B23. These figures also show that the FEA model using element B22 gives essentially the same results as the analytical solution

.

Table 3.2 Comparison of displacements between analytical and ABAQUS results

Model	Displacement (in)
Analytic	0.1271
B23	0.1255
B22	0.1259

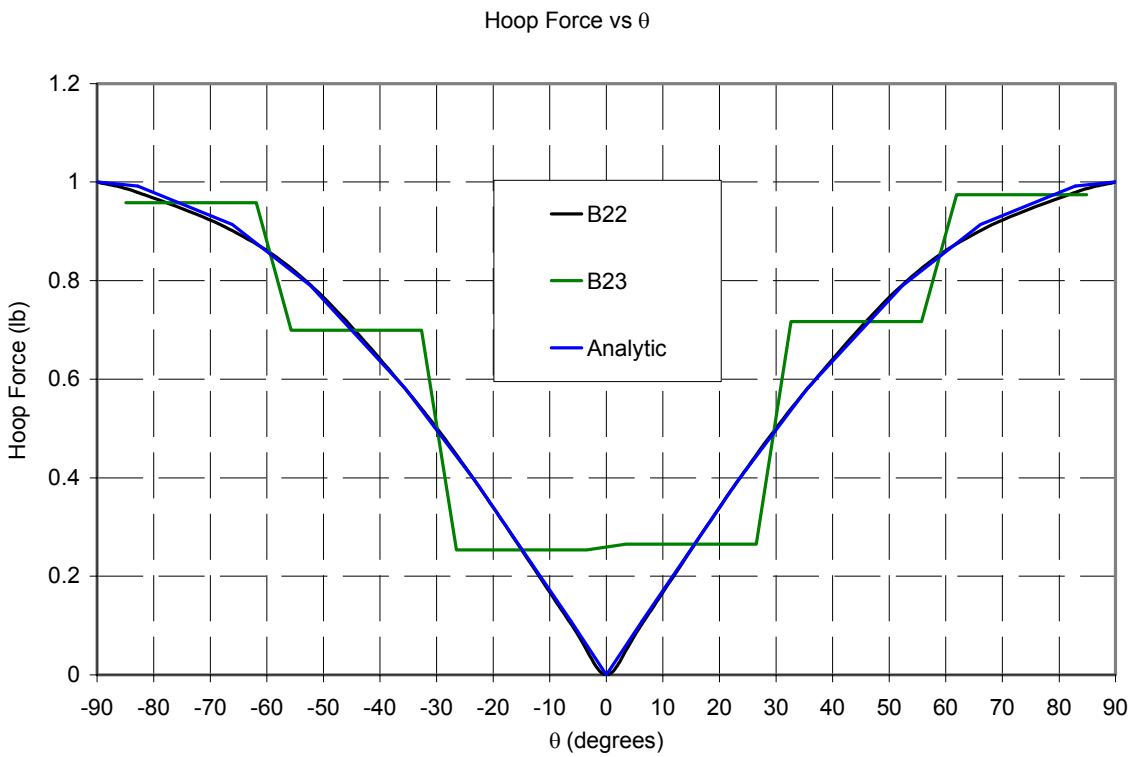

Fig. 3.5 Hoop Force distribution in the ring

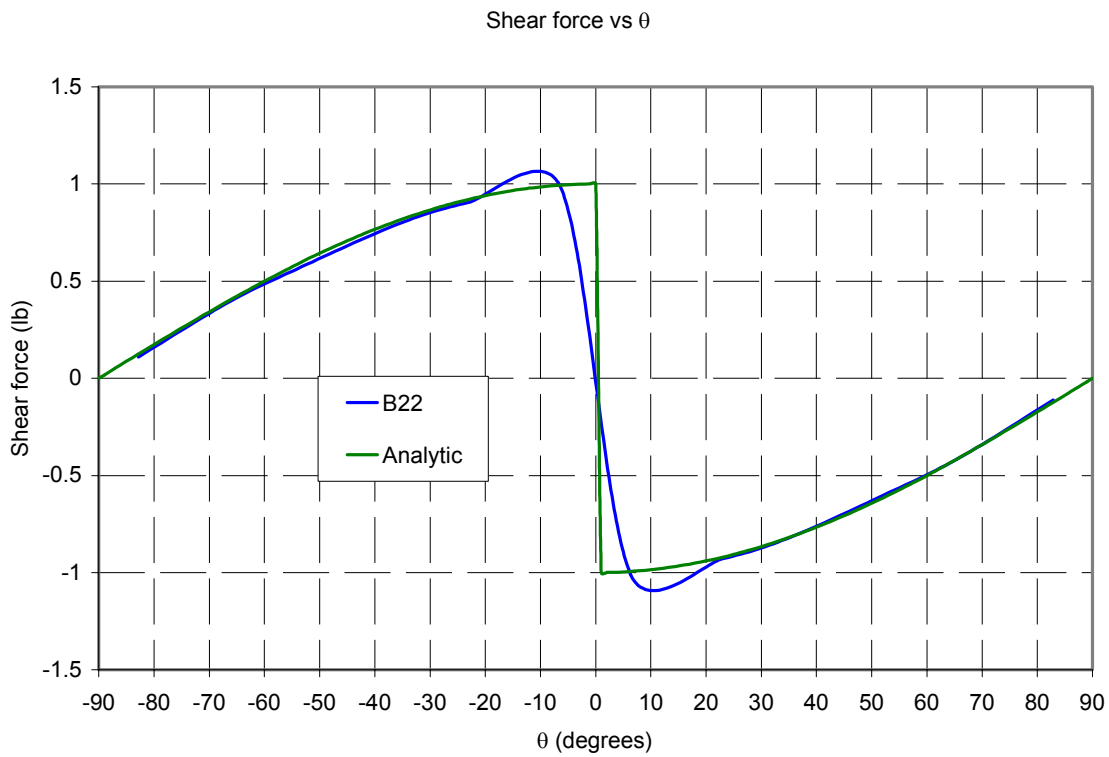

Fig. 3.6 Shear force distribution in the ring

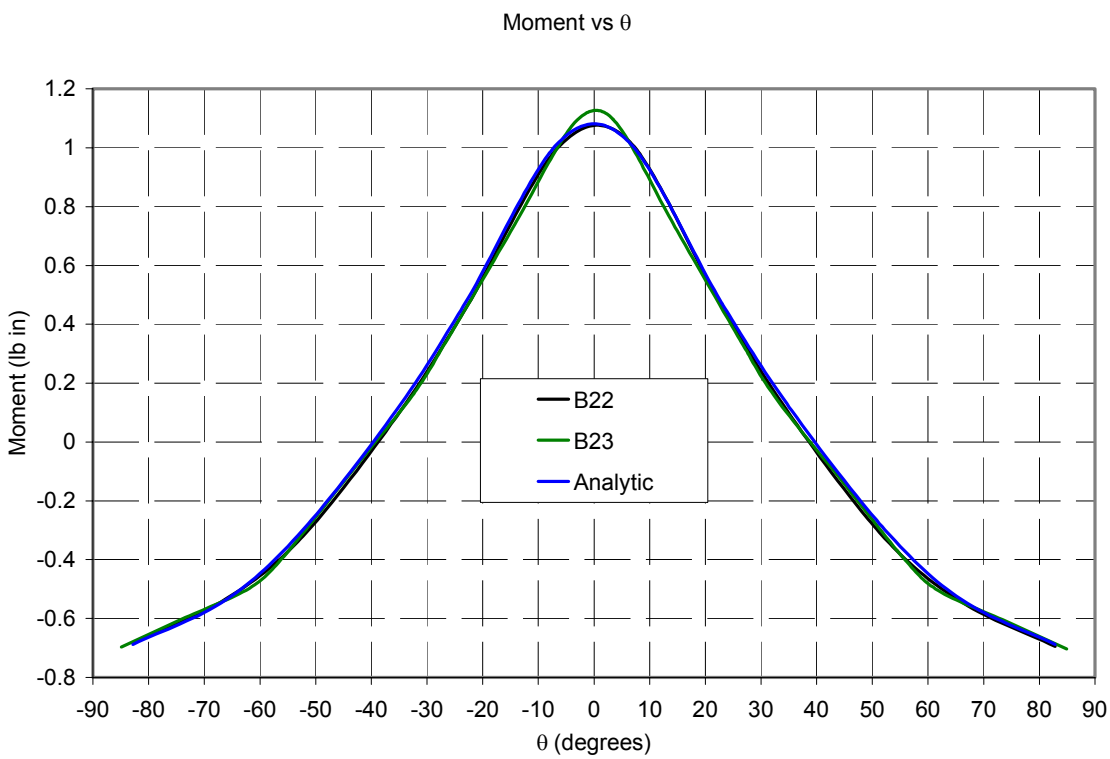

Fig. 3.7 Moment distribution in the ring

Notice that the results shown on Fig. 3.7 are consistent with the theoretical analysis of the bending moment distribution. The three curves have a bending moment of zero at about $40°$. Fig. 3.4 shows that the moment becomes zero at $39.54°$. This correlation proves the effectiveness of the ABAQUS models.

3.3 Analytical Solution for the Truncated Conical Shell

The configuration is a thin-walled, truncated conical shell with open ends as is depicted in Fig. 3.8. The reference surface of the thin shell is a taken to be its middle surface, and the middle surface is generated by revolving a straight line meridian about the axis of revolution. The cone angle between the axis of revolution and a meridian is $\pi/2 - \alpha$. Let (x, θ) denote coordinates in the middle surface, where x is the location along a meridian and polar angle θ is the location along a circle of latitude. The origin of x is at the vertex, $x = x_1$ at the open

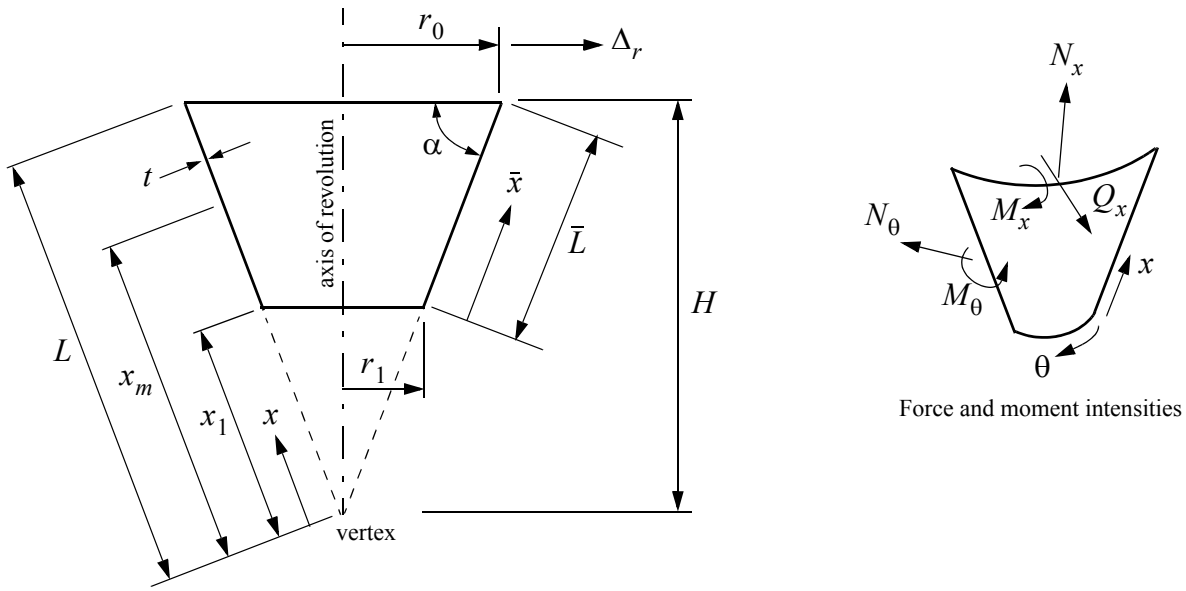

Fig. 3.8 Geometric parameters, and force and moment intensities of a conical shell

end with the smaller radius r_1, $x = L$ at the open end with the larger radius r_0, and $0 < x_1 < L$. Let $\bar{x}$ denote the meridional coordinate defined by $\bar{x} = x - x_1$, where $0 \le \bar{x} \le \bar{L}$ and $\bar{L} = L - x_1$. The shell is subjected to a prescribed radial displacement Δ_r at the end $\bar{x} = \bar{L}$ and the end $\bar{x} = 0$ is free. The prescribed radial displacement is uniform around the circumference, and there are no other loads acting on the shell. It is assumed the shell wall has uniform thickness t, and that the material of the wall is linear elastic and isotropic having a modulus of elasticity denoted by E and Poisson's ratio denoted by ν. Hence, the response of the shell is axisymmetric, or independent of θ, and torsionless. Since the reaction loads associated with the prescribed radial displacement are self-equilibrated, the response is confined to a small region of the shell wall in the vicinity of $\bar{x} = \bar{L}$. The opposite end at $\bar{x} = 0$ is not disturbed by the loading, because it is assumed that the meridional length $\bar{L}$ is much greater than the wall thickness t. The meridional length of the disturbed region is approximately $\sqrt{R_0 t}$, where R_0 denotes the radius of curvature of the circle of latitude in the

middle surface at $\bar{x} = \bar{L}$, which is given by $R_0 \sin\alpha = r_0$. This linear elastic solution presented below was taken from the book by Baker, et al. [4], and the original work cited in [4] was done by E. Hampe (1964).

Define a dimensionless meridional coordinate $\xi = \bar{x}/\bar{L}$, $0 \le \xi \le 1$. The quantities of interest are the distributions of the meridional force intensity $N_x(\xi)$, circumferential force intensity $N_\theta(\xi)$, meridional transverse shear force intensity $Q_x(\xi)$, the meridional bending moment intensity $M_x(\xi)$, and the radial displacement $\Delta(\xi)$. Refer to the force and moment intensities shown in Fig. 3.8. These quantities are given by

$$N_x(\xi) = \{4Dk^3 \cot\alpha \Delta_r [F_{10}F_7(\xi) + F_8F_9(\xi)]\}/(F_1 \sin\alpha) \tag{7}$$

$$N_\theta(\xi) = \{Et\Delta_r[-F_{10}F_9(\xi) + 2F_8F_8(\xi)]\}/(F_1 x_m \cos\alpha) \tag{8}$$

$$Q_x(\xi) = \{4Dk^3\Delta_r[F_{10}F_7(\xi) + F_8F_9(\xi)]\}/(F_1 \sin\alpha) \tag{9}$$

$$M_x(\xi) = \{2Dk^2\Delta_r[-F_{10}F_{10}(\xi) + 2F_8F_7(\xi)]\}/(F_1 \sin\alpha) \tag{10}$$

$$\Delta = \{\Delta_r[-F_{10}F_9(\xi) + 2F_8F_8(\xi)]\}/F_1 \tag{11}$$

$$\beta = \{2k\Delta_r[F_{10}F_8(\xi) - F_8F_{16}(\xi) - F_8F_{15}(\xi)]\}/(F_1 \sin\alpha) \tag{12}$$

where

$$k = \sqrt[4]{3(1-\nu^2)}/\sqrt{tx_m \cot\alpha} \tag{13}$$

$$D = Et^3/[12(1-\nu^2)] \tag{14}$$

The functions $F_i(\xi)$, $i = 1, 7, 8, 9, 10, 15, 16$ are listed in Table 3.3. Note that $F_i(1) \equiv F_i$.

The geometric and material parameters, and the specified displacement for the example are listed in Table 3.4. This analytic solution is plotted with the finite element solution in the next section.

Table 3.3 Distribution functions for the truncated conical shell

$F_1(\xi)$	$\sinh^2(kL\xi) - \sin^2(kL\xi)$
$F_7(\xi)$	$\cosh(kL\xi)\cos(kL\xi)$
$F_8(\xi)$	$\sinh(kL\xi)\sin(kL\xi)$
$F_9(\xi)$	$\cosh(kL\xi)\sin(kL\xi) - \sinh(kL\xi)\cos(kL\xi)$
$F_{10}(\xi)$	$\cosh(kL\xi)\sin(kL\xi) + \sinh(kL\xi)\cos(kL\xi)$
$F_{15}(\xi)$	$\cosh(kL)\sin(kL)$
$F_{16}(\xi)$	$\sinh(kL)\cos(kL)$

Table 3.4 Parameters for the truncated conical shell

Parameter (refer to Fig. 3.8)	Value
Δ_r	0.020 in.
α	69°
L	5.36 in.
$\bar{L}$	2.57 in.
x_m	4.075 in.
t	0.020 in.
H	5.0 in.
E	295,000 psi
ν	0.35

3.4 ABAQUS Model of the Truncated Conical Shell

The shell described in the last section was modeled with the axisymmetric shell element denoted as SAX1 in the ABAQUS library of elements. The SAX1 element has two nodes, and uses linear interpolation functions and one-point Gauss integration. It can be used for a thin or thick walled shell. The geometry and material properties for the model are listed in Table 3.4. Equal and oppositely directed outward radial displacements were specified at two

symmetrically opposite nodes at the top of the shell. To determine how sensitive the solution was to the number of elements, two models with different mesh refinement were programmed using axisymmetric shell elements SAX1. The SAX1 element is a two-node linear axisymmetric thin or thick shell. The first model consisted of 100 SAX1 elements while the second one was composed of 200 SAX 1 elements. The difference between the results given by the refined and coarse models was not significant. However, for accuracy purposes the model containing 200 elements was the best. Figure 3.10 on page 38 also shows a cone model using S4R elements. The S4R element eventually became the element of choice. This four-node stress/displacement shell with reduced integration accounts for finite membrane strains and allows change of thickness. It is of great importance to remember that the ultimate finite element model must have the capability of variable thickness.

A circular cylinder with the same parameters shown on Table 3.4 was modeled as well. This was done due to the fact that the cylinder has an angle $\alpha = 90°$. It can be seen from Fig. 3.10 to Fig. 3.12 that the solutions for the cylinder have very small discrepancies with respect to the solutions for the conical axisymmetric shell. The results from the two truncated cone models, the cylinder (whenever applicable) and theoretical calculations are compared in Figure 3.9-Figure 3.13.

The comparison between the analytic results to the theoretical results, proved to be a very important step in the completion of this project. The complete agreement between analytic and theoretical results gave us the needed confidence on the model to start modeling the actual cup. The results shown on this section are of great importance due to the fact that they constitute the basis for the development of a more complex model which will be discussed in the next section.

This chapter explained and introduced the reader to the procedure followed to gain confidence while developing and using a finite element code. From simple beam analysis to truncated cone theory and ring analysis, this chapter showed the early evolutionary steps of the model development. In the next chapter, the reader will be introduced to the actual model of the plastic cup with all its geometrical characteristics and material complexities.

Figure 3.15 on page 43 summarizes the steps taken to reach the goal of having a working finite element model of the cup.

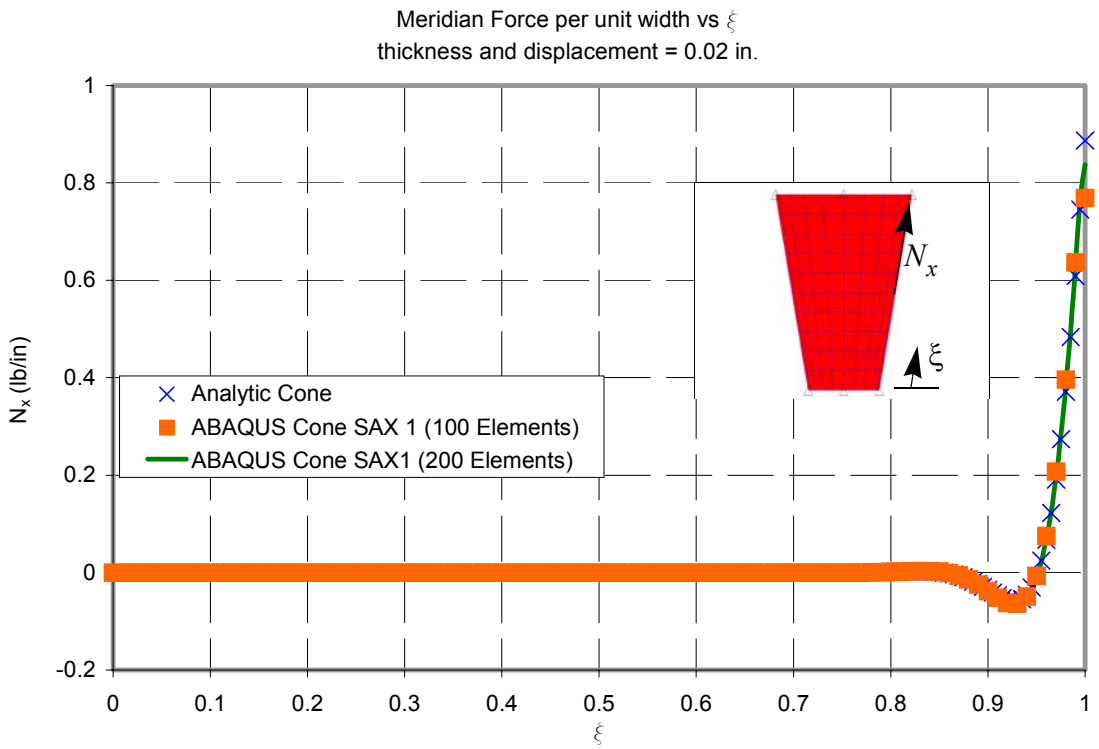

Fig. 3.9 Distribution of the meridional force intensity in the conical shell

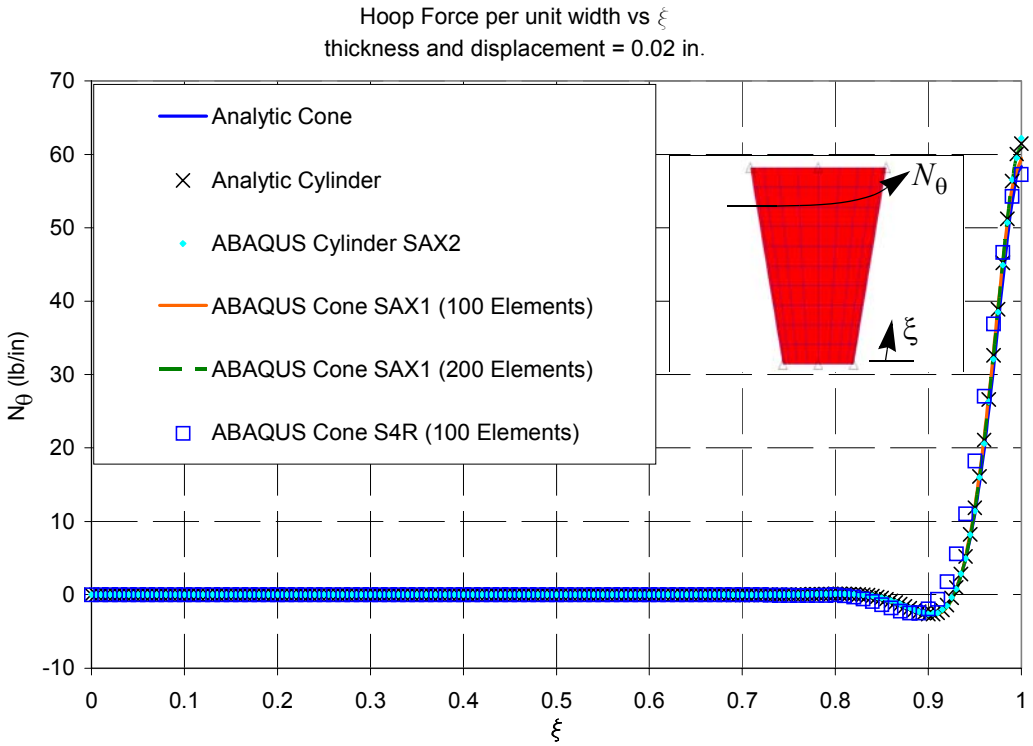

Fig. 3.10 Distribution of the circumferential force intensity in the conical shell

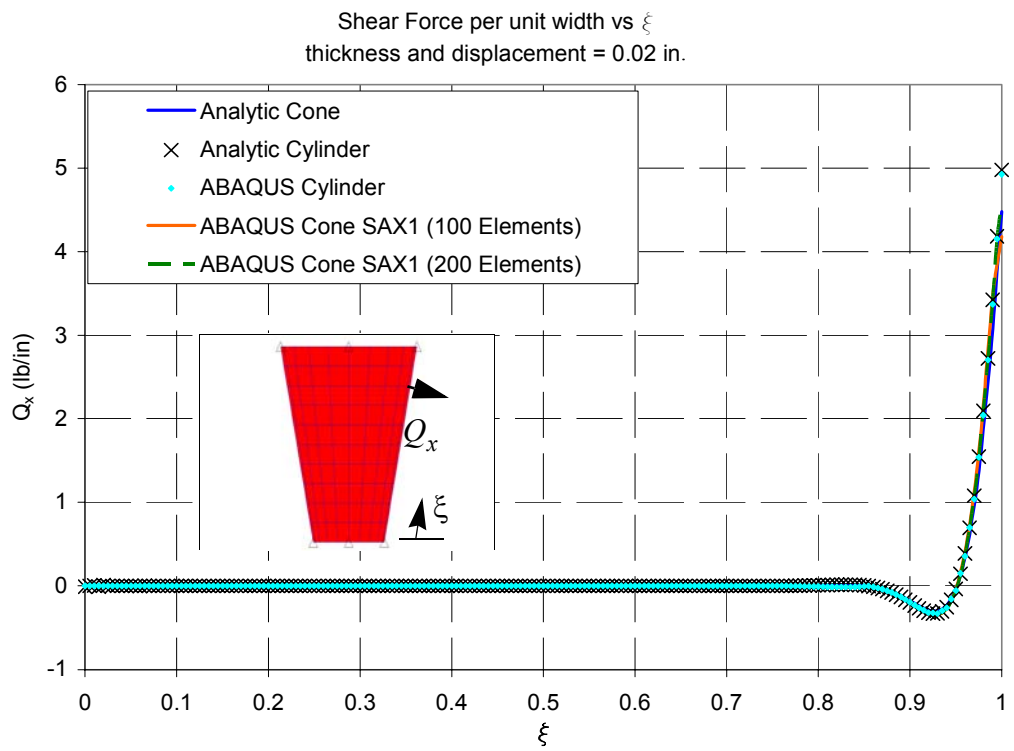

Fig. 3.11 Distribution of the meridional transverse shear force intensity in the conical shell

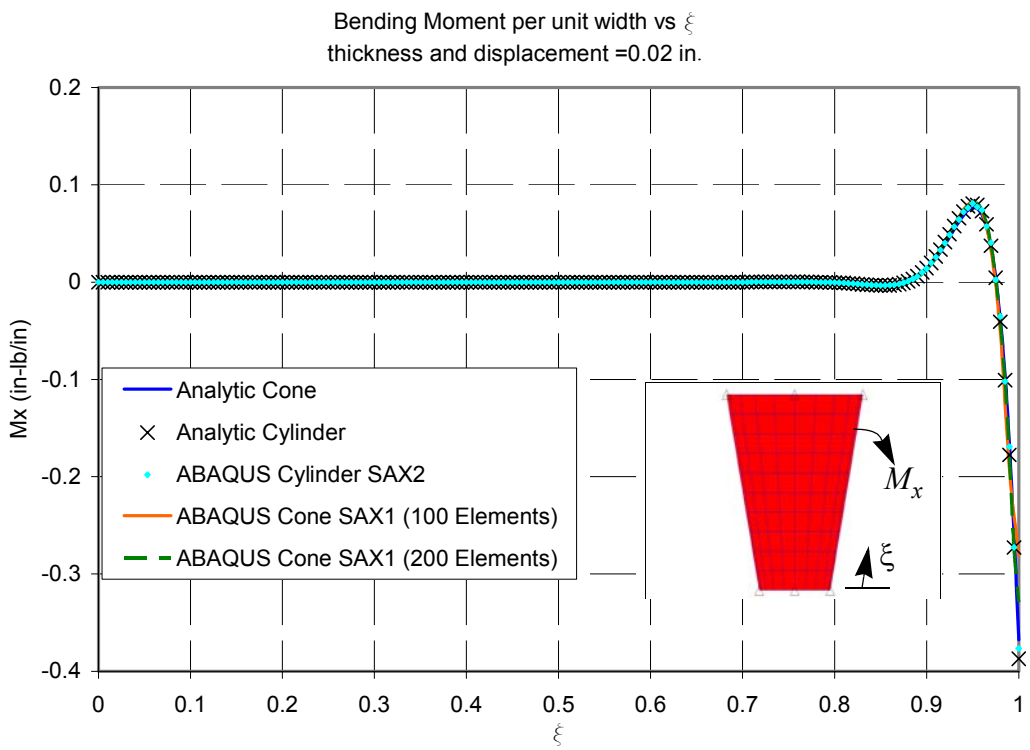

Fig. 3.12 Distribution of the meridional bending moment intensity in the conical shell

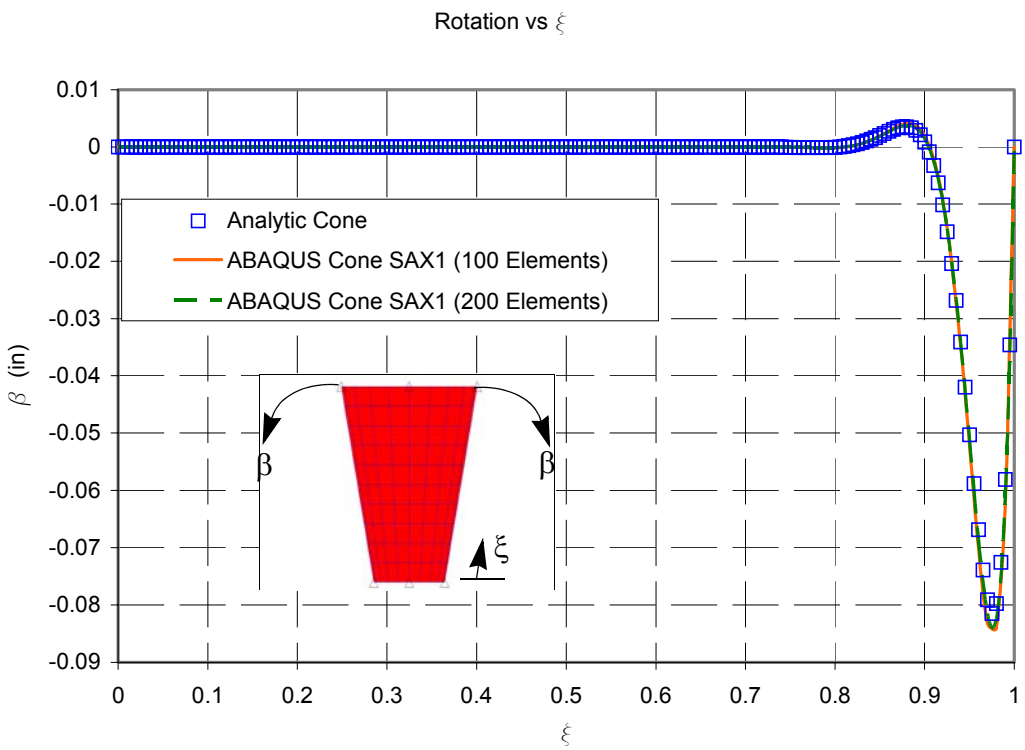

Fig. 3.13 Distribution of the rotation in the conical shell

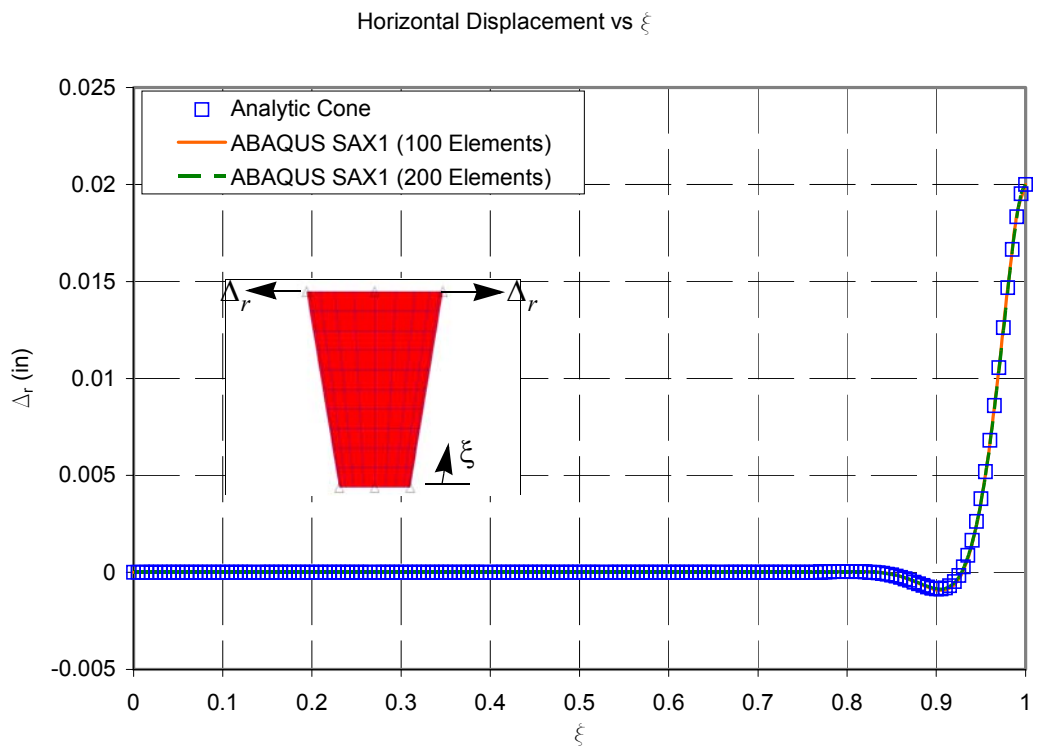

Fig. 3.14 Distribution of the radial displacement in the conical shell

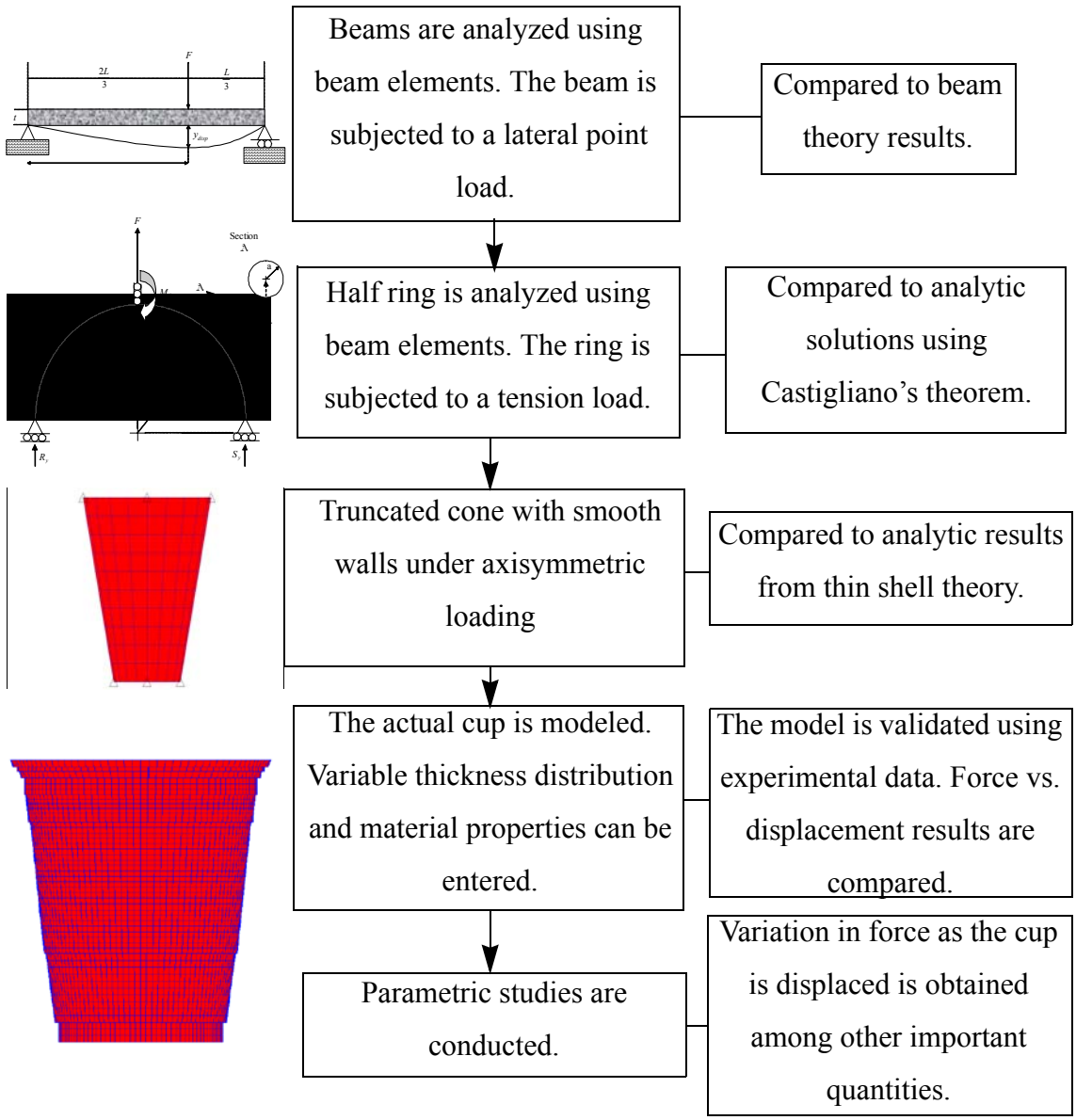

Fig. 3.15 Finite element modeling procedure

3.5 Finite Element Model of the Ring Test

As described in Section 2.4 on page 18, several ring, or rim, specimens of the cup were tested under tensile load. Having these data available permitted a validation of finite element model of the ring portion of the cup. A schematic of the ring and its dimensions is shown in Figure 3.16. The ring model consists of fifty S4R5 shell elements in the circumferential direction and three elements in the meridional direction. For simplicity purposes and due to symmetry, only one half of the ring was modeled. The ends of the ring model have x-symmetric boundary conditions $U1 = UR2 = UR3 = 0$ prescribed at $x = 0$, and a point tensile load of magnitude 1.6 lb. is imposed at $x = 1.84$ in.. The material is isotropic with a modulus of elasticity of 295 ksi and a Poisson's ratio of 0.35. The wall has a uniform thickness of 0.02 in.

The linear elastic analysis from the ABAQUS [5] model is compared to the test results in Fig. 3.17. The slope of the load-displacement response from the analysis is in very good agreement with the test data in the linear portion of that data. This agreement provided confidence to the proceed to the full cup model discussed in the next chapter.

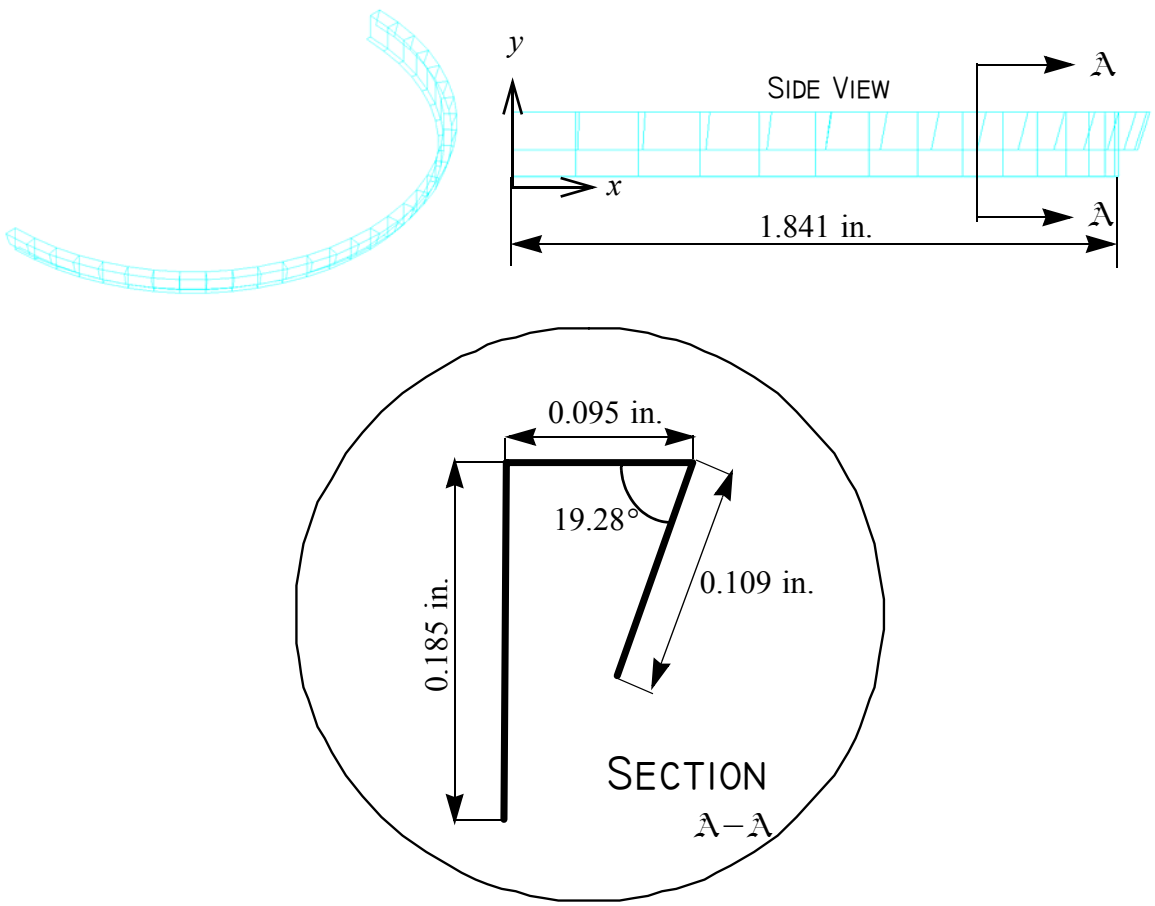

Fig. 3.16 Ring schematic and dimensions

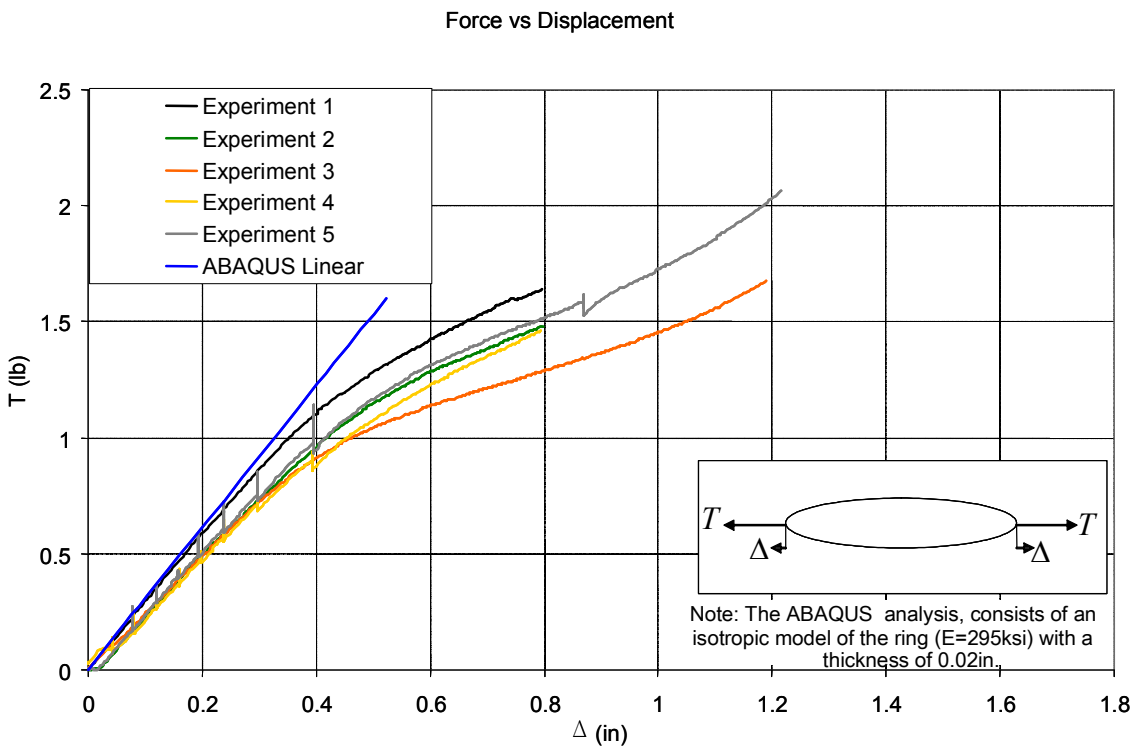

Fig. 3.17 Ring tensile force distribution as a function of displacement

CHAPTER 4

The Cup Finite Element Model

The finite element model of the cup developed in this chapter includes a contact algorithm to simulate the lateral compression test apparatus used by Dow. Model creation is done using the software packages MSC.Patran[1] and ABAQUS/CAE. The analysis solver is the ABAQUS/Standard software package. The graphical user interface in Patran is a forms-based, mouse-driven menu system for the operation of all tasks associated with a finite element model, such as geometry creation and editing, automatic meshing, application of loads and boundary conditions, element selection, and assignment of material properties. Patran creates the ABAQUS/Standard input file. Likewise, ABAQUS/CAE is a forms-based, mouse-driven menu system for interactive modeling and visualization, which is used to conveniently change the ABAQUS input file for the various parametric studies. In Section 4.1 through Section 4.6 of this chapter, the use of the Patran finite element modeler is described with respect to the development of the cup model. Important options present in the ABAQUS/Standard input file are discussed in Section 4.7, and the use of ABAQUS/CAE for the parametric studies is discussed in Section 4.8 to Section 4.10.

1. MSC. Patran is a product of MSC.Corporation, 2 MacArthur Place, Santa Ana, CA 92707.

4.1 Geometry of the Cup Model

In order to create the finite element model of the cup, various stages had to be completed. The first stage was the creation of the three-dimensional geometry of the cup in Patran [6]. To create the ABAQUS input file, the ABAQUS option should be selected in the *Analysis Code* option of Patran. The strategy here was to sketch line segments. To do so, it is necessary to go to the *Geometry* menu, select *Action: Create, Object: Curve, Method: Point*. The *x-y* coordinates shown in Table 4.1 have to be input as connected points in the corresponding boxes shown in the menu screen. These coordinates have to be put into square brackets with a zero value for the *z*-coordinate. Following the input of these coordinates, the screen in Patran displays the profile like the one shown on Fig. 4.1.a. The final step to complete the geometry of the model is to revolve the profile from the *Geometry* menu. In the *Geometry* menu, select *Action: Create, Object: Surface, Method: Revolve*. The Revolve option will open a set of options on the screen. Click on the *Surface Id List* option and select all the line segments for the profile of the cup that will be contained in a region. Line segments assigned to regions facilitate specification of variable thickness modeling. Then click on the *Axis* box and type **Coord 0.2** to revolve the profile about the *y*-axis. Finally, select the *Total Angle* box under *Sweep Parameters* and type **180** to revolve the profile 180 degrees to model one-half of the cup. To effectively visualize the cup in the *x-y* plane, type **-90** in the *Offset Angle* box. Repeat the revolve procedure for every set of segments contained in a region. After this is completed, the Patran screen should be displaying the sketch shown on Fig. 4.1.b

Table 4.1 Coordinates of the cup profile

Point Number	x-coordinate	y-coordinate
1	0	0.204
2	0.972	0.204
3	1.029	0
4	1.221	0
5	1.221	0.308
6	1.276	0.308
7	1.409	1.414
8	1.4365	1.414
9	1.6405	3.493
10	1.6685	3.493
11	1.7085	3.931
12	1.734	3.931
13	1.734	4.196
14	1.7815	4.196
15	1.8005	4.3
16	1.841	4.3
17	1.841	4.485
18	1.9365	4.485
19	1.9	4.3756

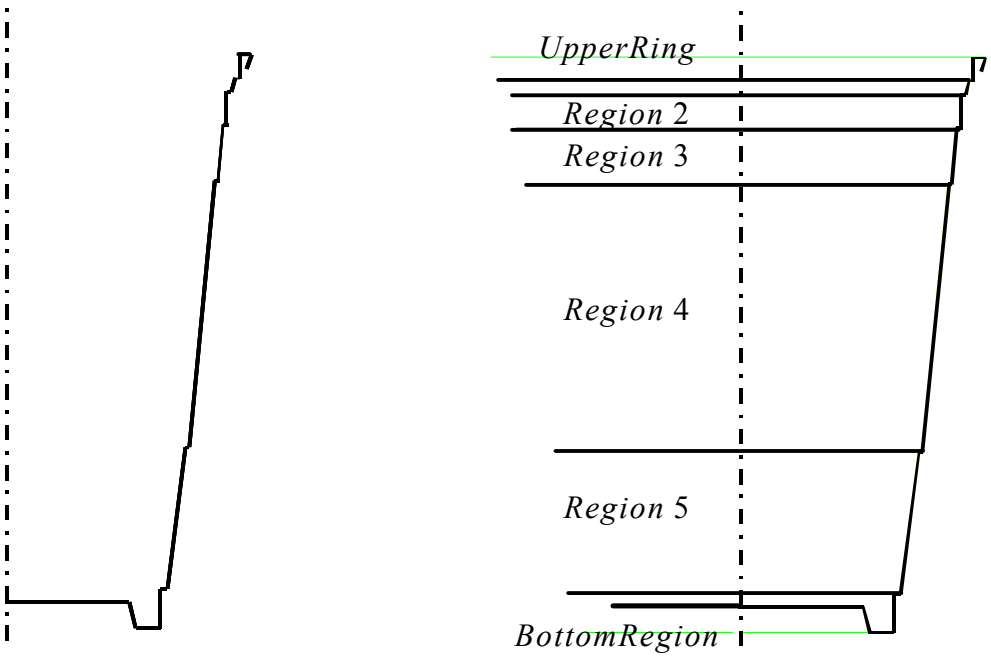

a) Profile of the cup using line segments

b) Revolved profile

Fig. 4.1 Geometry of the cup

4.2 Meshing of the Cup

The second step in the completion of the finite element model is to created a mesh in Patran. To start meshing the cup, select from the *Elements* menu *Action: Create, Object: Mesh Seed, Type: Uniform*. Select the option *Number of Elements* and type in the *Number=* box the numbers contained in Table 4.2. This is the original distribution of elements in the meridional and circumferential directions. These number can be changed according to the desires of the user. The numbers presented below were chosen such that the element size had an aspect ratio of approximately unity using a refined mesh. To seed the mesh in the circumferential direction, use the top view parallel to *x-z* plane. The *x-y* view is recommended to seed the mesh in the meridional direction. While seeding the mesh in the meridional direction, it is important to select the wall profile and the corresponding section located on the axis of revolution.

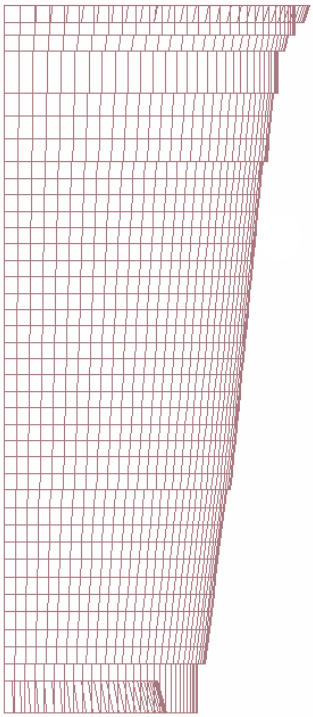

Fig. 4.2 Cup model with mesh

After the mesh seeding is done, select *Object: Mesh, Type: Surface* to finish the meshing process. Click on the *Surface List* box and select the whole cup. The following options should be activated: *Element Shape: Quad, Mesher: IsoMesh, Topology: Quad4*. Execute equivalence of the nodes by choosing *Action:Equivalence.* It is also recommended to optimize the node numbering by choosing *Action: Optimize*. Optimizing is done for purposes of simplicity in case a node or an element has to be found at a later time. Once the meshing process is finalized, the model is displayed as shown on Figure 4.2 .

Table 4.2 Original element number distribution

Region	Number of meridional elements	Number of circumferential elements
Ring region	2	60
2	1	60
3	3	60
4	20	60
5	10	60
Bottom region	1	60

4.3 Geometry of the Contact Cylinder

The movable loading nose in the lateral compression test apparatus has a 0.25-inch radius. In the contact algorithm the movable loading nose is modeled as a circular cylinder with 0.25-inch radius. The modeling of the contact cylinder follows similar procedures as the ones used in the geometric modeling of the cup. To add the contact cylinder, select the *Geometry* menu in Patran and follow these steps: *Action: Create, Object: Curve, Method: 2D Circle*. Select the *Input Radius* option and type **0.125** in the box located below this option for the dimension of the radius in inches. In the Center Point List box, type inside square brackets the coordinates $1.875, 3, -2$. The first coordinate with a value of 1.875 inches corresponds to the distance that is needed to have the cylinder very close to the cup, and not penetrating through the surface of the cup in what is termed overclosure. This first coordinate was obtained visually by trial and error. The second coordinate was chosen to satisfy the condition of having the cylinder contact the cup at one third from the top. The height of the cup is 4.485 in. and a value of 3 in. is two-thirds of this length measured from the bottom. Finally, *z*-coordinate of -2 inches is selected as the location from which the circle is extruded along the *z*-direction in Patran to create the cylinder. Recall that the *x-y* plane of symmetry of the cup is at z = 0 and with the length of the cylinder is specified as 4 in., extruding the circle to form the cylindrical surface from $z = -2$ simplifies the extrusion parameters. Once the circle is sketched, it is necessary to make it a

surface. To do so select *Action: Create, Object: Surface, Method: Extrude*. In the *Translation Vector* box, type **<0,0,4>**, and in the *Curve List* box select the circle. The dimensions of the contact cylinder are shown on Figure 4.3 .

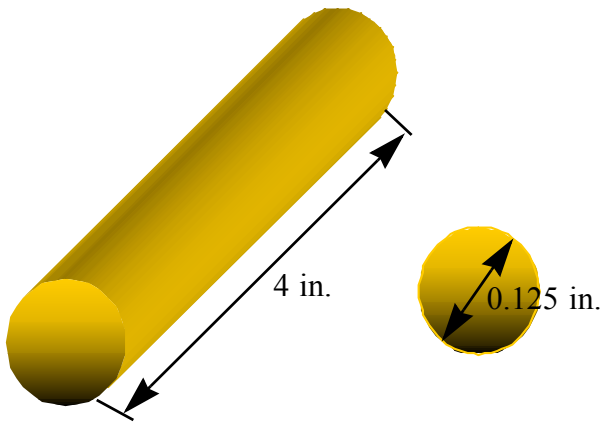

Fig. 4.3 Dimensions of contact cylinder

4.4 Meshing of the Contact Cylinder

Although it may not seem important because the cylinder is considered to be rigid relative to the cup, it is suggested that this entity contains some kind of meshing. To do so, from the *Elements* menu select *Action: Create, Object: Mesh Seed, Type: Uniform*. Choose the *Number of Elements* option and type **20**, which means twenty elements around the circumference of the cylinder to try to match the size of the elements on the circular surface of the cup wall. Select the *Curve List* box and highlight the cylindrical surface. Finally, select *Action: Create, Object: Mesh, Type: Surface* and apply the mesh. It is recommended to perform equivalence and optimize this model.

4.5 Contact Algorithm

The contact algorithm is required to mimic the physics of the movable loading nose contacting the shell wall of the cup. The contact algorithm is composed of two geometrical entities, the cup and the contact cylinder. Proper modeling of mechanical contact constraints is

implemented by the definition of master and slave surfaces. These surfaces can either be rigid-rigid or rigid-deformable. In this case, the cup contact model consists of a rigid surface that is the cylinder, and a deformable surface that is the cup. A master surface must have consistent orientation of the outward normal in order to detect the proper contact direction. It is important to have the slave surface on the same side as the master surface. Master surfaces have to be continuous across element edges in three-dimensional models. Overclosure of the nodes is usually an issue in contact algorithms, and that is why a visual overclosure has to be avoided. Although visual location of the surfaces does not guarantee overclosure free nodes, it greatly helps the algorithm. In later sections this issue will be revisited.

4.5.1 The Concept of Master and Slave Surfaces

The concept of master and slave elements is used in several finite element codes like PATRAN and ABAQUS [5] when modeling mechanical contact. This concept implies that the nodes contained in the slave surface must conform to the ones contained in the master surface. In this case, the region of the cup that will be in contact with the cylinder is the slave surface, while the cylinder itself acts as the master surface.

4.5.2 Reference Node

To initiate the contact algorithm in Patran, it is necessary to define a reference node. The reference node is contained in the master surface and acts as a control. This means that the reference node contains all the displacement and rotational information for the cylinder. To create a reference node, select the *Finite Elements* menu and choose *Action: Create, Object: Node, Method: Edit*. The *Node Location List* allows the user to select any point in the model, in this case the point selected is the construction point used to create the contact cylinder. The node number assigned to this new node should be recorded for future reference. Once a reference node has been defined, select the *Loads/BCs* menu and select *Action: Create, Object: Displacement, Type: Nodal*. Then input the translation vector as **<-0.5,0,0>** and an all **zero rotations vector**. That is, the cylinder is specified to displace in the negative *x*-direction 0.5 in. The *Application Region* needs to have the *FEM Filter* activated and in the *Select Nodes Box*, type **Node and the number that was assigned to the reference node**. To create contact

between two surfaces select *Action: Create, Object: Contact, Type: Element Uniform* and choose the *Rigid-Deform* option. The *Select Application Region* contains the options needed to determine the master and slave surfaces. Select *Geometry* as the *Geometry Filter*, the master and slave surfaces are both shell surfaces. Select *Active Region* and assign the surfaces that correspond to master and slave. In this case, the surface corresponding to the slave one is Region 4 of the cup.

4.6 Materials and Properties

Although HIPS after thermoforming exhibits orthotropic behavior, initially in Patran we specified the material as isotropic for simplicity. Later, the material can be re-specified in ABAQUS/CAE [7] as orthotropic as is described in Section 4.8.1. The *Materials* menu in Patran contains the options *Action: Create, Object: Isotropic, Method: Manual Input.* Assign a material name and select *Input Properties.* Enter the value of *Elastic Modulus* as **295000**, which is in dimensional units of psi, and enter *Poisson's Ratio* equal to **0.35**.

In the Element Properties menu, an existing property related to the contact algorithm should exist. This property is automatically created when the contact algorithm is created. Failure of this property to be displayed on the screen means that no contact algorithm has been created. Select *Action: Create, Object: 2D, Type: Shell* and assign a different *Property Set Name* to every region of the cup. The *Input Properties* box allows the user to input a shell thickness for the cup. This thickness can be constant or variable. If later the thickness value is to change, then this is done in ABAQUS/CAE as described in Section 4.8.2.

4.7 Creation of an ABAQUS Input File

When all the steps have been completed in Patran, it is necessary to export all this information into ABAQUS/Standard. The way Patran handles this conversion is by creating an input file having an extension.*inp*. This input file is generated by selecting the *Analysis* menu, then *Action: Analyze, Object: Entire Model, Method: Analysis Deck.* The input file contains various important commands that should be completely understood in order to get the desired results. This file contains the general format shown on Figure 4.4 on page 56 . The first line of

the input file reads **HEADING, SPARSE*; the *SPARSE* option should be removed in order to avoid problems when ABAQUS/CAE reads the file. Node location is denoted by the command **NODE* and it contains four columns designated to element number, *x*-coordinate, *y*-coordinate and *z*-coordinate. Every single node contained in the cup and in the cylinder is listed under this command. The following contents of the input file require additional comments and explanation that can be found in next subsection.

4.7.1 The Rigid Elements of the Master Surface

The rigid elements contained in the cylinder are listed under the command **ELEMENT TYPE=R3D4 ELSET=CYLINDER*. This command defines the element connectivity of the cylinder. In this model, the cylinder acting as the master surface contains R3D4 elements. Elements R3D4 are four-nodded, bilinear, quadrilateral rigid body elements with six degrees of freedom per node (three translations and three rotations). The command is followed by five columns containing the element number and the four nodes assigned to the element.

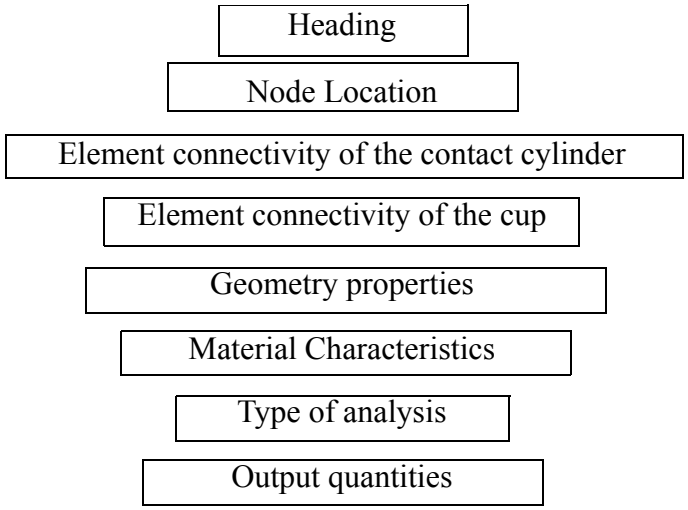

Fig. 4.4 Input file general format

4.7.2 ABAQUS Shell Elements

The cup model consists of 3629 S4R5 elements that are listed under the command **ELEMENT TYPE=S4R5 ELSET=CUP*. Element S4R5 is a four node, doubly curved thin shell element with five degrees of freedom per node. These degrees of freedom are the three translations and the two in-surface rotations. Element S4R5 is formulated for small strains and large rotations, and numerically imposes the Kirchhoff constraint of vanishing transverse shear deformation at discrete points on the reference surface. It features reduced integration and hourglass control. Nodal coordinates for this type of element require X, Y, Z Cartesian coordinates as inputs. Direction cosines normal to the shell at every node can be entered as an additional option. Five columns containing element number and nodes assigned are listed under the line command

4.7.3 Cross-sectional Behavior of a Shell

The cross-sectional behavior of a shell is defined using the **SHELL GENERAL SECTION* option or the **SHELL SECTION* option. The **SHELL GENERAL SECTION* option is for linear relationships between the bending moment intensities and the changes in curvatures, and between the in-surface force intensities and the membrane strains. Whenever the response of the shell is linear elastic and its stiffness is not dependent on changes in temperature, the **SHELL GENERAL SECTION* option may be used. If the section definition is included in the geometry properties part of the input file under the command **SHELL SECTION, ELSET=CUP, MATERIAL=POLYSTYRENE*, then the cross-sectional behavior is calculated by integration through the shell thickness. The **SHELL SECTION* option provides generality in material modeling; e.g., nonlinear material behavior. With this option any number of material points can be defined through the thickness and the material response can vary from point to point.

4.7.4 Homogeneous Section

When a shell wall is made from a single material, the user-specified name of the material appears in the parameter *MATERIAL* of the **SHELL SECTION* option; e.g., *MATERIAL=POLYSTYRENE*. The material name *POLYSTYRENE* refers to the **MATERIAL*

option block in the material data definition, as described in the next subsection. The data line following the **SHELL SECTION* option contains the shell wall thickness and the number of integration points to be used through the thickness of the shell section wall. The number of integration points can also be changed by the user if desired. The default value of five integration points should be adequate for the cup model.

4.7.5 Material Characteristics

The material properties are defined in the command **MATERIAL, NAME=POLYSTYRENE*. This option is used to indicate a material definition. This command is necessarily related to the **ELASTIC, TYPE=ISO* command. This **ELASTIC* command defines the material as isotropic linear elastic. In case the material is orthotropic, the parameter *TYPE=LAMINA*, which also implies a plane stress state in the lamina. However, ABAQUS/CAE has the capability to change material characteristics very easily. This procedure will be described in Section 4.8.1.

4.7.6 Type of Analysis

The type of analysis that will be performed by the ABAQUS solver can be found under the option **STEP, NLGEOM, INC=1000*. This option defines steps in the analysis as the state of the model evolves in response to the loading history. Parameters specified in the **STEP* option indicate linear or nonlinear solution procedures. In this case, the parameter *NLGEOM* specifies a geometrically nonlinear analysis. With contact displacements of the order 0.5 inches and an average wall thickness of 0.020 inches, it is anticipated that the rotations of the shell wall will be a significant contributor to the strains, and that equilibrium conditions must be satisfied on the deformed shell. Large rotations are accounted for in a geometrically nonlinear analysis. This option remains active all throughout the analysis. The parameter *INC* controls the maximum number of increments in a step. It is recommended that the value of *INC* remains at 1000, since complex geometry combined with a contact algorithm may require several increments to find the solution within a step.

4.7.7 Element Output

PATRAN determines the results of some quantities to be available as default after the analysis is conducted. This final section of the input file should not be altered since the commands listed there have no effect in the solution process. ABAQUS/CAE has the capability of displaying the results for any solution variable at any step in the analysis.

4.8 The ABAQUS CAE Environment

ABAQUS/CAE is a visual version of ABAQUS. Its graphic capabilities plus its user friendly environment make it convenient for the final stages of the finite element model construction. The previous stages of the model development were designed in such a way that CAE can be used to make changes in parameter values or include more complicated modeling features. In the following sub-sections, the final modeling stage and operation process are described. This interactive modeling procedure in ABAQUS/CAE is illustrated in Fig. 4.5.

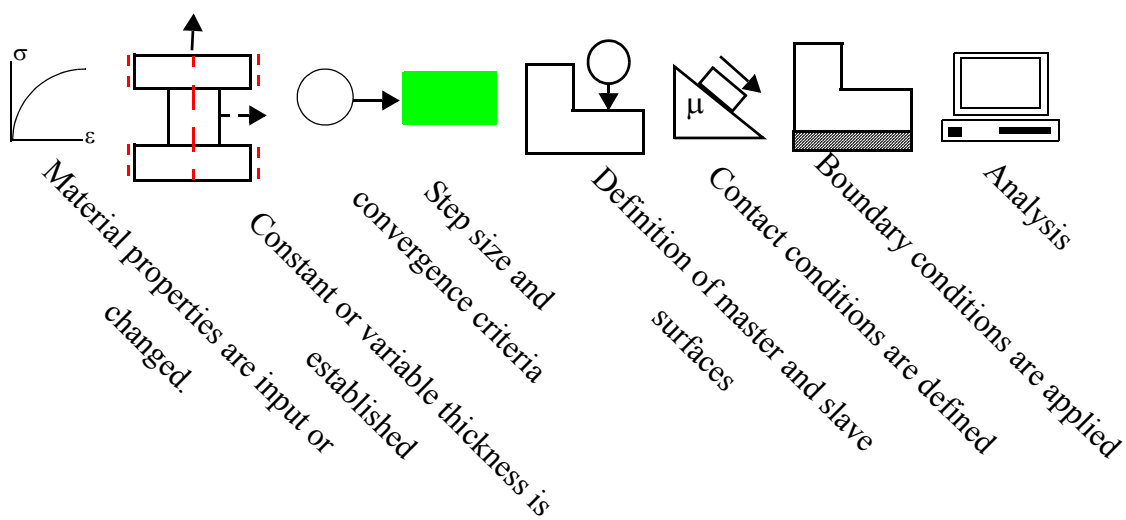

Fig. 4.5 ABAQUS CAE procedure summary

4.8.1 Create Material

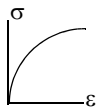

Fig. 4.6 Create material icon

The create material icon shown in Fig. 4.6 is found under the *Module: Property.* A material definition specifies the behavior of the selected material. This option allows the user to view the existing material assigned to the model in the previous steps. By selecting the material manager, which appears to the right of this icon, the user can change the material properties such as the modulus of elasticity or Poisson's ratio. The material manager can also be used to switch from isotropic to orthotropic properties. Whenever parametric studies on material orthotropy were performed on cup response, the option *Lamina* was specified. If the material specification is orthotropic, the following quantities should be entered: *E1;* the modulus of elasticity in the meridional direction, *E2;* the modulus of elasticity in the circumferential direction, *Nu12;* the major Poisson's ratio, and *G12, G13, and G23; the* shear moduli.

4.8.2 Create Section

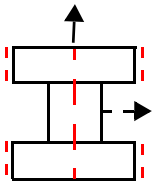

Fig. 4.7 Create section icon

Another important option in the *Module: Property* is the create section, whose icon is shown in Fig. 4.7. A section contains important information about geometrical properties of a part or a region of a part. The create section allows the user to create or modify an already existing section. In the cup model, the create section manager incorporates the six regions contained in the cup. The bottom region corresponds to section 1, region 5 corresponds to section 2 and so on (see Fig. 4.1.b). By selecting each section, the user can input the desired thickness of the section.

4.8.3 Create Step

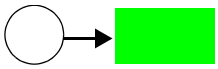

Fig. 4.8 Create step icon

The create step icon shown in Fig. 4.8 can be found under *Module: Step*. Since step criteria were specified in the input file, only few parameters need to be added in this section. The manager contains two steps, an initial and Step-1. The initial step is created at the beginning of the step sequence. This step is automatically created by ABAQUS and cannot be renamed, deleted or edited. This step carries information such as boundary conditions and interactions. It is important to

make sure all the prescribed boundary conditions and contact properties of the model start in this step. The manager also has the capability of turning on or off the *NLGEOM* parameter. For purposes of the cup response analysis, this option should be kept on. If step-1 is edited it should contain the capability of using *stabilization with dissipated energy fraction: 1* for convergence purposes. It should also have *automatic incrementation* with a maximum number of *increments* of **1000**. The *increment size* should be set to an *initial* value of **0.1** with a *minimum* of **1e-15** and a *maximum* of **0.25**.

4.8.4 Create Interaction

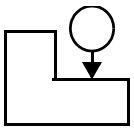

Fig. 4.9 Create interaction icon

The *Interaction Module* defines and manages mechanical interactions between regions of a model. Its icon is shown in Fig. 4.9. In this module it is necessary to assign the master and slave surfaces again. Select the interaction manager and create a *Surface to surface contact* in the *initial step*. Select the entire cylinder as the master surface and make sure the normals point radially outwards. A section that will be in contact with the cylinder in region 4 should be selected as the slave surface. Again, make sure the normal points outwards. Select the *Adjust only overclosed nodes* option just in case there is some overclosure that cannot be visually identified. The sliding formulation has to be chosen as *finite*, the reason for this choice is explained in the next sub-section.

4.8.5 Relative Surface Motion

Since a contact algorithm between a rigid surface an a deformable surface is being used, it is necessary to account for the relative motion between these two surfaces once they are in contact. The chosen approach to account for this relative motion between surfaces was finite sliding. Finite sliding is the most general approach and it allows arbitrary motion of the master and slave surfaces when they are in contact. This formulation features the capability of tracking the position of every node in the slave surface at any time step while contact progresses. The finite sliding formulation requires that every master element has a unique normal at all surface points. Failure to meet this requirement results in convergence problems due to slave nodes getting trapped wherever a discontinuity in the master surface normals is

found. Although ABAQUS smoothes the rigid surfaces to avoid the previously mentioned problem, it is necessary to create a fairly smooth rigid surface. In this case, the cylinder is a smooth curvilinear surface.

4.8.6 Create Interaction Property

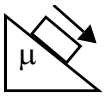

Fig. 4.10 Interaction property icon

The interaction property manager in the *Interaction Module* allows organization and manipulation of mechanical interactions between objects. Its icon is shown in Fig. 4.10. The contact property created in Patran should be visible with the designation I58. In this option, two very important formulations should be chosen. These formulations are described in the sub-sections below.

4.8.7 Tangential Behavior of the Contact Surfaces

When surfaces are in contact they usually transmit shear and normal forces across the interface. A relationship between these two forces is described as the friction between contacting bodies. There is a variety of friction models that can be implemented in the finite element model, however for simplicity purposes, a *frictionless* analysis is used.

4.8.8 Normal Behavior of the Contact Surfaces

The normal behavior of the contact surfaces determine the pressure-clearance model that is used in the analysis. In this case, the *hard contact* relationship is used. This characteristic allows no penetration of the slave nodes into the master surface, therefore no transfer of tensile stress across the interface is allowed. When the master and slave surfaces are in contact, the contact pressure can be transmitted between them. The surfaces, when separated, will obviously have a contact pressure equal to zero.

4.9 Boundary Conditions

Originally, a full model of the cup was developed for solution in ABAQUS/Standard. The average calculation time utilized by the solver was about nine hours. This original model featured the full cup being compressed by two opposing contact cylinders. The model proved

to be very inefficient and expensive. To reduce the calculation time and the complexity of the model, it was decided to use symmetry and to model just half of the cup, and to compress the half model with only one contact cylinder. The boundary conditions specified for the cup at the plane of symmetry were that translation in the 1-direction, or *x*-direction, rotation in the 2-direction, or about the *y*-axis, and rotation in the 3-direction, or about *z*-axis, all vanish. At the open end of the cup which is in contact with the side holding plate of the test fixture as shown in Fig. 1.4, the displacement in the 2-direction, or *y*-direction, is specified to vanish. These boundary conditions take place in the initial step of the analysis.

As mentioned in previous sections, the rigid element of the contact cylinder contains a reference node. All translational and rotational degrees-of-freedom of the rigid cylinder are prescribed at the reference node. To simulate the lateral compression test, the displacement of the reference node in the 1-direction, or *x*-direction, is prescribed to be non-zero and the other five degrees of freedom prescribed to be zero. Since it is desired to determine the response of the full cup when compressed one inch in the test fixture, the reference node in the half model is assigned a maximum displacement value of 0.5 inches in the 1-direction. This boundary condition will take effect in the first step of the analysis.

4.9.1 Boundary Conditions in the ABAQUS/CAE Environment

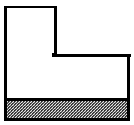

Fig. 4.11 Create boundary condition icon

The Load module contains the boundary conditions, and its icon is shown in Fig. 4.11. As described in the previous sub-section, the model requires boundary conditions that simulate symmetry of the half cup, constraint of the side holding plate at the open end of the cup, and the prescribed displacement of the contact cylinder. To create the symmetry boundary conditions, select the *Symmetry/Antisymmetry/Encastre* option, select the edge of the cup and then choose *XSYMM (U1=UR2=UR3=0).* The side holding plate located at the open end of the cup restricts the cup to move in the 2-direction, or $y-direction$; therefore, a boundary condition of *Displacement/Rotation* is created and the upper edge of the cup is selected. The boundary condition restricts displacement component *U2* to vanish. Finally, the reference node containing the value *U1=0.5* should be visible in the manager, it is important to restrict

all other five degrees of freedom if this has not been done before. The boundary conditions should be displayed on the model as shown in Fig. 4.12.

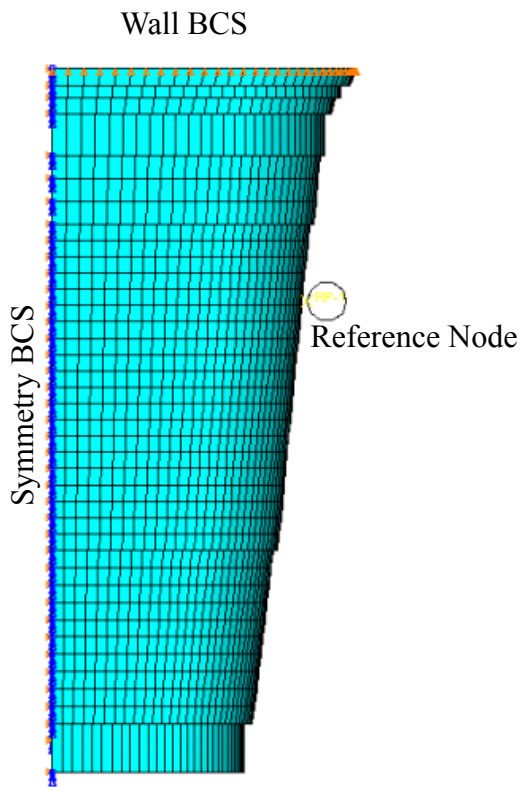

Fig. 4.12 Boundary conditions

4.10 Processing of the Model

Fig. 4.13 Create job icon

Once the finite element model is developed, it can still be changed in ABAQUS/CAE with respect to material and section properties in a very efficient way. For the parametric studies, changes from isotropic to orthotropic material behavior, and from a uniform thickness distribution along the meridian to variable thickness, are required. *The Job Module,* whose icon is shown in Fig. 4.13, submits the model with the specified parameters to the solver, and then retrieves the resulting evaluation functions. The average time of analysis for the cup model is 70 minutes and up to eight simultaneous models with different characteristics can run at the same time. A three- dimensional graphic of the half cup model in a deformed state is shown in Fig. 4.14.

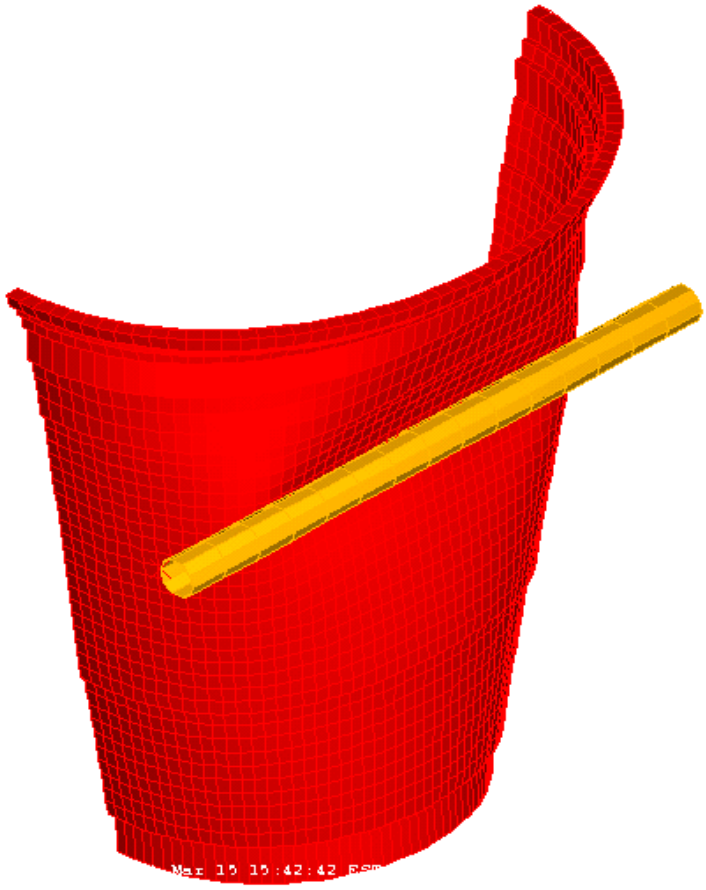

Fig. 4.14 Deformed state of the half cup model

This page is intentionally left blank

CHAPTER 5

Parametric Studies

Parametric studies constitute the most important part of the project. Several studies were performed using the finite element model described in Chapter 4. The lateral compressive response for five meridional thickness distributions of a ribbed cup with an isotropic wall are presented in Section 5.1. The effect of orthotropic wall properties on the response of a ribbed cup are presented in Section 5.2. A model without the circumferential stiffening ribs, or a smooth cup model, is presented in Section 5.3. A parametric study of the meridional thickness distribution on the response of the smooth cup model is presented in Section 5.4, followed by an orthotropic property study of the smooth cup in Section 5.5.

The general character of the lateral compressive response curve obtained from the finite element analyses for all models discussed in this chapter is shown in Fig. 5.1. Near the origin of this response curve, the load increases with increasing applied displacement until the load attains a small value. With a further increase in the displacement, the load remains relatively constant near this small value. This initial region near the origin represents the "take-up" in the contact model. In this first region, the cylinder barely makes contact with the cup and almost no force is exerted by the cup on the cylinder. After the initial take-up, the compressive response curves exhibit a nearly linear region with increasing applied displacement. This linear region is characterized by the slope, or the stiffness *k,* remaining nearly constant with increasing applied displacement. Following the linear region, there is a large deflection, nonlinear region of the response curve in which

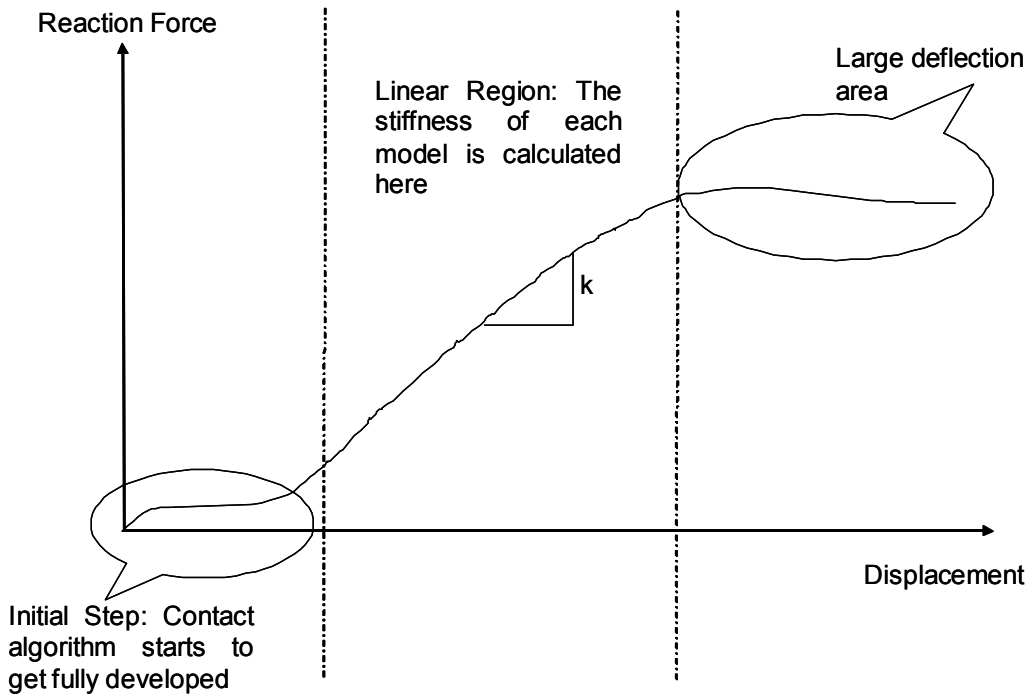

Fig. 5.1 P vs. Δ curve general trend and regions

the response softens and it may exhibit a limit point, or a relative maximum load. The initial take-up effects have been extracted from the response curves shown in Section 5.1 on page 68 and in Section 5.4 on page 89. That is, the origin of the response plot is shifted to the start of the linear region. The reason for extracting the take-up region is for comparative purposes to the test results given by Dow. In the Dow tests a small pre-load is applied to the cup before data is collected, which in effect eliminates the take-up region of the response predicted by the contact analysis.

5.1 Thickness Distribution Studies of a Ribbed Cup

To support the search for the best meridional thickness distribution of the cup, the effect of selected thickness distributions on the lateral compression response of the cup were undertaken. The material in the wall of the cup is assumed to remain isotropic in these parametric studies on the thickness distribution, having a modulus of elasticity of 295 ksi and a Poisson's ratio of 0.35. An overlaid plot of the deformed ribbed cup compared to its original

state before being compressed is shown in Fig. 5.2. The deformation pattern shown in this figure is typical of the response of a ribbed cup.

The cup is divided into six regions to quantify the thickness distribution: the bottom, the ring, and four major regions along the meridian as is shown in Fig. 4.1. The reason for identifying these six regions is that the wall thickness is measured at five points from the top plus the bottom, and these points of measurement lie in these six regions. The five parametric studies conducted are

- Different bottom thicknesses with wall thicknesses fixed
- Different wall thicknesses, a fixed bottom thickness, while maintaining constant volume
- Different thicknesses for region 5 with all other thicknesses fixed
- Proportional increases in the wall thicknesses with fixed bottom thickness I
- Proportional increases in the wall thicknesses with fixed bottom thickness II.

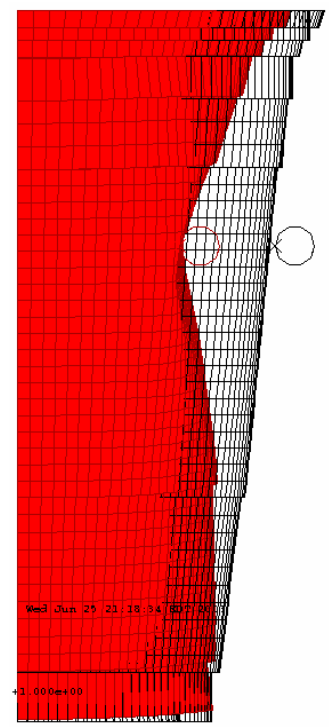

Fig. 5.2 Overlaid plot of a deformed ribbed cup

The six regions, the distance from the top where the thickness of a region is measured, and the meridional lengths of each region, are given in Table 5.1.

One way to quantify a thickness distribution is to simply average the six thickness values. Another measure is a weighted average thickness defined by

$$t_w = \left(\sum_{i=1}^{6} h_i l_i \right) \Big/ \left(\sum_{i=1}^{6} l_i \right) \qquad (1)$$

where h_i are the thicknesses specified at selected points in each region, and l_i are the meridional lengths of each region as listed in Table 5.1. These average thickness measures

along with the stiffness in the linear region are reported for each thickness distribution in tables that appear the following sections.

Table 5.1 Locations of thickness measurements and meridional lengths

Region		Distance from top where thickness is measured	Meridional length, l, (in)
1	Top Ring	0.27 in.	0.535
2	Wall	0.59 in.	0.265
3	Wall	0.98 in.	0.451
4	Wall	1.96 in.	2.093
5	Wall	3.93 in.	1.126
6	Bottom		1.660
			Sum = 6.13 in.

It is of interest to view a typical deformation sequence in the contact analysis. For a cup with variable thickness along the meridian a sequence is shown in Fig. 5.3. The sequence starts at a displacement Δ of 0 in. and it progresses until it reaches 1 in. This schematic provides the visual image of how the cup deforms at important stages of the contact analysis.

5.1.1 Different Bottom Thicknesses with Wall Thicknesses Fixed

The first set of thickness distributions consist of five distributions designated A to E, and they are listed in Table 5.2. Each distribution also designates a finite element model. In order to test the sensitivity of the load-displacement curve to bottom thickness, distributions A, B, C, D, and E were selected such that the wall thickness distribution remains constant while the bottom thickness increases from model A to model E. The thickness distribution for model A is referred as the reference distribution.

The load-deflection curves for models A to E are shown in Fig. 5.4., along with test data from a specimen from Dow, labeled Dow1 in the legend. The details of the Dow test are not known, but the fact that the results obtained from finite element models A to E lie in the same region of the response plot lends validity to the finite element models. The response

curves nearly coincide through the linear region for models A to E. Hence, in the linear region the bottom thickness has little effect on the response. This lack of sensitivity to changing bottom thickness is also quantified by the stiffness values listed in Table 5.2, which were calculated in the displacement range 0.1 to 0.2 in. The stiffness from models A to E vary between 4.2 to 4.4 lb/in; again, indicating that the change in bottom thickness in the ranges considered does not appreciably affect the response. The fact that the stiffness do not increase with increasing average thickness, or weighted average thickness, in Table 5.2 may be due to the numerical errors in the linear regression of the finite element data. Since the variation in stiffness is small, the fact that the stiffness do not strictly increase with the average thickness is not considered significant. It is noted that the Dow1 specimen has a stiffness of 2.252 lb/in. In the nonlinear region there are some differences in the response curves for distributions A to E. The smaller thickness models A and B have a larger load carrying capacity for an applied displacement between 0.3 and 0.9 in. than do the thicker models C, D and E. Also, the "knee" in the response curve, or where the softening begins at the end of linear region, occurs at a lower displacement for the thicker models than for models A and B.

Table 5.2 Thickness distributions A to E

Distance from the top of the cup	Model designation and thickness distribution (in)				
	A[a]	B	C	D	E
0.27 in.	0.029	0.029	0.029	0.029	0.029
0.59 in.	0.018	0.018	0.018	0.018	0.018
0.98 in.	0.016	0.016	0.016	0.016	0.016
1.96 in.	0.013	0.013	0.013	0.013	0.013
3.93 in.	0.012	0.012	0.012	0.012	0.012
Bottom	0.021	0.025	0.032	0.034	0.035
Average thickness in.	0.019	0.018	0.020	0.020	0.021
Weighted thickness in.	0.0168	0.0179	0.0198	0.0203	0.0206
Stiffness lb/in.	4.428	4.445	4.242	4.253	4.266

a. Reference distribution

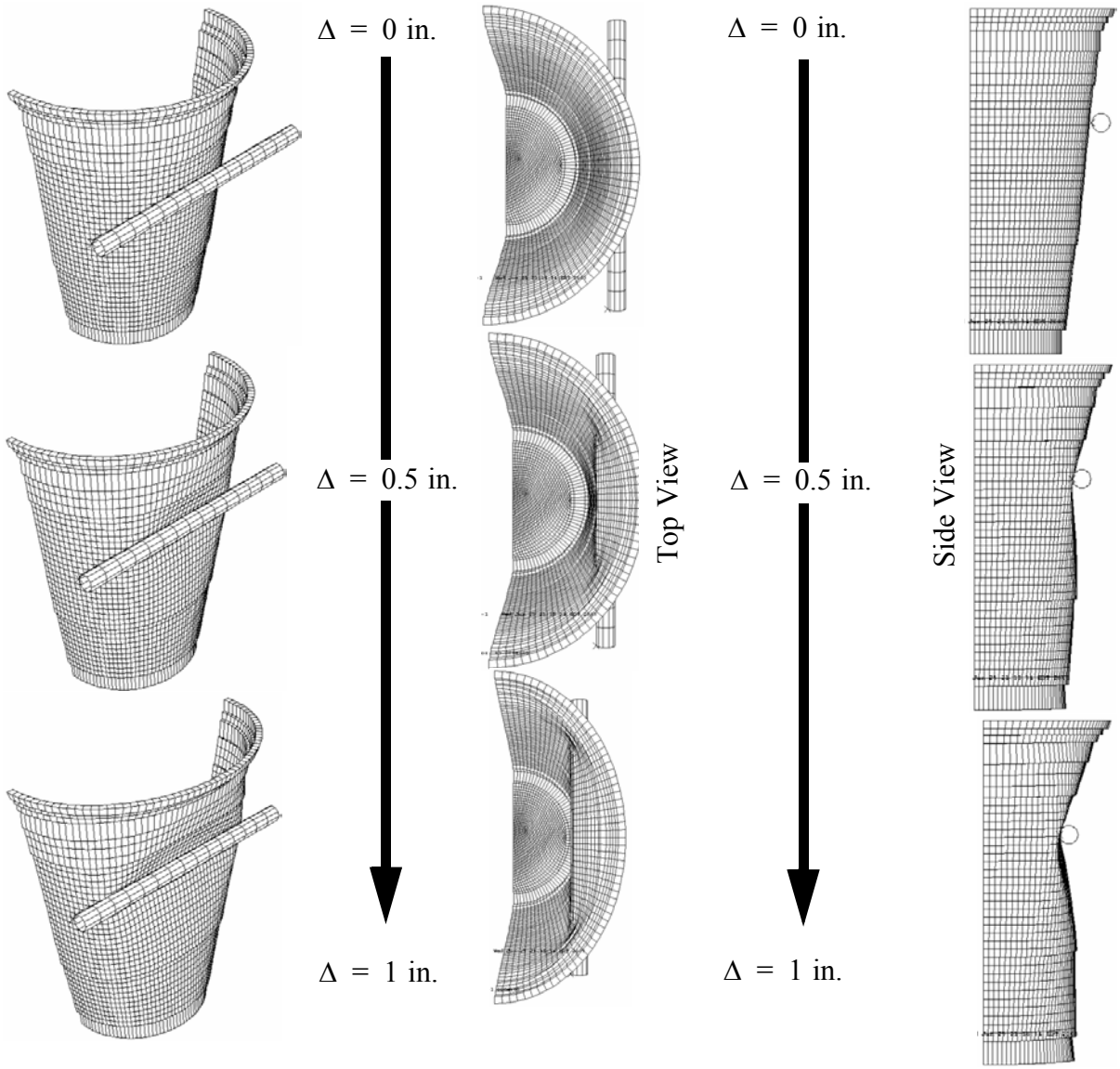

Fig. 5.3 Deformation sequence from the contact analysis

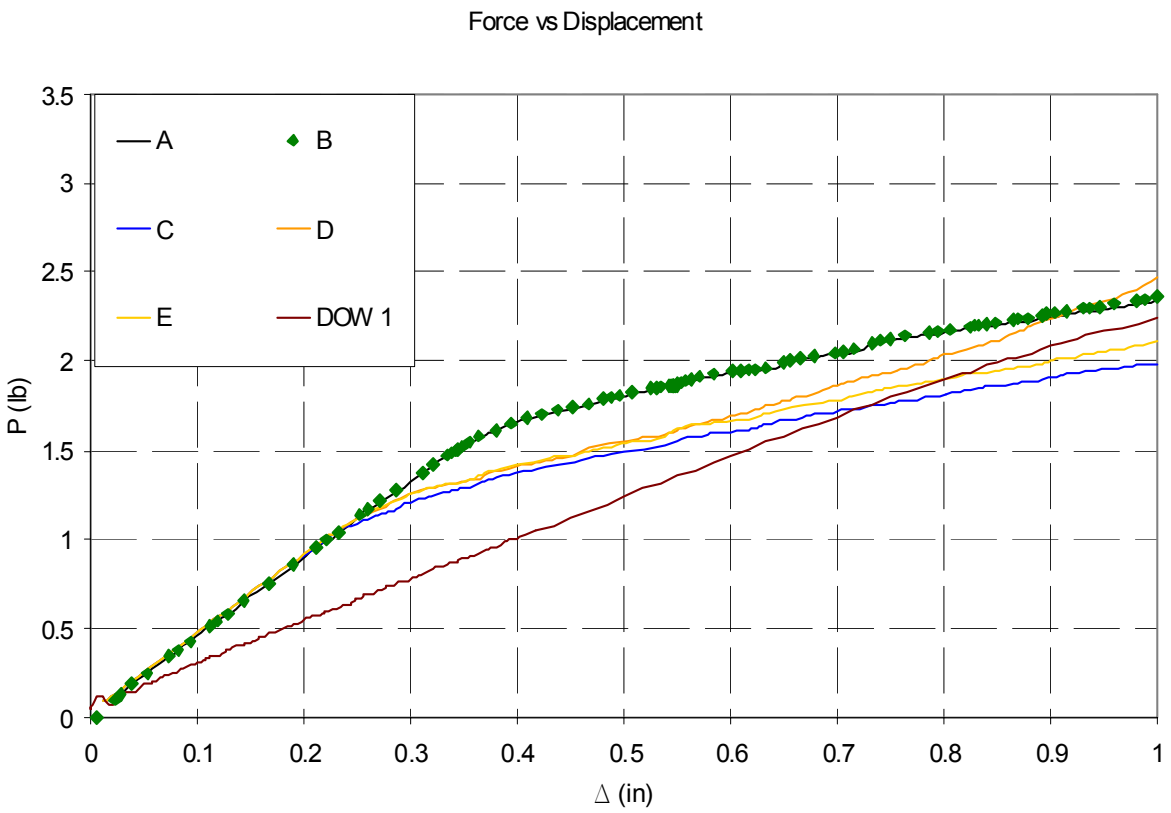

Fig. 5.4 Load-displacement curves for models A to E and from a Dow test

5.1.2 Different Wall Thicknesses, Fixed Bottom Thickness, while Maintaining Constant Volume

Distributions F, G, H and I listed in Table 5.3 have a variable thickness along the wall profile except for the bottom thickness which has been fixed to a value of 0.021 in. The response curves are shown in Fig. 5.5. In the linear region of the response, the curves nearly coincide to the scale of the plot. Model G with the largest weighted thickness has the largest stiffness of 4.53 lb./in., but the other models have stiffness in the range of 3.9 to 4.5 lb./in. In the nonlinear portion of the response there is a significant difference in the load carrying capacity of the cup. Model G carries the largest load followed by I, F, and H. Model H which has a uniform wall thickness except for the bottom, exhibits the least capacity to support the compressive load. Although, models H and I have about the same weighted thickness, model I carries a larger load in the nonlinear region of the response. The larger load capacity of model I with respect to model H is likely due to the fact that the ring of the former is twice as thick as the latter. Since the ring at the opening of the cup is relatively close to the application of the load, its stiffness plays a significant role in the resistance of the cup.

Table 5.3 Thickness distributions F to I

Distance from the top of the cup	Model designation and thickness distribution (in)			
	F	G	H	I
0.27 in.	0.025	0.025	0.015	0.031
0.59 in.	0.019	0.021	0.015	0.020
0.98 in.	0.016	0.018	0.015	0.017
1.96 in.	0.013	0.014	0.015	0.013
3.93 in.	0.013	0.011	0.015	0.009
Bottom	0.021	0.021	0.021	0.021
Average thickness, in.	0.019	0.019	0.017	0.019
Weighted thickness, in.	0.0167	0.0169	0.0166	0.0166
Stiffness, lb/in.	4.283	4.530	3.871	4.498

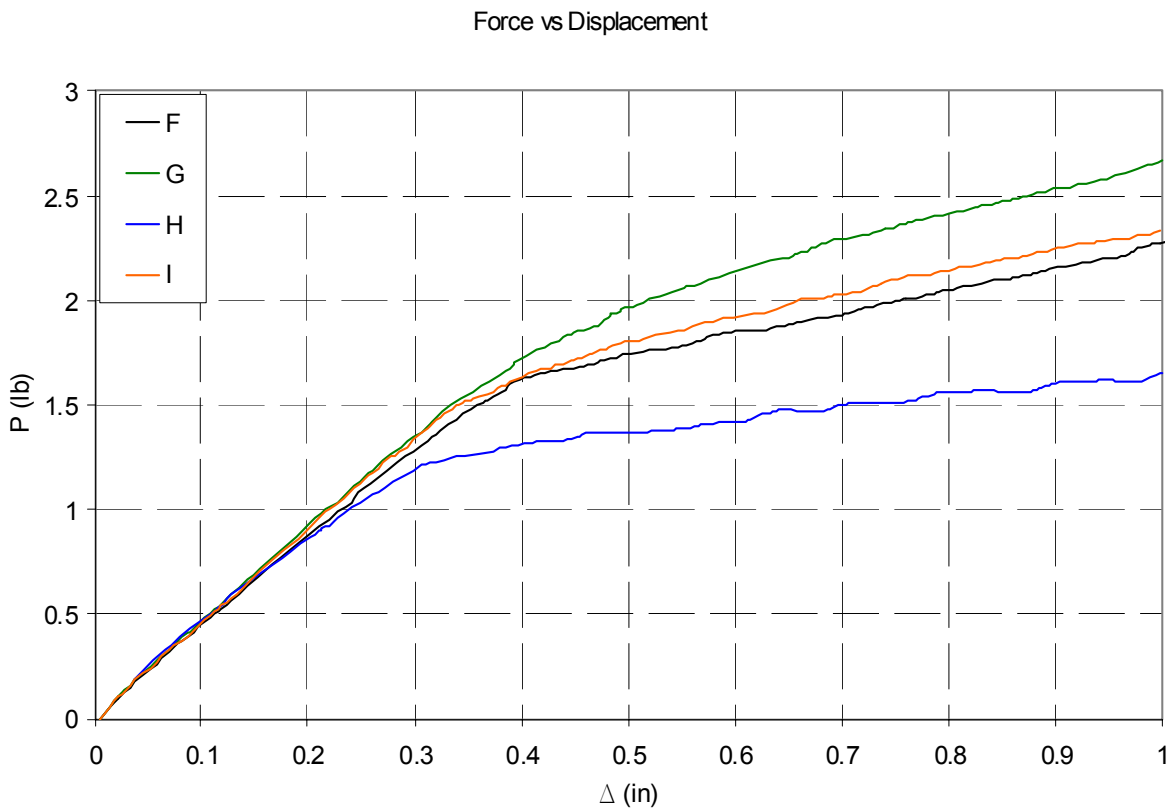

Fig. 5.5 Load-displacement curves for models F to I

5.1.3 Different Thicknesses for Region 5 with all other Thicknesses Fixed

Thickness distributions J to M listed in Table 5.4 have identical thickness except in region 5. The thickness in region 5 is measured at 3.93 in. from the top and it extends to the first rib above the bottom.

Table 5.4 Thickness distributions J to M

Distance from the top of the cup	Model designation and thickness distribution (in)			
	J	K	L	M
0.27 in.	0.021	0.021	0.021	0.021
0.59 in.	0.019	0.019	0.019	0.019
0.98 in.	0.017	0.017	0.017	0.017
1.96 in.	0.015	0.015	0.015	0.015
3.93 in.	0.009	0.011	0.013	0.015
Bottom region	0.021	0.021	0.021	0.021
Average thickness, in.	0.018	0.018	0.018	0.019
Weighted thickness, in.	0.0164	0.0167	0.0171	0.0175
Stiffness, lb./in.	4.765	4.824	4.895	4.965

The response curves for models J to M are shown Fig. 5.6. It is clear from the response curves that the thickness changes considered for region 5 have only a small effect in compressive response. Also, the stiffness in the linear region vary between the narrow range of 4.8 to 5.0 lb./in. as listed in Table 5.4. Since region 5 is relatively far from the application of the load, the response curves are not very sensitive to changes considered for region 5.

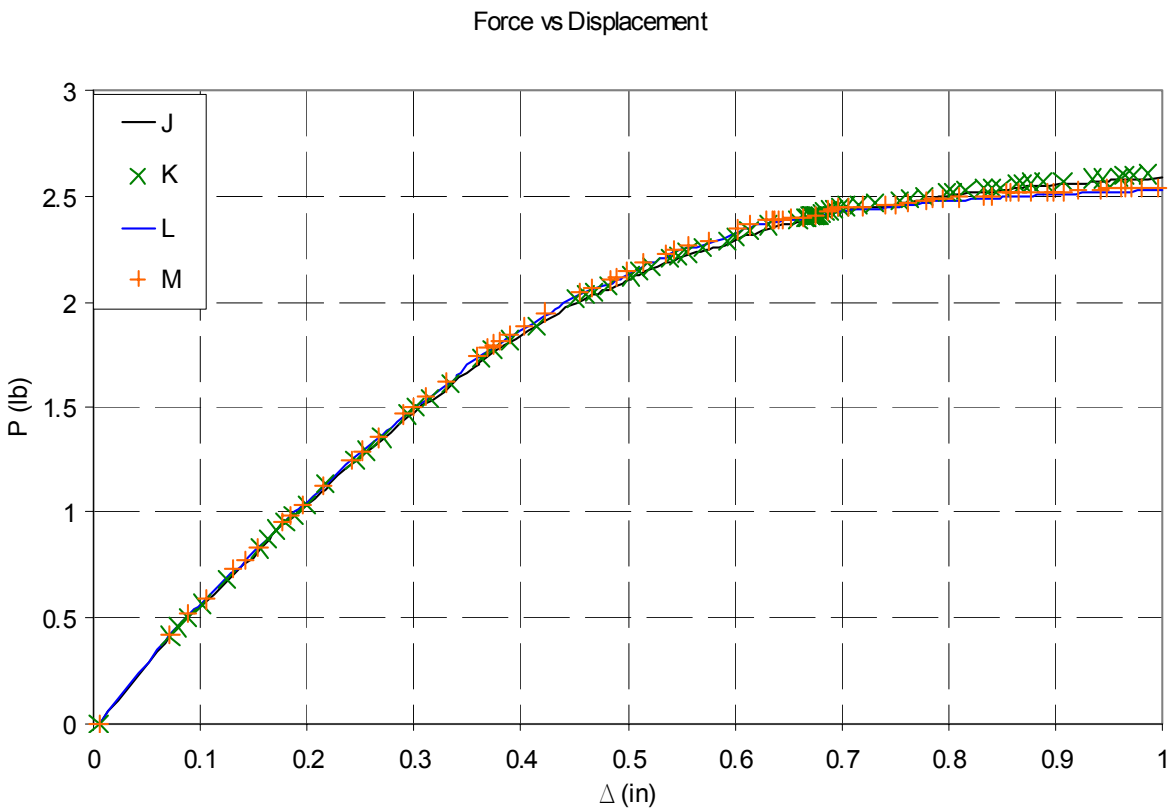

Fig. 5.6 Load-displacement curves for models J to M

5.1.4 Proportional Increases in the Wall Thicknesses with Fixed Bottom Thickness I

The next set of parametric studies consisted of proportional increases in the wall thickness from distribution N to distributions S as listed in Table 5.5. The thickness of the bottom is fixed at a value of 0.034 in. The response curves are shown in Fig. 5.7 along with the test data from a second specimen obtained from Dow, labeled Dow2 in the legend of the figure. The resistance of the cup increases from distribution N to S, which means the load carrying capacity increases for proportionally thicker walls. Similarly, the stiffness in the linear regions listed in Table 5.5 increase from distribution N to S.

Table 5.5 Thickness distributions N to S

Distance from the top of the cup	Model designation and thickness distribution (in.)				
	N	P	Q	R	S
0.27 in.	0.023	0.026	0.029	0.032	0.035
0.59 in.	0.014	0.016	0.018	0.020	0.022
0.98 in.	0.012	0.014	0.016	0.017	0.019
1.96 in.	0.011	0.012	0.013	0.015	0.016
3.93 in.	0.009	0.011	0.012	0.013	0.014
Bottom region	0.034	0.034	0.034	0.034	0.034
Average thickness, in.	0.017	0.019	0.020	0.022	0.023
Weighted thickness, in.	0.0181	0.0193	0.0203	0.0216	0.0226
Stiffness, lb./in.	2.873	3.630	4.253	5.218	6.234

A contour plot of the Mises stress normalized by the yield strength of 4000 psi from model S at 1.0 in. displacement is shown in Fig. 5.8. Model S has the largest values of thicknesses along the meridian of the models N to S. Consequently, model S has largest reaction forces. It can be seen that the major stress concentration is located at the edges of the contact region. The Mises stress only exceeds the yield strength in a very small, localized region at the edge of the contact cylinder.

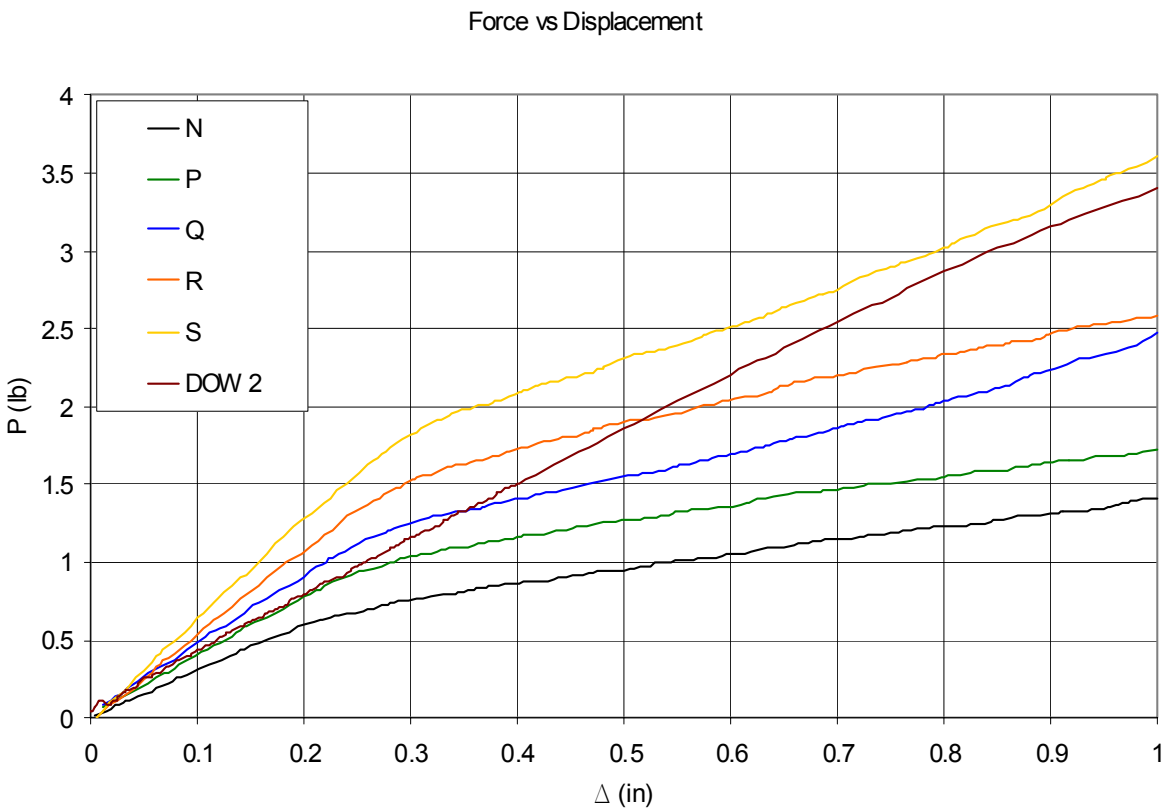

Fig. 5.7 Load-displacement curves for models N to S and for test specimen DOW 2

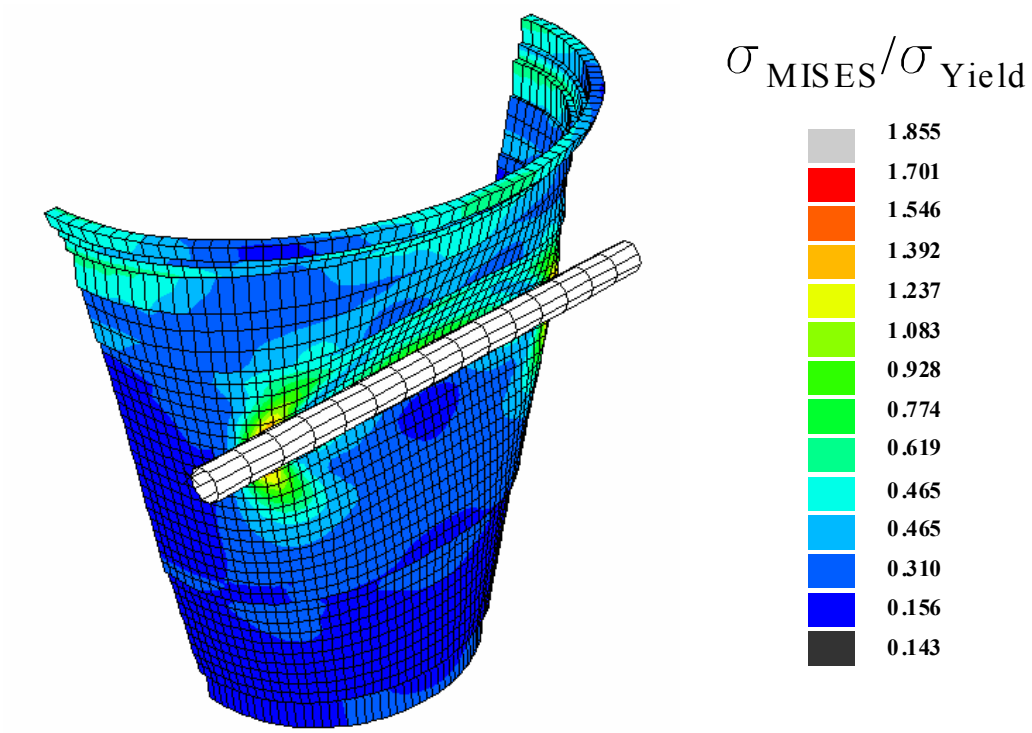

Fig. 5.8 Mises stresses for model S

5.1.5 Proportional Increases in the Wall Thicknesses with Fixed Bottom Thickness II. The last set of parametric studies consisted of proportional increases in the wall thickness from distribution T to distribution AB as listed in Table 5.6. The thickness of the bottom is fixed at a value of 0.021. in. A numerical problem was encountered when running model X. The solution was diverging with the given step and convergence criteria. To solve this problem, the number of increments was changed from 1200 to 1500. The initial step was reduced from 0.1 to 0.001 and the maximum step size was reduced from 0.25 to 0.01. These changes solved the convergence problem.

Table 5.6 Thickness distributions T to AB

Distance from the top of the cup	Model designation and thickness distribution (in.)								
	T	U	V	W	X	Y	Z	AA	AB
0.27 in.	0.020	0.023	0.025	0.027	0.029	0.031	0.034	0.036	0.039
0.59 in.	0.013	0.014	0.015	0.017	0.018	0.019	0.021	0.023	0.024
0.98 in.	0.011	0.012	0.013	0.015	0.016	0.017	0.018	0.020	0.021
1.96 in.	0.009	0.010	0.011	0.012	0.013	0.014	0.016	0.017	0.018
3.93 in.	0.008	0.009	0.010	0.011	0.012	0.013	0.014	0.015	0.016
Bottom region	0.021	0.021	0.021	0.021	0.021	0.021	0.021	0.021	0.021
Average thickness, in.	0.014	0.015	0.016	0.017	0.018	0.019	0.021	0.022	0.023
Weighted thickness, in.	0.013	0.014	0.015	0.016	0.017	0.018	0.019	0.020	0.021
Stiffness, lb/in.	2.174	2.697	3.217	3.893	4.430	5.212	6.357	7.314	8.163

The response curves are shown in Fig. 5.9. The resistance of the cup increases from distribution T to AB, which means the load carrying capacity increases for proportionally thicker walls. Similarly, the stiffness in the linear regions listed in Table 5.6 increase from distribution T to AB.

A summary of the five parametric studies is illustrated by the bar graph shown in Fig. 5.10. Bars of the average thickness and of the stiffness for each distribution are depicted in the figure. Although the average thickness shows little variation between the distributions, the

stiffness vary substantially. The average thickness of a distribution is not sufficient to characterized its stiffness.

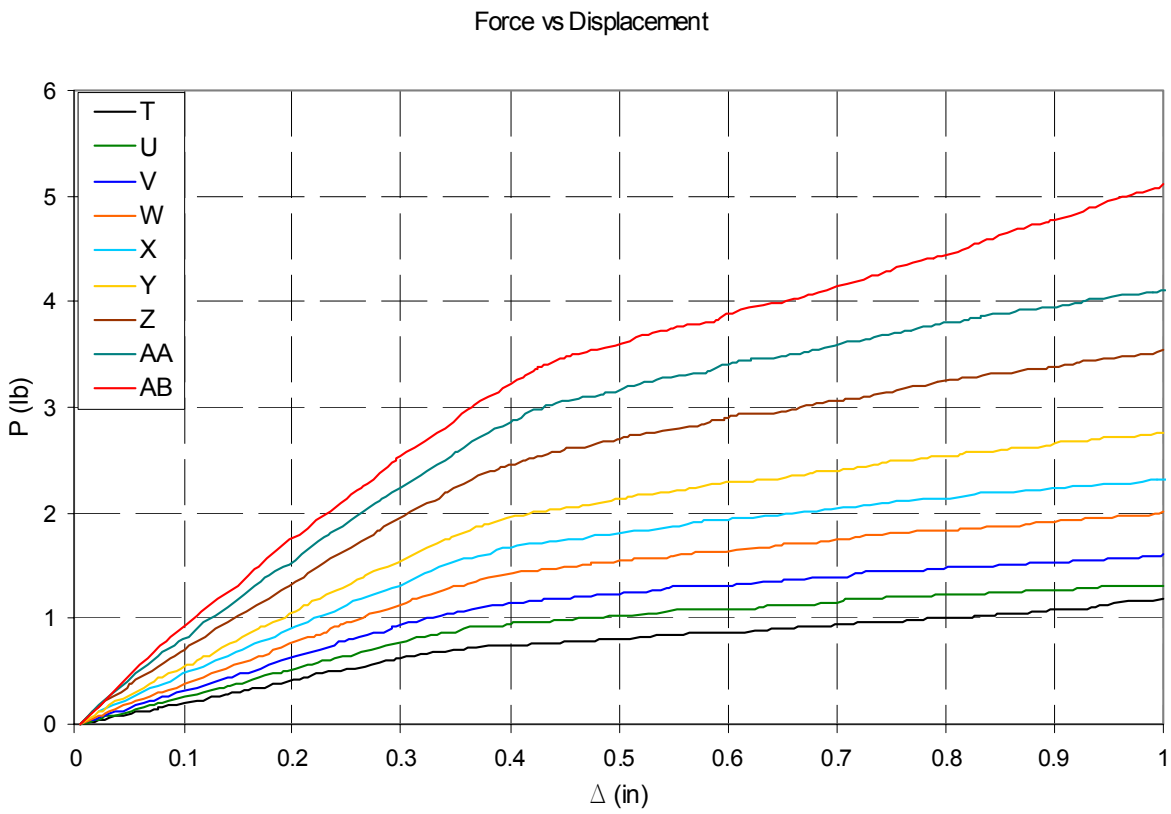

Fig. 5.9 Load-displacement curves for models T to AB

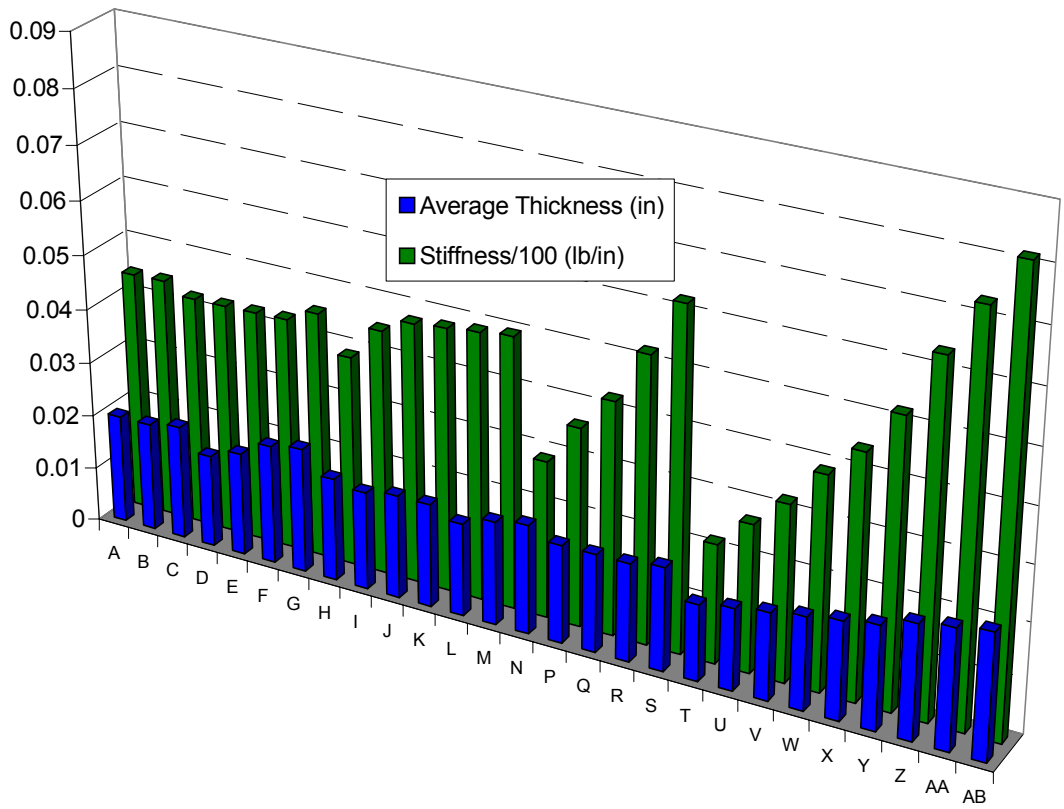

Fig. 5.10 Average thickness and stiffness summary

5.2 Orthotropic Sensitivity Analysis on Ribbed Cup

An orthotropic sensitivity analysis was conducted in order to determine the effects of different combinations of the meridional modulus of elasticity E_m, and circumferential modulus of elasticity E_c, on the compression response. The values for modulus of elasticity range from 295 ksi to 420 ksi. The principal Poisson's ratio is held fixed at 0.35 in these parametric studies. Assuming the principal modulus is the circumferential one, the principal Poisson's ratio is the ratio of the meridional normal strain to the circumferential normal strain under a uniaxial state of circumferential normal stress. Hence, the minor Poisson's ratio is in the range of 0.246 to 0.498. Since the shear modulus for the HIPS material is not readily available, it is assumed to remained fixed at its value in the isotropic case of 109 ksi. Also, the wall thickness is held constant at 0.02 in.

5.2.1 Constant Circumferential Modulus of Elasticity

The value of the circumferential modulus E_c was fixed at 295 ksi. The load-displacement curves for E_m = 295, 320, 345, 370, 395, and 420 ksi are shown in Fig. 5.11. Convergence problems were encountered by the solver while processing the models containing the meridional modulus values of E_m = 345 ksi and E_m = 420 ksi. The solution for this was to change the convergence and step size properties. The number of increments was changed from 1200 to 1500, the increment size was specified to be 0.001 with a maximum step size of 0.01. These changes solved the numerical problems. The two curves corresponding to E_m = 345 ksi and E_m = 420 ksi in Fig. 5.11 are distinguished from the others by the very low reaction forces in the take-up region of the response. The response curves outside the take-up region show that the reaction forces increase with increasing meridional modulus. Also, the stiffness in the linear region of the response increases with increasing modulus as shown in Table 5.7

Table 5.7 Stiffness values for *Ec* = 295 ksi and selected values of *Em*

Em, ksi	295	320	345	370	395	420
Stiffness, lb/in	7.092	7.357	7.565	7.832	8.089	8.299

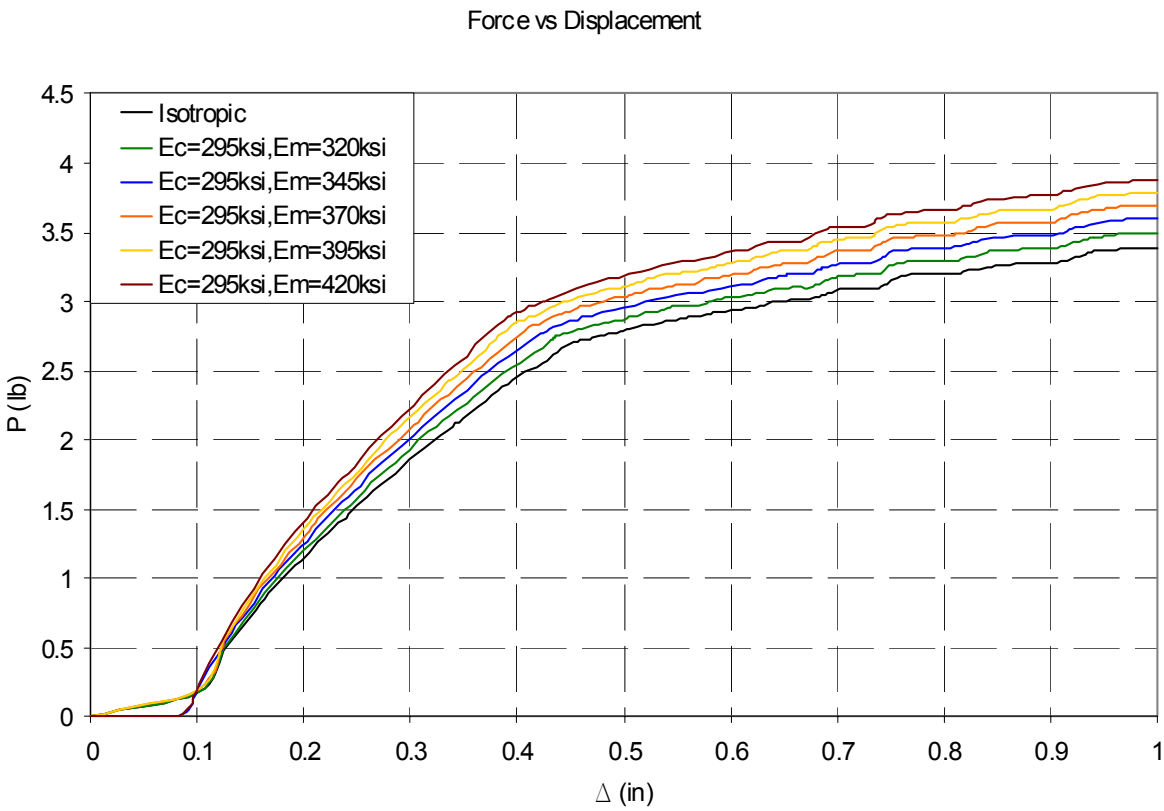

Fig. 5.11 Response curves for the orthotropic sensitivity analysis with constant circumferential modulus

5.2.2 Constant Meridional Modulus of Elasticity

The meridional modulus is fixed at E_m = 295 ksi while the values taken for the circumferential modulus were E_c = 295, 320, 345, 380, 395, and 420 ksi. The load-displacement curves are shown in Fig. 5.12. Outside the take-up regions the reaction force increases with increasing circumferential modulus. Also, the stiffness in the linear region of the response increases with increasing modulus as shown in Table 5.8. Convergence problems were again encountered by the solver for E_c = 320 and 345 ksi. In these cases, the step size parameters were changed to a

maximum number of increments of 2000 with an initial step of 0.001 and a maximum step size of 0.009.

Table 5.8 Stiffness values for *Em* = 295 ksi and selected values of *Ec*

Ec, ksi	295	320	345	370	395	420
Stiffness, lb/in	7.092	7.180	7.336	7.494	7.640	7.782

A summary of both of the orthotropic parametric studies for the ribbed cup is provided by the bar chart shown in Fig. 5.13, in which stiffness for each set of parameters is plotted on the ordinate. The isotropic case corresponds to both moduli equal to 295 ksi. It can be observed that the stiffness is more sensitive to changes in the meridional modulus of elasticity than for the circumferential modulus.

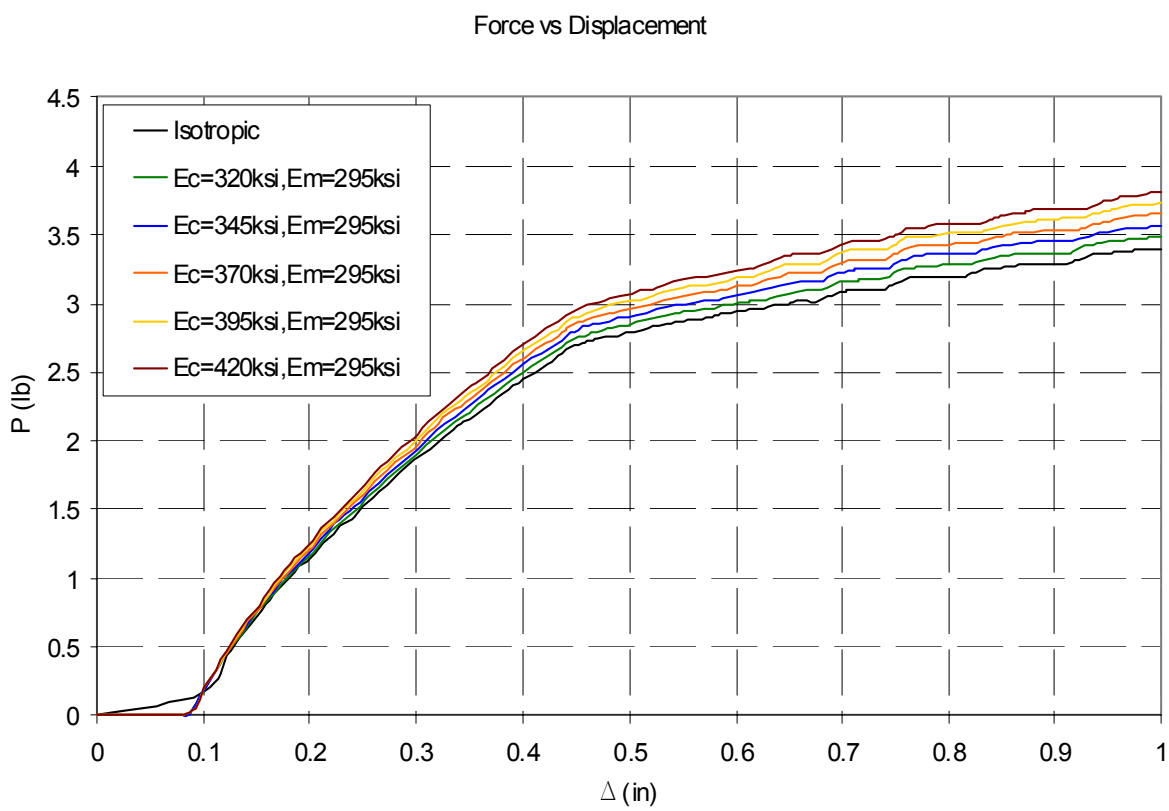

Fig. 5.12 Response curves for the orthotropic sensitivity analysis with constant meridional modulus

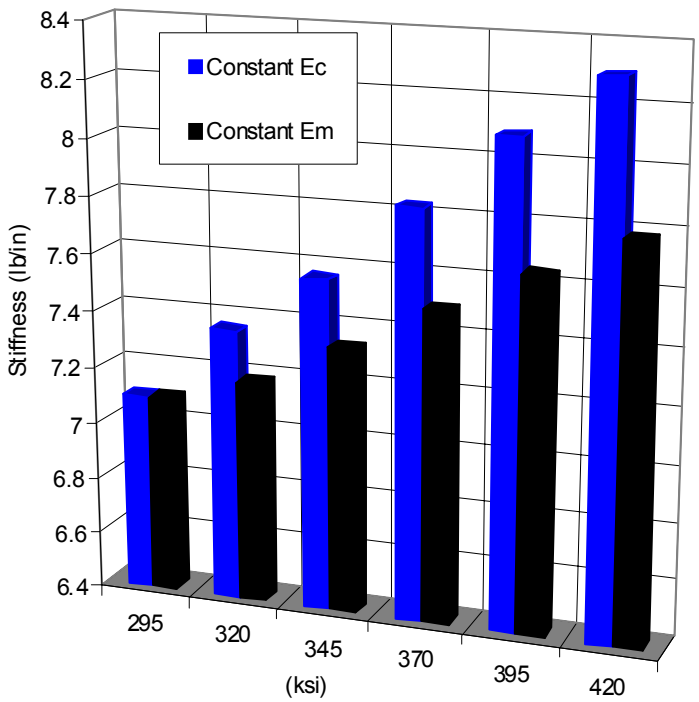

Fig. 5.13 Stiffness values comparison for the ribbed cup

5.3 The Smooth Cup Model

To determine the effects of the circumferential ribs on the response of the cup, a model of a cup with no ribs was developed. This model referred as the smooth model since the meridian in the center of the cup is a straight line. It has no ribs but it keeps the original geometry of the bottom part and the upper ring. To compare the geometries of the ribbed and smooth cup models, the meridional profiles are superimposed in the drawing shown in Fig. 5.14. The smooth model employs the same elements S4R5, and the same algorithms, as used for the ribbed model, which was described in Chapter 4. Table 5.9 contains the necessary points to reproduce the smooth wall profile.

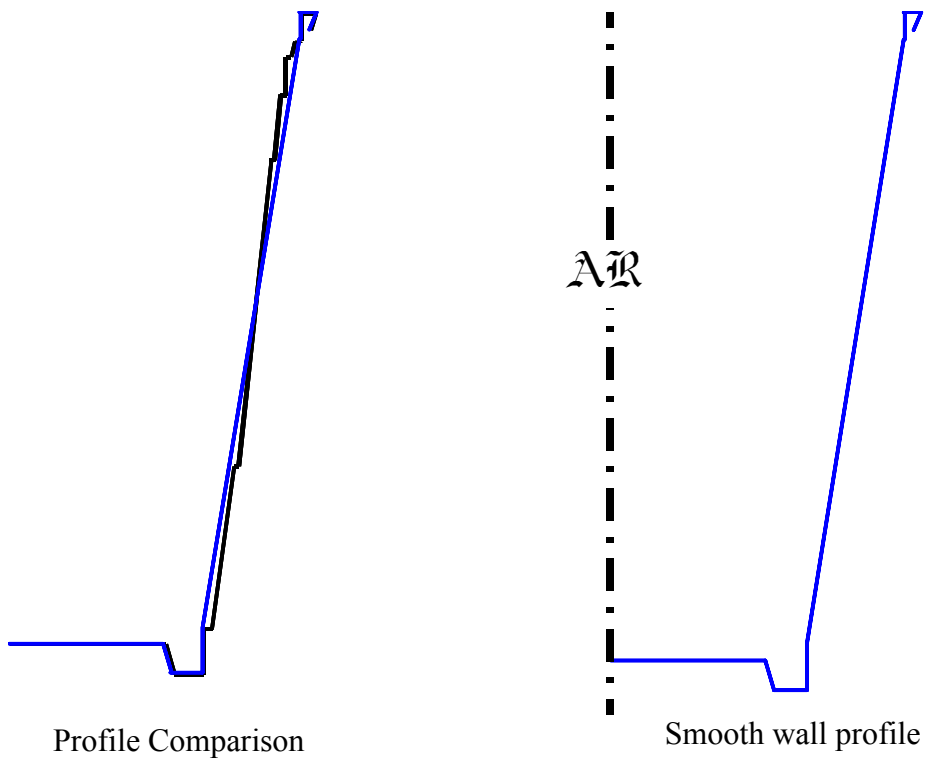

Fig. 5.14 Smooth cup model

Table 5.9 Coordinates of the smooth cup profile

Point Number	x-coordinate	y-coordinate
1	0	0.204
2	0.970	0.204
3	1.020	0
4	1.220	0
5	1.220	0.308
6	1.380	1.414
7	1.700	3.493
8	1.770	3.931
9	1.810	4.196
10	1.830	4.300
11	1.830	4.485
12	1.930	4.485
13	1.900	4.376

5.4 Variable Thickness Distribution Study of the Smooth Cup

The set of thickness distributions denoted by *Ts* to *ABs* listed in Table 5.10 is used as a basis to study the thickness variation on the smooth cup model. The thickness distributions listed in Table 5.10 for the smooth cup correspond to the distributions *T* to *AB* in the ribbed cup study of Table 5.6. The thickness of bottom remains fixed at 0.021in., while the smooth cup wall has a piecewise constant thickness distribution corresponding to regions 2 to 5 of the ribbed cup. Hence, the smooth cup models have smooth meridian in regions 2 to 5, but the wall thickness changes from one region to the next as shown in Table 5.10.

The response curves for the nine distribution *Ts* to *ABs* are shown in Fig. 5.15. The response curves show that the reaction force increases as the wall thickness increases. A peculiar result is the waviness exhibited by the curves. After careful analysis and with the help of the *CPRESS* option in ABAQUS/CAE, the cause of the waviness was determined to be due to the mechanics of the contact. The *CPRESS* command output is available whenever a master

and a slave surface exist. This command displays a contour plot of contact pressure at surface nodes between the master and slave surfaces. As indicated by the inset graphics of the contact pressure in Fig. 5.15 for thickness case *Zs*, the contact area is changing with the displacement of the cylinder. For the applied displacement of slightly less that 0.5 in., the contact pressure is non-zero in two contact areas towards the ends of the cylinder. At a displacement of 0.5 in, note that the pressure is non-zero in an additional area at the center of the cylinder. At a displacement slightly greater than 0.5 in., the contact pressure is non-zero at the two contact areas near the end of the cylinder. Hence, the locations of the contact are changing as the displacement increases through 0.5 in from two areas at the ends of the cylinder, to two areas at the ends plus an area in the middle, and then back to two at areas ends. At the peak the wavy section where the displacement is 0.5 in, the cylinder then makes contact at three locations on the cup. With the next increment in the applied displacement, the cylinder breaks contact with the central region of the cup having again only two contact locations.

Table 5.10 Thickness distributions Ts to ABs for the smooth cup

Distance from the top of the cup	Model designation and thickness distribution (in.)								
	Ts	Us	Vs	Ws	Xs	Ys	Zs	AAs	ABs
0.27 in.	0.020	0.023	0.025	0.027	0.029	0.031	0.034	0.036	0.039
0.59 in.	0.013	0.014	0.015	0.017	0.018	0.019	0.021	0.023	0.024
0.98 in.	0.011	0.012	0.013	0.015	0.016	0.017	0.018	0.020	0.021
1.96 in.	0.009	0.010	0.011	0.012	0.013	0.014	0.016	0.017	0.018
3.93 in.	0.008	0.009	0.010	0.011	0.012	0.013	0.014	0.015	0.016
Bottom region	0.021	0.021	0.021	0.021	0.021	0.021	0.021	0.021	0.021
Average thickness, in.	0.014	0.015	0.016	0.017	0.018	0.019	0.021	0.022	0.023
Weighted thickness, in.	0.013	0.014	0.015	0.016	0.017	0.018	0.019	0.020	0.021
Stiffness, lb/in.	1.686	2.022	2.350	2.688	3.421	3.918	5.025	5.754	6.468

The stiffnesses in the linear region of the response are listed for each distribution in Table 5.10 and plotted in the bar graph of Fig. 5.16. The stiffnesses for the smooth cup are less

than the corresponding stiffnesses of the ribbed cup; compare stiffnesses in Table 5.6 to Table 5.10. Hence, the ribbed cup is stiffer than the corresponding smooth cup if both cups have the same thickness distribution.

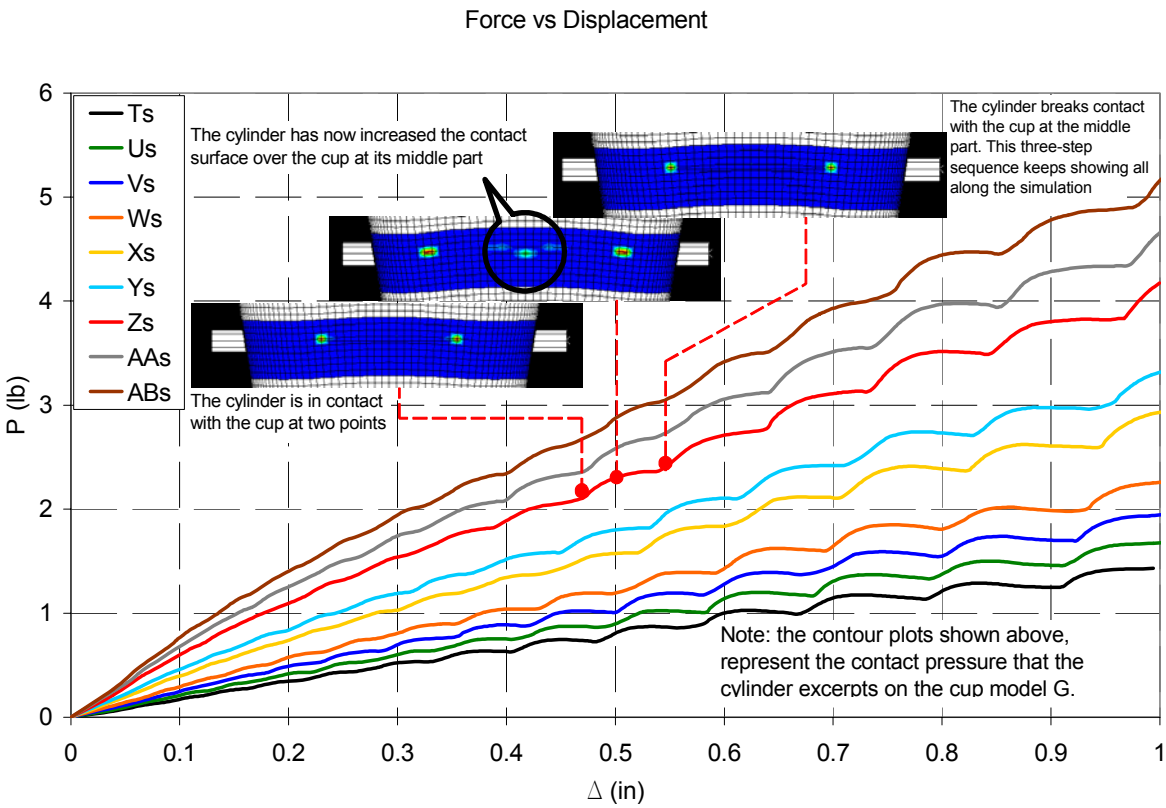

Fig. 5.15 Load-displacement curves for thickness distributions Ts to ABs of the smooth cup

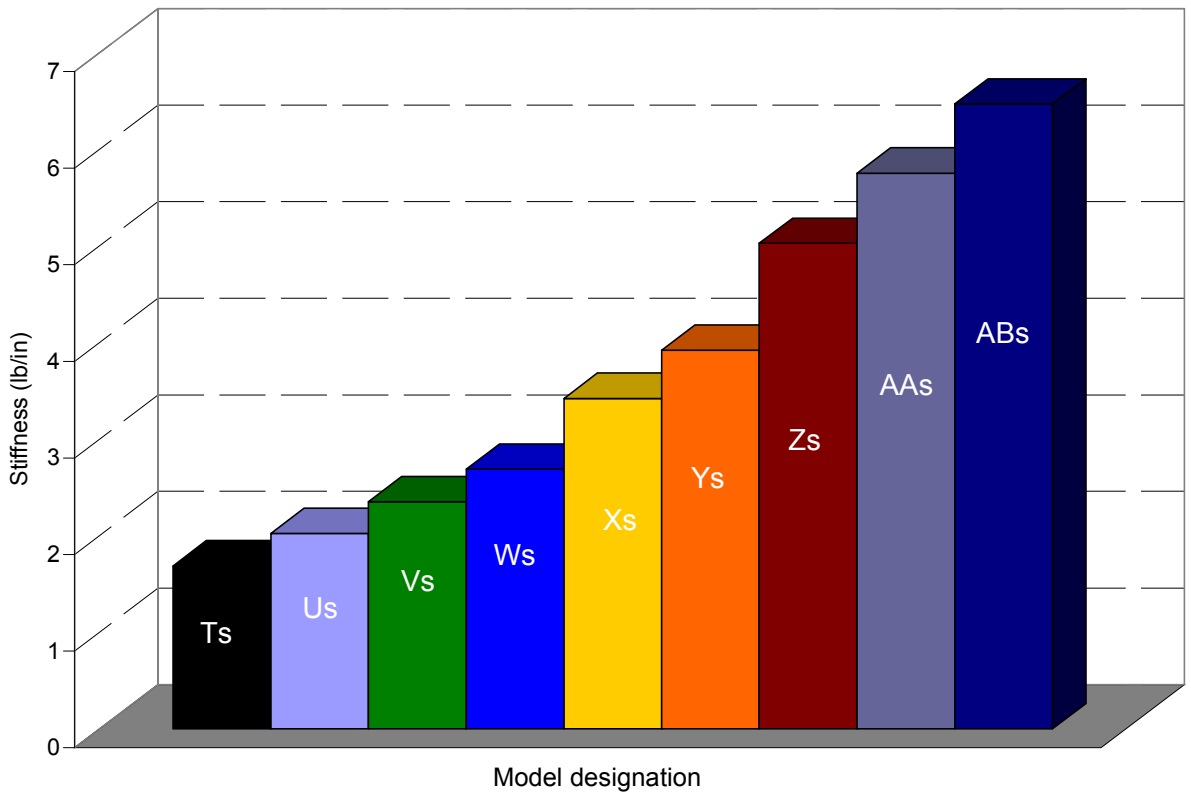

Fig. 5.16 Stiffness values for the smooth cup

5.5 Orthotropic Sensitivity Analysis on Smooth Cup

The same general procedures described in Section 5.2.1 on page 84 and Section 5.2.2 on page 85 are used to determine how sensitive the smooth cup is to changes in circumferential modulus of elasticity and the meridional modulus of elasticity. The response curves for fixed *Ec* = 295 ksi and *Em* = 295, 320, 345, 370, 395, and 420 ksi are shown in Fig. 5.17. The response curves for fixed *Em* = 295 ksi and *Ec* = 295, 320, 345, 370, 395, and 420 ksi are shown in Fig. 5.18. For the isotropic case both moduli are equal to 295 ksi. The waviness in the curves is apparent again in this set of results. The cause of this has been explained on Section 5.4 on page 89. The reaction force increases with increasing modulus in both cases. Also, the stiffness in the linear region increases with increasing modulus as is shown in Table 5.11. The stiffness for both orthotropic studies are plotted in the bar graph in Fig. 5.19. The stiffness is more sensitive to changing meridional modulus than for changing circumferential modulus, except for 370 ksi. This sensitivity is also reflected in the stiffness values listed in Table 5.11. Compared to the ribbed cup stiffness shown in Figure 5.13 on page 87 , the smooth cup has less sensitivity than the ribbed cup.

Table 5.11 Stiffness values of a smooth cup for either fixed *Ec* or *Em*

Variable modulus in ksi	295	320	345	370	395	420
Stiffness in lb/in. for Ec = 295 ksi	5.885	6.091	6.221	6.282	6.610	6.776
Stiffness in lb/in. for Em = 295 ksi	5.885	6.062	6.121	6.313	6.358	6.692

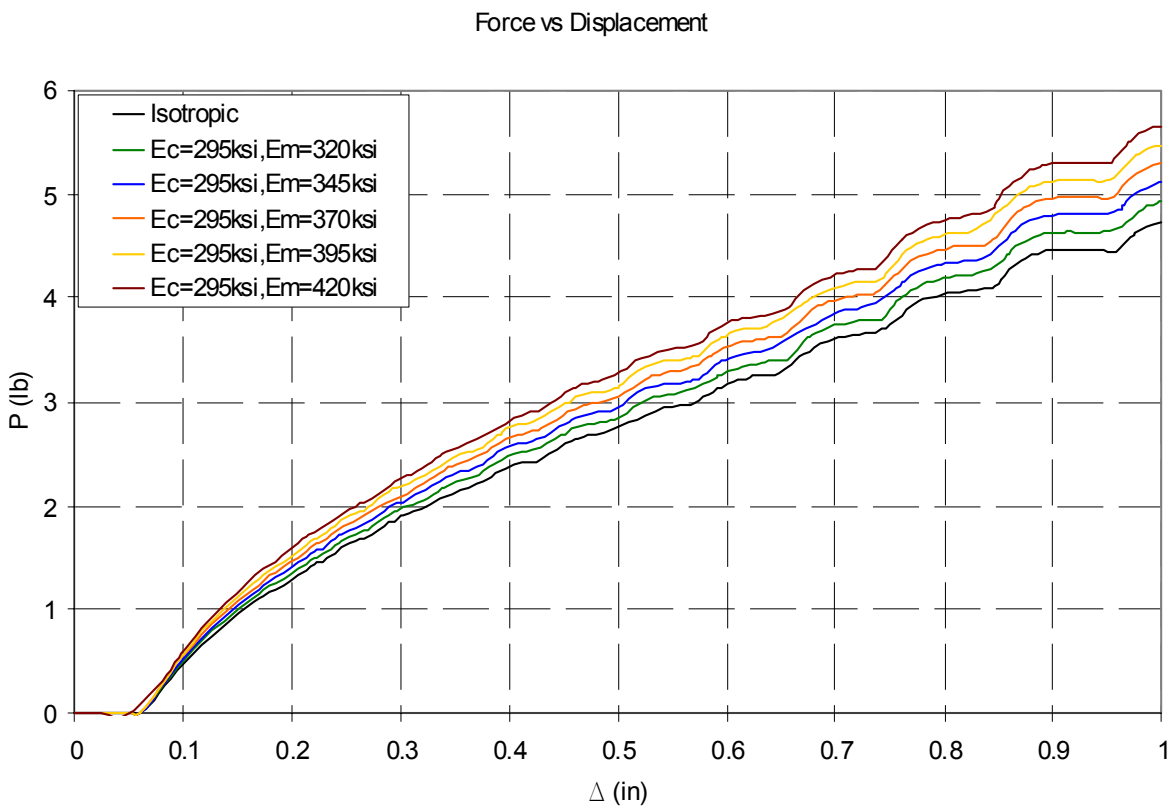

Fig. 5.17 Orthotropic sensitivity analysis for constant circumferential modulus of the smooth cup

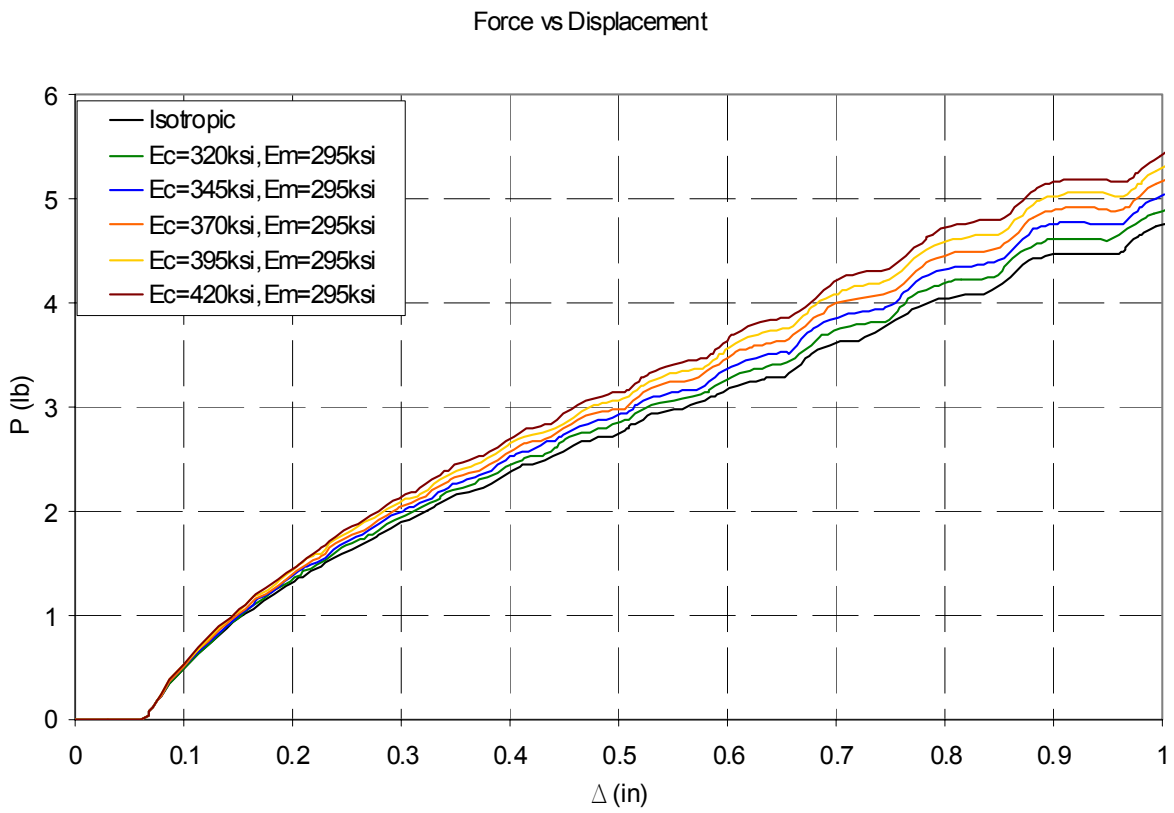

Fig. 5.18 Orthotropic sensitivity analysis for constant meridional modulus of the smooth cup

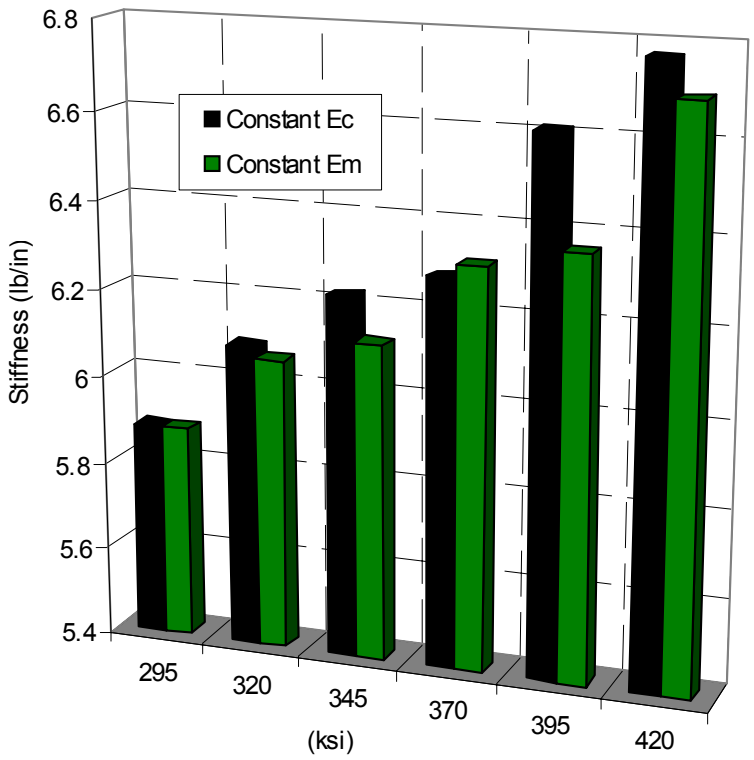

Fig. 5.19 Stiffness values comparison for the smooth cup

CHAPTER 6

Summary and Concluding Remarks

The load-deflection response of a typical sixteen-ounce plastic drink cup was simulated using the small strain, large rotation shell analysis capability in the ABAQUS finite element software package. A contact algorithm was used to model a test in which the cup is squeezed in a load frame to mimic the action of a person holding the cup in their hand. The truncated conical shell model of the cup developed in ABAQUS used shell element S4R5. The meridian of the cup is specified by the coordinates listed in Table 4.1 and it is sketched in Fig. 4.1. This meridian contains abrupt radial changes in its profile that represent circumferential ribs in the cup wall. The material of the cup is high impact polystyrene (HIPS), and it is assumed to be linear elastic in the analysis. Generic material properties are listed in Table 1.1. Coupons cut from the wall of a cup were subjected to tensile tests in the meridional and circumferential directions conducted at Dow Plastics and in the Engineering Science and Mechanics (ESM) Department at Virginia Tech. The stress-strain curves from these coupon tests are presented in Chapter 2, and average values of the moduli are listed in Table 2.1. Moduli used in ABAQUS model of the cup are in the range of the coupon test data obtained from both sources. The cup has a ring, or rim, at its open end, and separate tests of it subjected to diametrical tension were conducted in ESM as discussed in Section 2.4. Good correlation between the linear finite element analysis of the rim test and the test data was achieved as is shown in Fig. 3.17 on page 46 .

Confidence in using ABAQUS to construct the model of the lateral compression test of the cup was achieved by modeling simpler problems with known analytical solutions as discussed in Chapter 3. A detailed process to construct the finite element model using Patran and ABAQUS/CAE is outlined in Chapter 4. The load-deflection response curves obtained from the simulation exhibit a "knee" and a softening behavior with increasing applied displacement, while the data provided by Dow exhibits a linear response as shown in Fig. 5.4 on page 73 and Fig. 5.7 on page 79 . However, the values of the loads and deflections from the simulation are in the same range as the test data.

To study the effect of the circumferential ribs, a smooth cup model was developed which has no ribs. The smooth cup model has the same dimensions for the upper ring and bottom region as the ribbed cup model, but its profile along the meridian was changed to a straight continuous line. For the thickness distribution studies of the smooth cup, the same piece-wise constant thicknesses along the wall segments corresponding to the segments of the ribbed cup were used. The meridian of the smooth cup is shown with respect to the ribbed cup model in Fig. 5.14. Parametric studies conducted on the ribbed cup model and the smooth cup model are presented in Chapter 5.

A total of 27 ribbed cup models were analyzed with different thickness distributions considering the material to be isotropic with a modulus of elasticity of 295ksi and a Poisson's ratio of 0.35. For the range thicknesses considered, changing the thicknesses in segments of the wall remote from the applied load had little effect on the load-deflection response curves. For example, the load-deflection response was insensitive to changing bottom thickness and Region 5 thicknesses as reported in Section 5.1.1 and Section 5.1.3. It was also observed that the ring at the open end was a significant contributor to the stiffness of the cup. The response curves for changing wall thickness, while maintaining constant volume, differ in the non-linear response regime. However, the linear response regimes are nearly the same as is shown in Fig. 5.5. Finally, it was observed that the stiffness increases with proportional increases in the thicknesses of all segments of wall as described on Section 5.1.4 and Section 5.1.5.

Orthotropy studies focused on the effect of changing the ratio of the meridional to circumferential modulus in a range 295ksi to 420ksi in increments of 25ksi. These studies determined the sensitivity of the cup's compressive response by keeping one modulus of elasticity constant while the other varied. In this case of the cup model with variable orthotropic material characteristics, Poisson's ratio was fixed at 0.35, the shear modulus was fixed at 109 ksi, and the thickness along the meridian was fixed at 0.02 in. Several convergence problems were encountered during this set of analyses. Therefore, the original convergence and step size criteria described in Chapter 4 had to be changed in order to get converged results. Fortunately, once the numerical problems were solved, we were able to get consistent response curves with respect to changing moduli values. Changes in step size and convergence criteria changed the way the take-up region in the response near the origin develops. Whenever convergence problems were encountered, the take-up region exhibited almost no load increase for an increasing the applied displacements from zero. It was observed that the stiffness is more sensitive to increasing meridional modulus than increasing circumferential modulus as depicted on Fig. 5.19.

Load-deflection response curves for the smooth cup are nearly linear, but have small waviness due to changes in the contact area as described by the graphic insets of Fig. 5.15 on page 91 . The waviness is due to the exchange from two to three contact areas between the rigid cylindrical indenter rod (master surface) and the cup wall (slave surface) as the displacement of the rod is increased. This changing contact condition was not observed in the response of the ribbed cup model.

This page is intentionally left blank

References

[1]Mangonon, Pat L., The Principles of Materials Selection for Engineering Design, Prentice Hall. Melbourne, FL (1999), p. 677.

[2]STYRON A-TECH 1220. High Impact Polystyrene Resins Product Information. Trademark of The Dow Chemical Company.

[3]Young, Warren C., Roark's Formulas for Stress and Strain, Sixth Edition, McGraw-Hill, Inc., New York (1989), p. 263.

[4]Baker, E.H, et al., Structural Analysis of Shells, Robert E. Krieger Publishing Company, Malabar, FL, (1972), p. 93 and 127.

[5]ABAQUS/Standard Version 6.3 User's Manual, Hibbitt, Karlsson, & Sorensen, Inc., 1080 Main St., Pawtucket, Rhode Island, 2001.

[6]Patran Version 7 User's Manual, The MacNeal-Schwendler Corporation, 815 Colorado Boulevard, Los Angeles, CA 90041.

[7]ABAQUS/CAE Version 6.3 User's Manual, Hibbitt, Karlsson, & Sorensen, Inc., 1080 Main St., Pawtucket, Rhode Island, 2001.

Appendix A

A.1 Sample ABAQUS Input File for a Ribbed Cup Model

```
*Heading
** Job name: Ribbed Model name: Ribbed
**
** PARTS
**
*Part, name=PART-1-1
*End Part
**
** ASSEMBLY
**
*Assembly, name=Assembly
**
*Instance, name=PART-1-1, part=PART-1-1
*Node
      1,       1.6489,      2.92649,           2.
      2,        1.625,      2.99996,           2.
      3,      1.71142,       2.8811,           2.
      4,      1.64885,      3.07345,           2.
      :
      :
   4250, -4.47016e-09,        0.204,    -0.102265
   4251, -8.94473e-09,        0.204,    -0.204632
   4252,  -6.7084e-09,        0.204,     -0.15347
   4253,        1.625,      2.99996,           2.
*Element, type=R3D4
```

```
5500, 160, 159, 157, 156
5501, 159, 154, 153, 157
5502, 154, 145, 144, 153
  :
  :
5647,  13,  15,   5,   3
5648,  15,  17,   7,   5
5649,  17,  19,   9,   7
*Element, type=S4R5
5650, 3776, 3829, 3828, 3775
5651, 3829, 3880, 3879, 3828
5652, 3880, 3929, 3928, 3879
  :
  :
9275,  299,  298,  345,  346
9276,  346,  345,  416,  344
9277,  344,  416,  413,  414
9278,  414,  413,  479,  415
*Elset, elset=S1, generate
 8979,  9278,     1
*Elset, elset=S2, generate
 8859,  8978,     1
*Elset, elset=S3, generate
 8619,  8858,     1
*Elset, elset=S4, generate
 7359,  8618,     1
*Elset, elset=S5, generate
 6699,  7358,     1
*Elset, elset=S6, generate
 5650,  6698,     1
*Elset, elset=_I2, internal, generate
 5650,  6698,     1
*Elset, elset=_I3, internal, generate
 6699,  7358,     1
*Elset, elset=_I4, internal, generate
 7359,  8618,     1
*Elset, elset=_I5, internal, generate
 8619,  8858,     1
*Elset, elset=_I6, internal, generate
 8859,  8978,     1
*Elset, elset=_I7, internal, generate
 8979,  9278,     1
```

```
** Region: (Section-1-_I2:_I2)
*Elset, elset=_I2, internal, generate
 5650,  6698,     1
** Section: Section-1-_I2
*Shell Section, elset=_I2, material=POLYSTYR
0.021, 5
** Region: (Section-2-_I3:_I3)
*Elset, elset=_I3, internal, generate
 6699,  7358,     1
** Section: Section-2-_I3
*Shell Section, elset=_I3, material=POLYSTYR
0.012, 5
** Region: (Section-3-_I4:_I4)
*Elset, elset=_I4, internal, generate
 7359,  8618,     1
** Section: Section-3-_I4
*Shell Section, elset=_I4, material=POLYSTYR
0.013, 5
** Region: (Section-4-_I5:_I5)
*Elset, elset=_I5, internal, generate
 8619,  8858,     1
** Section: Section-4-_I5
*Shell Section, elset=_I5, material=POLYSTYR
0.016, 5
** Region: (Section-5-_I6:_I6)
*Elset, elset=_I6, internal, generate
 8859,  8978,     1
** Section: Section-5-_I6
*Shell Section, elset=_I6, material=POLYSTYR
0.018, 5
** Region: (Section-6-_I7:_I7)
*Elset, elset=_I7, internal, generate
 8979,  9278,     1
** Section: Section-6-_I7
*Shell Section, elset=_I7, material=POLYSTYR
0.029, 5
*End Instance
*Nset, nset=_G21, internal, instance=PART-1-1
 4253,
*Nset, nset=_G20, internal, instance=PART-1-1
 4253,
*Nset, nset=_G19, internal, instance=PART-1-1
```

```
 4253,
*Nset, nset=_G18, internal, instance=PART-1-1
 4253,
*Nset, nset=_G17, internal, instance=PART-1-1
 4253,
*Nset, nset=_G14, internal, instance=PART-1-1
 4253,
*Nset, nset=_G7, internal, instance=PART-1-1
 4253,
*Nset, nset=BCSEDGE, instance=PART-1-1
  304,  305,  306,  361,  415,  431,  479,  496,  497,  498,  499,  544,
563,  610,  630,  671
  692,  741,  763,  805,  828,  882,  905,  962,  985, 1042, 1068, 1119,
1145, 1194, 1222, 1262
 1290, 1330, 1358, 1397, 1426, 1464, 1494, 1531, 1562, 1598, 1630, 1665,
1698, 1732, 1766, 1799
 1834, 1866, 1903, 1934, 1973, 2003, 2043, 2072, 2114, 2142, 2185, 2212,
2257, 2283, 2328, 2353
 2399, 2426, 2475, 2507, 2555, 2583, 2629, 2658, 2709, 2733, 2794, 2817,
2879, 2901, 2963, 2984
 3047, 3068, 3129, 3149, 3211, 3230, 3285, 3305, 3361, 3382, 3435, 3458,
3509, 3533, 3581, 3598
 3643, 3662, 3702, 3721, 3760, 3776, 3814, 3829, 3866, 3880, 3916, 3929,
3964, 3976, 4010, 4021
 4052, 4062, 4090, 4099, 4124, 4132, 4154, 4161, 4180, 4186, 4202, 4207,
4220, 4224, 4234, 4237
 4244, 4246, 4250, 4251, 4252
*Nset, nset=MOVE, instance=PART-1-1
 4253,
*Elset, elset=CONT, instance=PART-1-1, generate
 5500,  5649,     1
*Nset, nset=_PICKEDSET10, internal, instance=PART-1-1
 161, 164, 165, 168, 170, 172, 175, 176, 179, 180, 182, 184, 186, 188, 189,
192
 197, 198, 200, 201, 206, 207, 210, 214, 216, 221, 224, 226, 227, 230, 239,
242
 245, 250, 253, 256, 261, 262, 270, 271, 274, 283, 285, 286, 288, 298, 301,
305
 306, 308, 309, 310, 317, 320, 332, 333, 345, 348, 358, 359, 364, 367, 371,
372
 377, 380, 383, 413, 416, 417, 420, 421, 422, 423, 424, 425, 426, 427, 432,
433
```

```
 434, 435, 438, 439, 443, 445, 446, 448, 451, 452, 453, 454, 455, 456, 457,
458
 459, 479, 481, 484, 485, 486, 487, 488, 489, 490, 500, 501, 502, 512, 513,
514
 517, 518, 519, 520, 521, 522, 523, 524, 525, 544
*Nset, nset=_PICKEDSET11, internal, instance=PART-1-1
  304,  305,  306,  361,  415,  431,  479,  496,  497,  498,  499,  544,
563,  610,  630,  671
  692,  741,  763,  805,  828,  882,  905,  962,  985, 1042, 1068, 1119,
1145, 1194, 1222, 1262
 1290, 1330, 1358, 1397, 1426, 1464, 1494, 1531, 1562, 1598, 1630, 1665,
1698, 1732, 1766, 1799
 1834, 1866, 1903, 1934, 1973, 2003, 2043, 2072, 2114, 2142, 2185, 2212,
2257, 2283, 2328, 2353
 2399, 2426, 2475, 2507, 2555, 2583, 2629, 2658, 2709, 2733, 2794, 2817,
2879, 2901, 2963, 2984
 3047, 3068, 3129, 3149, 3211, 3230, 3285, 3305, 3361, 3382, 3435, 3458,
3509, 3533, 3581, 3598
 3643, 3662, 3702, 3721, 3760, 3776, 3814, 3829, 3866, 3880, 3916, 3929,
3964, 3976, 4010, 4021
 4052, 4062, 4090, 4099, 4124, 4132, 4154, 4161, 4180, 4186, 4202, 4207,
4220, 4224, 4234, 4237
 4244, 4246, 4250, 4251, 4252
*Elset, elset=__PICKEDSURF8_SPOS, internal, instance=PART-1-1, generate
 5500,  5649,     1
*Elset, elset=__PICKEDSURF9_SPOS, internal, instance=PART-1-1
 7361, 7362, 7363, 7364, 7365, 7366, 7381, 7382, 7383, 7384, 7385, 7386,
7401, 7402, 7403, 7404
 7405, 7406, 7421, 7422, 7423, 7424, 7425, 7426, 7441, 7442, 7443, 7444,
7445, 7446, 7461, 7462
 7463, 7464, 7465, 7466, 7481, 7482, 7483, 7484, 7485, 7486, 7501, 7502,
7503, 7504, 7505, 7506
 7521, 7522, 7523, 7524, 7525, 7526, 7541, 7542, 7543, 7544, 7545, 7546,
7561, 7562, 7563, 7564
 7565, 7566, 7581, 7582, 7583, 7584, 7585, 7586, 7601, 7602, 7603, 7604,
7605, 7606, 7621, 7622
 7623, 7624, 7625, 7626, 7641, 7642, 7643, 7644, 7645, 7646, 7661, 7662,
7663, 7664, 7665, 7666
 7681, 7682, 7683, 7684, 7685, 7686, 7701, 7702, 7703, 7704, 7705, 7706,
7721, 7722, 7723, 7724
 7725, 7726, 7741, 7742, 7743, 7744, 7745, 7746, 7761, 7762, 7763, 7764,
7765, 7766, 7781, 7782
```

```
 7783, 7784, 7785, 7786, 7801, 7802, 7803, 7804, 7805, 7806, 7821, 7822,
7823, 7824, 7825, 7826
 7841, 7842, 7843, 7844, 7845, 7846, 7861, 7862, 7863, 7864, 7865, 7866,
7881, 7882, 7883, 7884
 7885, 7886, 7901, 7902, 7903, 7904, 7905, 7906, 7921, 7922, 7923, 7924,
7925, 7926, 7941, 7942
 7943, 7944, 7945, 7946, 7961, 7962, 7963, 7964, 7965, 7966, 7981, 7982,
7983, 7984, 7985, 7986
 8001, 8002, 8003, 8004, 8005, 8006, 8021, 8022, 8023, 8024, 8025, 8026,
8041, 8042, 8043, 8044
 8045, 8046, 8061, 8062, 8063, 8064, 8065, 8066, 8081, 8082, 8083, 8084,
8085, 8086, 8101, 8102
 8103, 8104, 8105, 8106, 8121, 8122, 8123, 8124, 8125, 8126, 8141, 8142,
8143, 8144, 8145, 8146
 8161, 8162, 8163, 8164, 8165, 8166, 8181, 8182, 8183, 8184, 8185, 8186,
8201, 8202, 8203, 8204
 8205, 8206, 8221, 8222, 8223, 8224, 8225, 8226, 8241, 8242, 8243, 8244,
8245, 8246, 8261, 8262
 8263, 8264, 8265, 8266, 8281, 8282, 8283, 8284, 8285, 8286, 8301, 8302,
8303, 8304, 8305, 8306
 8321, 8322, 8323, 8324, 8325, 8326, 8341, 8342, 8343, 8344, 8345, 8346,
8361, 8362, 8363, 8364
 8365, 8366, 8381, 8382, 8383, 8384, 8385, 8386, 8401, 8402, 8403, 8404,
8405, 8406, 8421, 8422
 8423, 8424, 8425, 8426, 8441, 8442, 8443, 8444, 8445, 8446, 8461, 8462,
8463, 8464, 8465, 8466
 8481, 8482, 8483, 8484, 8485, 8486, 8501, 8502, 8503, 8504, 8505, 8506,
8521, 8522, 8523, 8524
 8525, 8526, 8541, 8542, 8543, 8544, 8545, 8546
*Elset, elset=__PICKEDSURF8_SPOS, internal, instance=PART-1-1, generate
 5500,  5649,     1
*Surface, type=ELEMENT, name=_PICKEDSURF8, internal
__PICKEDSURF8_SPOS, SPOS
*Elset, elset=__PICKEDSURF9_SPOS, internal, instance=PART-1-1
 7361, 7362, 7363, 7364, 7365, 7366, 7381, 7382, 7383, 7384, 7385, 7386,
7401, 7402, 7403, 7404
 7405, 7406, 7421, 7422, 7423, 7424, 7425, 7426, 7441, 7442, 7443, 7444,
7445, 7446, 7461, 7462
 7463, 7464, 7465, 7466, 7481, 7482, 7483, 7484, 7485, 7486, 7501, 7502,
7503, 7504, 7505, 7506
 7521, 7522, 7523, 7524, 7525, 7526, 7541, 7542, 7543, 7544, 7545, 7546,
7561, 7562, 7563, 7564
```

```
 7565, 7566, 7581, 7582, 7583, 7584, 7585, 7586, 7601, 7602, 7603, 7604,
7605, 7606, 7621, 7622
 7623, 7624, 7625, 7626, 7641, 7642, 7643, 7644, 7645, 7646, 7661, 7662,
7663, 7664, 7665, 7666
 7681, 7682, 7683, 7684, 7685, 7686, 7701, 7702, 7703, 7704, 7705, 7706,
7721, 7722, 7723, 7724
 7725, 7726, 7741, 7742, 7743, 7744, 7745, 7746, 7761, 7762, 7763, 7764,
7765, 7766, 7781, 7782
 7783, 7784, 7785, 7786, 7801, 7802, 7803, 7804, 7805, 7806, 7821, 7822,
7823, 7824, 7825, 7826
 7841, 7842, 7843, 7844, 7845, 7846, 7861, 7862, 7863, 7864, 7865, 7866,
7881, 7882, 7883, 7884
 7885, 7886, 7901, 7902, 7903, 7904, 7905, 7906, 7921, 7922, 7923, 7924,
7925, 7926, 7941, 7942
 7943, 7944, 7945, 7946, 7961, 7962, 7963, 7964, 7965, 7966, 7981, 7982,
7983, 7984, 7985, 7986
 8001, 8002, 8003, 8004, 8005, 8006, 8021, 8022, 8023, 8024, 8025, 8026,
8041, 8042, 8043, 8044
 8045, 8046, 8061, 8062, 8063, 8064, 8065, 8066, 8081, 8082, 8083, 8084,
8085, 8086, 8101, 8102
 8103, 8104, 8105, 8106, 8121, 8122, 8123, 8124, 8125, 8126, 8141, 8142,
8143, 8144, 8145, 8146
 8161, 8162, 8163, 8164, 8165, 8166, 8181, 8182, 8183, 8184, 8185, 8186,
8201, 8202, 8203, 8204
 8205, 8206, 8221, 8222, 8223, 8224, 8225, 8226, 8241, 8242, 8243, 8244,
8245, 8246, 8261, 8262
 8263, 8264, 8265, 8266, 8281, 8282, 8283, 8284, 8285, 8286, 8301, 8302,
8303, 8304, 8305, 8306
 8321, 8322, 8323, 8324, 8325, 8326, 8341, 8342, 8343, 8344, 8345, 8346,
8361, 8362, 8363, 8364
 8365, 8366, 8381, 8382, 8383, 8384, 8385, 8386, 8401, 8402, 8403, 8404,
8405, 8406, 8421, 8422
 8423, 8424, 8425, 8426, 8441, 8442, 8443, 8444, 8445, 8446, 8461, 8462,
8463, 8464, 8465, 8466
 8481, 8482, 8483, 8484, 8485, 8486, 8501, 8502, 8503, 8504, 8505, 8506,
8521, 8522, 8523, 8524
 8525, 8526, 8541, 8542, 8543, 8544, 8545, 8546
*Surface, type=ELEMENT, name=_PICKEDSURF9, internal
__PICKEDSURF9_SPOS, SPOS
** Constraint: RigidBody-1
*Rigid Body, ref node=_G21, elset=CONT
*End Assembly
```

```
**
** MATERIALS
**
*Material, name=POLYSTYR
*Elastic
295000., 0.35
**
** INTERACTION PROPERTIES
**
*Surface Interaction, name=I58
1.,
*Friction, slip tolerance=0.005
0.,
*Surface Behavior, no separation, pressure-overclosure=HARD
**
** BOUNDARY CONDITIONS
**
** Name: Disp-BC-1 Type: Displacement/Rotation
*Boundary
_PICKEDSET10, 2, 2
** Name: Disp-BC-2 Type: Symmetry/Antisymmetry/Encastre
*Boundary
_PICKEDSET11, XSYMM
**
** INTERACTIONS
**
** Interaction: I58-1
*Contact Pair, interaction=I58, adjust=0.0
_PICKEDSURF9, _PICKEDSURF8
** ----------------------------------------------------------------
**
** STEP: Step-1
**
*Step, name=Step-1, nlgeom, extrapolation=PARABOLIC, inc=1500
Linear Static Analysis
*Static, stabilize=2e-05
0.001, 1., 1e-15, 0.01
**
** BOUNDARY CONDITIONS
**
** Name: Disp-BC-3 Type: Displacement/Rotation
*Boundary
```

```
MOVE, 1, 1, -0.6
** Name: Disp-BC-4 Type: Displacement/Rotation
*Boundary
MOVE, 2, 2
** Name: Disp-BC-5 Type: Displacement/Rotation
*Boundary
MOVE, 3, 3
** Name: Disp-BC-6 Type: Displacement/Rotation
*Boundary
MOVE, 4, 4
** Name: Disp-BC-7 Type: Displacement/Rotation
*Boundary
MOVE, 5, 5
** Name: Disp-BC-8 Type: Displacement/Rotation
*Boundary
MOVE, 6, 6
**
** OUTPUT REQUESTS
**
*Restart, write, frequency=0
*Print, contact=YES
**
** FIELD OUTPUT: F-Output-1
**
*Output, field, variable=PRESELECT
**
** HISTORY OUTPUT: H-Output-1
**
*Output, history, variable=PRESELECT
*El Print, freq=999999
*Node Print, freq=999999
*End Step
```

This page is intentionally left blank

Vita

Ignacio Dapic Rodriguez is a graduate research assistant in the Aerospace and Ocean Engineering at Virginia Polytechnic and State University. He was born on June 18, 1979 to Ignacio Dapic and Violeta Rodriguez in Mexico City, Mexico. After receiving his high school diploma with a 4.0 GPA from Instituto Tecnologico y de Estudios Superiores de Monterrey Campus Estado de Mexico, he attended Florida Institute of Technology to achieve his life-long dream: become an aerospace engineer. The 2001 NASA-FAA aircraft design competition represented one of his biggest challenges when he lead the Florida Tech team to this competition. Under the advisory and expertise of an international authority in flying cars and roadable aircraft such as Prof. Palmer Stiles, the Florida Tech team created a flying car that was ultimately submitted to the design competition. The summer of that same year, he earned his Bachelor's degree with High Honors. After success-

fully completing his undergraduate studies in Melbourne, FL. where he was inducted to Tau Beta Pi (The Engineering Honor Society) and awarded as Outstanding Senior in Aerospace Engineering, he decided to enroll in a Master's degree at Virginia Polytechnic Institute and State University. In February 2002, The DOW Chemical Company funded Ignacio Dapic to conduct finite element analysis research on plastics. He graduated in May 2003 with a Master's of Science in Aerospace Engineering under the advisory of Dr. Eric Johnson. On June 9th, 2003 Ignacio Dapic successfully defended his thesis titled "Numerical Model for the Lateral Compression Response of a Plastic Cup." During his years as a graduate student in Blacksburg, VA he became a member of the Graduate Student Committee and was inducted to The International Honor Society Delta Phi Beta and The Outstanding Student Honor Society.